SIMULATION OF SOIL EVAPORATION AND ITS RELATION TO HEAVY WATER ISOTOPOLOGUE ENRICHEMENT IN SOIL USING DIFFERENT MODEL APPROACHES

Jana SCHNEIDER

Supervisors:
Prof. Dr. Jan Vanderborght, supervisor
Prof. Dr. Youri Rothfuss, supervisor
(Univ. Liège)

Members of the Examination Committee:
Prof. Dr. ir. Jan Diels, assessor
Prof. Dr. Bart Nicolaï, assessor
Prof. Dr. Rainer Helmig, assessor
(Univ. Stuttgart)
Prof. Dr. Isabelle Braud, additional member
(INRAE)
Prof. Dr. Steven Bouillon, additional member
Prof. Dr. Maarten Roeffaers, chair

Dissertation presented in partial fulfillment of the requirements for the degree of Doctor of Bioscience Engineering (PhD)

January 2026

Doctoraatsproefschrift nr. 2081 aan de faculteit Bio-ingenieurswetenschappen van de KU Leuven

Uitgegeven in eigen beheer, Jana Schneider, Essen, Germany

Acknowledgement

After studying evaporation processes for many years my doctoral work comes to an end.

During all this time I received great support from a lot of people, exchanging their knowledge and experience but also helping as friends with motivation, persistence and open ears at any time.

I could not have undertaken this journey without Jan Vanderborght, who did a perfect job as a supervisor, always keeping track of the work, knowing when he is needed and always guiding and supporting at the right times. I gained a lot of knowledge from you and your expertise but also from your analytical and solution focused mindset towards the scientific problems we faced.

I also would like to thank Youri Rothfuss for being a great educational daily supervisor, teaching me a lot about isotopologues and not minding spending countless hours with me analyzing results during my time at the Research Center Jülich. Thank you Youri for sparking my interest in isotopologues.

A special thanks to Isabelle Braud, who was a great support and exceptional help to get along with SiSPAT-Isotope. I was always impressed by your ability to remember so many peculiarities of SiSPAT-Isotope and your passion for continuing the work with it.

Another big thank you goes to our project research group, especially to Stefanie Kiemle, Katharina Heck and Rainer Helmig, dedicating time and energy towards our collaborative research, never losing your enthusiasm.

I am also grateful to my doctoral and examination committee, who generously provided knowledge and expertise, helping me improve my thesis.

I had a great time at the Research Center Jülich looking back to an outstanding team of colleagues leading me through difficult times and always being supportive over all the years we spent together. When I first started, I could have never imagine what I have achieved today.

A special thanks goes to my friends and family always believing in me even at times where everything seemed to be impossible. In this context Joel must be mentioned explicitly, being by my side only for a short period of my doctoral time, he maybe suffered the most under sharing me with my ambition to finally finish the research.

Thank you Joel for being patient, encouraging, my greatest supporter and fan. Having you by my side changed a lot for me and I appreciate each hour we spent together in our small home office.

Summary

Water scarcity is an increasing challenge to global agriculture in times of climate change and world population growth. Understanding water loss through evapotranspiration becomes critical for sustainable water management practices. A major part of this water loss is caused by soil evaporation, especially in arid regions, where it can account for up to 95% of water loss.

Despite its importance, significant knowledge gaps remain in modeling and monitoring complex energy and mass transfer processes that drive soil evaporation. Current modeling approaches range from simplified isothermal models to complex non-isothermal multi-phase models with varying degrees of accuracy.

Furthermore, field and laboratory measurements face technical challenges, such as capturing diurnal water flux variations or controlling experimental conditions like in wind tunnel studies.

With our research we aimed to address some of these limitations by testing and comparing different model approaches against high-frequency laboratory and field measurements. Our goal was to identify under which conditions simplifications used in evaporation models are appropriate.

Therefore, in our first study we used the FAO Penman-Monteith method combined with soil water flow simulations using the Richards equation for predicting soil evaporation. The model was evaluated using lysimeter measurements. Needed soil hydraulic properties were estimated from soil texture using the ROSETTA pedotransfer functions, from in situ measured water retention curves, or from soil surface water contents using inverse modeling.

We found that the Richards equation approach adequately predicted cumulative evaporation but could not capture diurnal dynamics due to neglecting vapor transport processes in the soil. The results depended strongly on the chosen set of soil hydraulic properties. In situ measured soil properties produced much better predictions than texture-based estimations. Moreover, soil surface structure has a major

impact on evaporation rates, e.g. tillage can reduce total evaporation rates and limit water movement from deeper layers to the surface.

In our second study we analyzed evaporation-driven enrichment of heavier water isotopologues in unsaturated porous media by comparing two different numerical models, SiSPAT-Isotope and DuMu^x, with experimental data.

The main difference between both models is the handling of very dry soil conditions. In DuMu^x, the soil can dry out completely, whereas in SiSPAT-Isotope the soil does not become drier than the residual water content. This leads to similar simulation results of heavy isotopologue enrichment if the residual water saturation is low. For high residual water saturations, SiSPAT- Isotope simulated considerably lower heavy isotopologue enrichment than DuMu^x.

Furthermore, in SiSPAT- Isotope we increased the laminar boundary layer thickness in the free air flow over time to reproduce a decrease in evaporation rates. This was necessary due to numerical instabilities but consequently led to incorrect simulation of the location of the evaporation front and isotopic ratio profiles.

We compared our simulations with experimental data and concluded that diffusive transport processes in the laminar boundary layer and in the dried-out surface soil layer need to be adequately represented in the model to reproduce isotopologue enrichment profiles in the soil.

Samenvatting

Waterschaarste is een steeds grotere uitdaging voor de wereldwijde landbouw in tijden van klimaatverandering en groei van de wereldbevolking. Inzicht in waterverlies door evapotranspiratie wordt cruciaal voor duurzaam waterbeheer. Een groot deel van dit waterverlies wordt bepaald door bodemverdamping, vooral in droge gebieden, waar dit tot 95% van het waterverlies kan veroorzaken.

Ondanks het belang van bodemverdamping blijven er grote hiaten in de kennis over het modelleren en monitoren van complexe energie- en massatransferprocessen die de bodemverdamping aandrijven. De huidige modelbenaderingen variëren van vereenvoudigde isotherme modellen tot complexe niet-isotherme meerfasenmodellen met verschillende nauwkeurigheid.

Bovendien hebben veld- en laboratoriummetingen te maken met technische uitdagingen, zoals het waarnemen van variaties in verdampingsfluxen tijdens een dag of het controleren van de experimentele omstandigheden in windtunnelstudies.

Met ons onderzoek wilden we bepaalde beperkingen aanpakken door verschillende modelbenaderingen te testen en te vergelijken met hoogfrequente laboratorium- en veldmetingen. Ons doel was om te bepalen onder welke omstandigheden bepaalde vereenvoudigingen in verdampingsmodellen geschikt zijn.

In onze eerste studie gebruikten we de FAO Penman-Monteith methode gecombineerd met simulaties van de bodemwaterstroming met behulp van de Richards vergelijking voor het voorspellen van de bodemverdamping. Het model werd geëvalueerd met behulp van lysimeter-metingen. De benodigde hydraulische eigenschappen van de bodem werden geschat op basis van de bodemtextuur met behulp van de ROSETTA pedotransferfuncties, op basis van in situ gemeten waterretentiecurven of op basis van het watergehalte aan het bodemoppervlak met behulp van inverse modellering.

We ontdekten dat de Richards-vergelijking de cumulatieve verdamping adequaat voorspelde, maar de dagelijkse dynamiek niet kon weergeven doordat damptransportprocessen in de bodem

werden verwaarloosd. De resultaten waren sterk afhankelijk van de gekozen set van hydraulische bodemeigenschappen. In situ gemeten bodemeigenschappen leverden veel betere voorspellingen op dan op textuur gebaseerde schattingen. Bovendien heeft de structuur van het bodemoppervlak een grote invloed op de verdampingssnelheden, bijv. grondbewerking kan de totale verdampingssnelheden verminderen en de waterbeweging van diepere lagen naar het oppervlak beperken.

In onze tweede studie analyseerden we verdampingsgedreven aanrijking van zwaardere water isotopologen in onverzadigde poreuze media door twee verschillende numerieke modellen te vergelijken: SiSPAT-Isotope en DuMu^x, met experimentele gegevens.

Het belangrijkste verschil tussen beide modellen is de beschrijving van zeer droge bodemomstandigheden. In DuMu^x kan de bodem volledig uitdrogen, terwijl in SiSPAT-Isotope de bodem niet droger kan worden dan het residuele vochtgehalte. Dit leidt tot vergelijkbare simulatieresultaten voor de aanrijking van zwaardere isotopologen indien de residuele waterverzadiging laag is. Voor hoge residuele vochtgehaltes simuleerde SiSPAT-Isotope een aanzienlijk lagere aanrijking van isotopologen dan DuMu^x.

Verder hebben we in SiSPAT- Isotope de dikte van de laminaire grenslaag in de vrije luchtstroom vergroot in de tijd om een afname van de verdampingssnelheid te reproduceren. Dit was nodig vanwege numerieke instabiliteiten, maar leidde tot een onjuiste simulatie van de locatie van het verdampingsfront en het isotopologueieconcentratieprofiel.

We vergeleken onze simulaties met experimentele gegevens en besloten dat diffusieve transportprocessen in de laminaire grenslaag en in de uitgedroogde bodemlaag aan het oppervlak correct gerepresenteerd moeten worden om aanrijkingsprofielen van isotopologen in de bodem te reproduceren

Abbreviations and Symbols

Latin symbols

Symbol	Unit	Definition
a_{vG}	m^{-1}	Inverse of the air entry value
BL		Bad Lauchstädt soil
b	-	Parameter describing soil geometry
C_v^{ia}	kg m^{-3}	Isotopic concentration at the atmosphere
C_v^{is}	kg m^{-3}	Isotopic concentration at the soil surface
C_α^i	kg m^{-3}	Isotopic concentration in phase α
c_s	J kg^{-1} K^{-1}	Specific heat capacity
c_α	J kg^{-1} K^{-1}	Heat capacity of phase α
D_v	m^2 s^{-1}	Vapor diffusion coefficient
D_v^i	m^2 s^{-1}	Isotopic vapor diffusion coefficient
$D_\alpha^{\kappa,j}$	m^2 s^{-1}	Binary diffusion coefficient
$D_{\alpha,pm}^{\kappa}$	m^2 s^{-1}	Effective diffusion coefficient
DBM		Bimodal model of Durner
DD		Dedelow soil
E	mm d^{-1}	Evaporation
E_{cum}	mm	Cumulative evaporation
$E_{cum,I}$	m	Cumulative evaporation during stage-I
E_m	mm d^{-1}	Measured evaporation rates
E_{pot}	mm d^{-1}	Potential evaporation rate
E_{sim}	mm d^{-1}	Simulated evaporation rate
E^i	kg m^{-2} s^{-1}	Surface isotopic flux
ET	mm d^{-1}or kg	Evapotranspiration
ET_0	mm d^{-1}	Reference evapotranspiration
e_a	kPa	Mean daily ambient vapor pressure
e_{sat}^0	kPa	Mean saturated vapor pressure
FAO		Food and Agriculture Organization of the United Nations
g	m s^{-2}	Gravitational acceleration
H	W m^{-2}	Sensible heat flux
H_g	J m^2 s^{-1}	Heat flux
h	m	Matric pressure head
h_i	m	Initial water pressure head

Symbol	**Unit**	**Definition**
h_α	J kg $^{-1}$	Specific enthalpy
I	mm d^{-1}	Irrigation
$K_{l,h}$	m s^{-1}	Isothermal hydraulic conductivity for liquid flow
$K_{l,T}$	m s^{-1}	Thermal hydraulic conductivity for liquid flow
$K_{r,\alpha}$	-	Relative hydraulic conductivity
$K_{s,\alpha}$	m s^{-1}	Saturated hydraulic conductivity for phase α
K_{tilled}	m s^{-1}	Hydraulic conductivity of a tilled surface
$K_{v,h}$	m s^{-1}	Isothermal hydraulic conductivity for vapor flow
$K_{v,T}$	m s^{-1}	Thermal hydraulic conductivity for vapor flow
K_α	m s^{-1}	Hydraulic conductivity of phase α
k_a	m^2	Soil permeability
k_i	m^2	Intrinsic permeability
$k_{r,\alpha}$	-	Relative permeability of phase α
k_s	m^2	Saturated or absolute permeability
k_α	m^2	Effective permeability
L_c	m	Characteristic length of evaporation
L_v	J kg $^{-1}$	Latent heat vaporization
LE	W m^{-2}	Outgoing latent heat flux
l	-	Pore connectivity
M^{H_2O}	g mol^{-1}	Molar mass of water
M^{i}	g mol^{-1}	Isotopic molar mass
m_{total}	kg	Total mass
m_{vG}	-	Shape parameter (van Genuchten)
m^i	kg	Mass of the isotopic species
N^K	-	Particle number
n	mol	Moles
n_c	-	Pore size distribution index (Brooks-Corey)
n_K	-	Kinetic exponent
n_{vG}	-	Pore-size distribution index (van Genuchten)
n^i	mol	Moles of isotopic species
n'_K	-	Kinetic exponent
P	mm d^{-1}	Precipitation rate

Symbol	**Unit**	**Definition**
P_i	kg or mm	Precipitation
PDI		Peter-Durner-Iden
PM		Penman-Monteith method
PTF		Pedotransfer function
p_c	Pa	Capillary pressure
p_g	Pa	Gas phase pressure
$p^{\kappa}_{sat,Kelvin}$	Pa	Kelvin pressure
p_l	Pa	Liquid phase pressure
p_α	Pa	Phase pressure
Q_g	W m^{-2}	Soil heat flux
q^K	kg m^{-3} s^{-1}	Source/sink term
R	J mol^{-1} K^{-1}	Universal gas constant
R_N	W m^{-2}	Incoming net solar radiation
R_{VSMOW}	-	Reference isotopic ratio given by the Vienna Standard Mean Ocean Water
R^i_α	-	Isotopic ratio in phase α
RH	-	Relative humidity
$RMSD_u$		Unsystematic difference
$RMSD_s$		Systematic difference
r_a	s m^{-1}	Aerodynamic resistance factor
r_{aT}	s m^{-1}	Turbulent aerodynamic resistance
r_{am}	s m^{-1}	Molecular aerodynamic resistance
r_{av}	s m^{-1}	Bulk surface aerodynamic resistance for water vapor
r_i	s m^{-1}	Resistance to isotopic species transport
r_s	s m^{-1}	Surface bulk resistance
S	mm	Water storage
S_{evap}	m d$^{-0.5}$	Soil desorptivity
S_l	-	Liquid saturation
S_g	-	Gas saturation
S_{we}	-	Effective wetting saturation
S_{wr}	-	Residual water saturation
S_α	-	Phase saturation
SB		Sauerbach soil
SE		Selhausen soil
SHP		Soil hydraulic properties
SR	mm d^{-1}	Surface runoff losses
T	K	Temperature

Symbol	Unit	Definition
T_r	mm d^{-1}	Transpiration
T_{ref}	K	Reference temperature
t	s	Time
u	m s^{-1}	Friction velocity
u_2	m s^{-1}	Wind speed at 2 m above the ground
u_α	J kg^{-1}	Specific internal energy
vG	-	Van Genuchten
vGM	-	Van Genuchten Mualem
V_{pore}	m^3	Pore volume
V_{total}	m^3	Total volume
V_α	m^3	Phase volume
v	m^2 s^{-1}	Air kinematic viscosity
$\boldsymbol{v}_\alpha$	m s^{-1}	Fluid phase velocity
WL	kg	Lysimeter weight
WT	kg	Seepage tank weight
w	kg kg^{-1}	Weight of the pore domain to total pore volume
X_α^κ	kg kg^{-1}	Mass fraction of component κ in phase α
z_{om}	m	Roughness length

Greek symbols

Symbol	Unit	Definition
α	-	Priestly-Taylor coefficient
α_{eq}^{i}	-	Equilibrium fractionation factor
α_{iK}	-	Kinetic fractionation factor
α_{vG}	m^{-1}	Empirical van Genuchten shape parameter
β^{i}	-	Factor relating liquid and vapor concentration
γ	kPa $°C^{-1}$	Psychometric constant
Δ	kPa $°C^{-1}$	Slope of the saturation vapor pressure
δ	-	Adaptive threshold
δ_z	m	Boundary layer thickness
δ^{i}	‰	Isotope delta notation
ε	-	Error
θ	m^3 m^{-3}	Volumetric water content
θ_i	m^3 m^{-3}	Initial water content
θ_l	m^3 m^{-3}	Volumetric liquid water content
θ_r	m^3 m^{-3}	Residual volumetric water content
θ_{sat}	m^3 m^{-3}	Saturated volumetric water content
θ_{sur}	m^3 m^{-3}	Soil surface volumetric water content
θ_v	m^3 m^{-3}	Water vapor content expressed in volume of liquid water
λ	MJ kg^{-1}	Latent heat of evaporation
λ_{pm}	W m^{-1} K^{-1}	Effective thermal conductivity
λ_s	W m^{-1} K^{-1}	Solid thermal conductivity
μ_α	Pa s	Dynamic fluid viscosity
ρ_a	kg m^{-3}	Air density
ρ_s	kg m^{-3}	Mass density of the solid phase
ρ_w	kg m^{-3}	Water density
ρ_α	kg m^{-3}	Mass density of phase α
σ	N m^{-1}	Surface tension of the-gas-fluid phase
σ_g	-	Geometric standard deviation of geometric mean diameter
τ	-	Tortuosity factor

Symbol	Unit	Definition
ϕ	-	Porosity
ψ	Pa	Matric potential
ω	-	Averaging window width

Indices and exponents

Symbol	Definition
air	Dry air
a	Air/atmosphere
α	Phase
c	Capillary
cum	Cumulative
eq	Equal
ff	Free-flow
g	Gaseous phase
H_2O	Water
i	Isotopologue
l	Liquid phase
m	Measured
pm	Porous-medium domain
ref	Reference
s	Solid phase/ soil
s	Saturated
t	Time interval
v	Vapor
vG	Van Genuchten
w	Wetting phase/water
we	Effective wetting
wr	Residual water
κ	Component

List of Figures

List of Tables

Contents

1 General Introduction and Objectives

1.1 Introduction

Water is one of the most critical resources for sustainable agricultural development worldwide(Chartzoulakis & Bertaki, 2015). Climate change and the expected growth of the world population will increase irrigated areas and consequently water demand. However, more freshwater will be required to meet the increasing demand of domestic and industrial use, leading to water supplies being diverted from agriculture (Assouline et al., 2015; Rost et al., 2008). Global irrigation water use reached 2500 km^3 a^{-1}, representing ca. 70 % of total human blue water use. The global agricultural blue water consumption including transpiration, bare soil evaporation, water bodies and canopies amounts to 90 % of overall blue water consumption (Rost et al., 2008). Additionally, the expected changes in precipitation and drought patterns associated with global warming will increase water scarcity (Dai, 2011; Lehmann et al., 2019). Dai (2011) analyzed the Palmer Drought Severity Index (PDSI) for the period 1900-2008 and identified extensive drying across Africa, East Asia, South Asia, and several other regions between 1950 and 2008, largely attributable to global warming. During this time, the proportion of the world's land area classified as dry increased by approximately 1.74 % per decade.

Nowadays, agriculture consumes up to 70 % of the world's water resources, with particularly high consumption in semi-arid and arid regions(Boretti & Rosa, 2019). To fulfill the demand for agricultural products from an increasing global population, agriculture must expand and therefore will require more water for irrigation(Beier et al., 2023). Accurate estimations of water demand in agricultural areas are important for effective agricultural water management. Proper water management is important to face challenges of a growing global population and a growth in crop production (Chukalla et al., 2025).

The second largest component of the terrestrial water balance is evapotranspiration (ET) after precipitation (Volk et al., 2024). The Food and Agriculture Organization of the United Nations (FAO) defines ET as a combination of two processes, evaporation from the bare soil surface and transpiration from the plant canopy, both processes describe water losses to the atmosphere by a phase transition from liquid to gas. Evaporation and transpiration occur simultaneously(Allen et al., 1998; Jensen & Allen, 2016).

In the global hydrological cycle, approximately 60% of precipitation on land returns to atmosphere by soil evaporation (ca. 20%) or by transpiration (ca. 40%) (Oki & Kanae, 2006 in Or et al., 2013). Schlesinger and Jaseschko (2014) compared 81 studies that have partitioned evapotranspiration into its components, and summarized that soil evaporation in these studies represents ca. 20 - 40% of global evapotranspiration. Within continental hydrologic partitioning, most evaporation (65 % ± 26 %) originates from soils rather than from surface waters such as rivers and streams (Good et al., 2015). Van der Ent et al. (2010) used an accounting procedure based on ERA-Interim reanalysis data to calculate moisture recycling ratios. They estimated that approximately 40% of terrestrial precipitation is derived from land-surface evaporation, and that 57% of the total terrestrial evaporation subsequently falls again as precipitation over land. A field study in a semiarid ponderosa pine forest conducted over four years showed the significance and temporal variability of evapotranspiration in the water balance. In this study the water budget was dominated by ET which accounts for ca. 95% of precipitation (Brandes & Wilcox, 2000).

Evaporation from soil is predominant when crops are small, and the soil surface is bare for many weeks (Mellouli et al., 2000). At the time of sowing, nearly 100% of ET originates from bare soil evaporation (Allen et al., 1998). During this period, soil moisture content in the upper soil layer is critical for plant growth, including seed germination, seedling establishment and the growth of young crops.

For rainfed agriculture in arid and semiarid regions, bare soil causes significant soil moisture loss, negatively impacting the crop yield. In Tunisia, a study conducted over a time period of 20 years found that bare soil evaporation accounted for 75% of annual precipitation(Riou, 1977 in Mellouli et al., 2000). Similarly, in Syria up to 75% of soil moisture is lost by bare soil evaporation under barely (Cooper et al., 1987 in Mellouli et al., 2000). Information about bare soil evaporation processes is crucial for water management practices such as irrigation scheduling, weather forecasting, and water resource management (Gebler et al., 2015; Hu et al., 2018; Jung et al., 2010; Yang et al., 2000 in Gong et al., 2025).

The following sections provide a brief introduction to the fundamentals of bare soil evaporation, measurement methods, and modeling approaches, followed by the research objectives and research conducted as part of this thesis. Finally, we conclude with the results and give an outlook on future research.

1.2 Vadose Zone and Bare Soil Evaporation

The vadose zone, also known as the unsaturated zone, plays a significant role in the hydrologic cycle. It is defined as the geologic layer expanding from the land surface to the groundwater table of the first unconfined aquifer (Stephens et al., 2018) (Figure 1-1). Water movement in the vadose zone or unsaturated flow is driven by capillary and gravitational forces. Unsaturated flow in the soil is closely linked to flow processes at the soil surface such as infiltration during rainfall events, upward liquid water flow towards evaporation surfaces and downward liquid flow that drains and redistributes water during dry periods (Arora et al., 2019; Hillel, 2004). Evaporation from the soil surface involves a combined process of heat and mass transfer, with rates influenced by energy input, diffusive and advective transport processes in the soil, and diffusive and turbulent mixing in the air flowing over the soil surface (Haghighi & Or, 2013). It is influenced by the relative humidity of the air and the flow regime of the surrounding atmosphere (Mosthaf, Helmig, & Or, 2014).

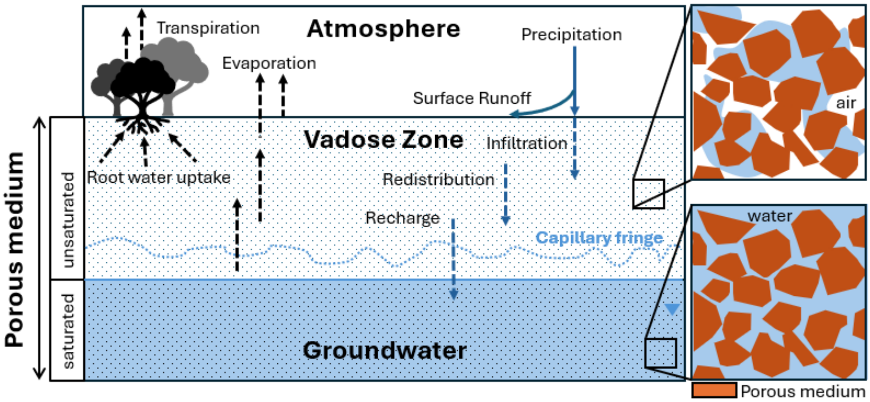

Figure 1-1: Schematic display of processes between atmosphere, vadose zone and groundwater. Water precipitates from the atmosphere on the surface where it runs off or is infiltrating into the porous medium. The unsaturated zone of the porous medium is called vadose zone and controls water infiltration rates, movement and storage within the subsurface influencing plant growth, groundwater recharge and surface water dynamics. Above the saturated porous medium / groundwater storage, there is a capillary fringe where water is drawn by capillary action. Due to root water uptake and therewith transpiration as well as evaporation processes, water returns to the atmosphere.

Soil evaporation follows a three stage process (Figure 1-2) (Idso et al., 1974). During the first stage, evaporation is driven by atmospheric conditions, the limiting factor for the evaporation rate is the amount of available energy to vaporize soil moisture in the upper soil layer and by vapor pressure deficit between surface and atmosphere. First stage evaporation can be compared to evaporation of free water surfaces (Bittelli, et al., 2008). Due to a relatively constant drying rate this stage is termed constant-rate period (Mosthaf et al., 2014).

When the water content in the upper soil layer decreases and the evaporative demand at the surface cannot be met by the liquid connections supplying the interface, the second stage of evaporation begins. During this stage, evaporation is constrained by the diffusive transport of water in the soil, both in the liquid and gas phases. Diffusive liquid water flow does not refer to molecular diffusion here but to a flow process that is driven by a gradient in water pressure, which corresponds to gradient in water content or liquid water ‘concentration’, while the flow due to gravity is neglected. The liquid water flow diffusivity is equal to the water conductivity divided by the water capacity of the soil, i.e. the change in water content with a change in water pressure. Diffusive water transport in the gas phase, i.e. vapor transport, is driven by vapor concentration gradients and occurs by molecular diffusion, governed by the effective diffusion coefficient in soil. As long as the diffusive processes are not limited by the presence of a boundary deeper in the soil across which no diffusive transport can take place, the evaporation rate during stage-II decreases inversely proportional with the square root of time:

$$E_{stage-II}(t) \propto \frac{1}{\sqrt{t}} \qquad \text{1-1}$$

When the evaporation process becomes limited by a deeper soil boundary, e.g., when the soil below the wetted surface layer is significantly drier, diffusion of vapor and liquid water is no longer well described by a semi-infinite domain. Under these conditions, evaporation departs from diffusion-controlled behavior and transitions to Stage III evaporation, which is characterized by an exponentially decreasing evaporation rate (Brutsaert, 2014).

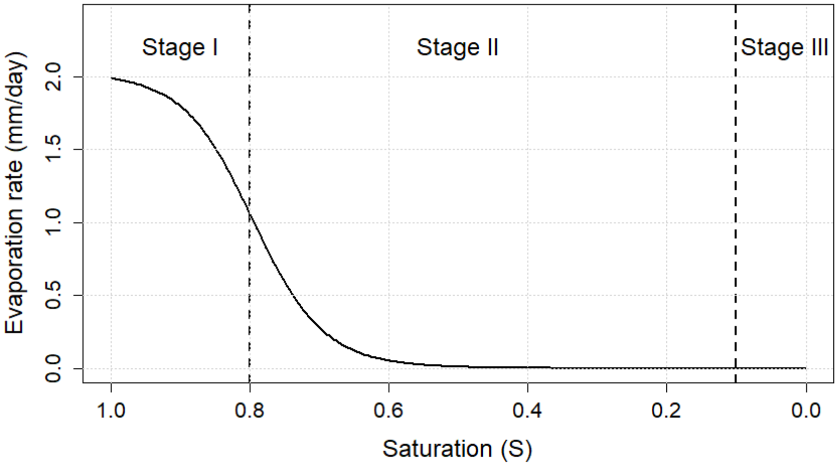

Figure 1-2: Schematic figure of evaporation stages from a porous medium. Soil evaporation proceeds through three stages: an energy-limited constant-rate stage controlled by atmospheric demand (stage-I), fol-

lowed by a diffusion-limited stage in which declining water content restricts vapor and liquid transport within the soil (stage-II). In stage-III, diffusive transport to the evaporating surface is limited by a no-flow boundary condition deeper in the soil.

1.3 Soil as a Porous Medium

Often the upper layer of the vadose zone is formed by a porous medium, such as soil. A porous medium is defined as a material containing interconnected void spaces or pores, through which liquids and gas can move. Pore size, shape and distribution of pores can vary and influence transmission and storage abilities. The solid phase of soil is composed of mineral particles of varying sizes and shapes, along with organic matter. The interactions between the solid, liquid, and gaseous phases create a dynamic system of ongoing chemical and biological processes, resulting in continuously evolving soil properties (Yaron et al., 1996).

1.3.1 State Variables and Soil Hydraulic Properties

To describe water and air flow and retention in soil, state variables, hydraulic properties and their parametric representation are needed.

State variables characterize the instantaneous condition of water and air in the soil. Important state variables are saturation (S), capillary pressure (p_c), which is closely related to the matric potential (ψ) of the soil water, and gravitational potential or height.

Soil hydraulic properties (SHPs) describe how the air and water phases behave as a function of the state variables, for example the water retention curve relating saturation or water content (θ) to the capillary pressure or the matric potential. Another example is the hydraulic conductivity function relating hydraulic conductivity to saturation or matric potential. Quantities such as porosity (ϕ), permeability (k), and saturated hydraulic conductivity (K_S) define limits for those relationships.

Soil hydraulic properties can be represented by models such as the van Genuchten-Mualem or Brooks-Corey hydraulic conductivity model (Brooks & Corey, 1964; van Genuchten, 1980). For those models parameters are needed which can be determined by parameter estimation methods such as pedotransfer functions (PTFs). PTFs are used to derive parameters from already available soil information such as texture or bulk density. Alternatively, parameters may be obtained from laboratory measurements or inverse modeling.

1.3.1.1 State Variables

Saturation

Saturation (S) [-] refers to the proportion of the pore space filled with a specific phase α. The sum of all phase saturations equals one (Eq. *1-3*) (Mosthaf, 2014):

$$S_\alpha = \frac{V_\alpha}{V_{pore}} \tag{1-2}$$

$$\sum_\alpha S_\alpha = 1 \tag{1-3}$$

For describing the water accessibility and availability for transport, the effective wetting phase saturation S_{we} is mostly used. It refers to the degree to which the soil is saturated in relation to its ability to hold water at a given tension or matric potential. In the following S_{we} is described as a function of the residual water (wetting) saturation S_{wr}, the saturation S_w, the residual gas (non-wetting) saturation S_{nr} (van Genuchten, 1980):

$$S_{we} = \frac{S_w - S_{wr}}{1 - S_{wr} - S_{nr}} \tag{1-4}$$

S_{we} can also be described by using volumetric water content which is defined as $\theta = \phi S_w$, using the residual water content $\theta_r = \phi S_{wr}$ and the saturated water content $\theta_{sat} = \phi(1 - S_{nr})$ [m^{-3} m^{-3}], where ϕ is the porosity of the porous medium (Fetzer, 2018):

$$\phi = \frac{V_{pore}}{V_{total}} \quad 1\text{-}5$$

V_{pore} [m^3] is the ratio of the pore volume and V_{total} [m^3] the total volume of the porous medium:

S_{wr} and θ_r represent the residual saturation or water content that remains in the soil and cannot be removed by applying higher capillary pressure or matric potential gradients over a soil volume. It can be interpreted as the water content at which the remaining water content is not connected anymore and does not flow when a pressure or potential gradient is applied.

Capillary Pressure

The geometry of the pore space and the different wetting energies of the solid phase by gas and liquid phases govern the distribution of these phases and the geometry of their interfaces, which is characterized by the interface curvature, in the porous medium. Surface tensions of gas-liquid interfaces result in pressure jumps across curved gas-liquid interfaces, which are proportional to the curvature of the interface. Soil particle surfaces are typically water-wettable which means that energy is released when air at the particle interface is replaced by water so that water pressure is lower than the air pressure. The capillary pressure p_c [Pa] can be defined as the difference between the pressure in the gas (air) phase p_g (non-wetting) [Pa] and the liquid (water) phase p_l (wetting) [Pa] in a porous medium (Class, 2007):

$$p_c = p_g - p_l \tag{1-6}$$

Matric Potential and Matric Potential Head

The matric potential (ψ) [Pa] refers to the change in energy per volume of water of an infinitesimal volume of free water, which is originally at the same pressure as the gas phase in the porous medium, when it is added to porous medium without changing the water saturation. The water pressure in the porous medium is equal to:

$$p_l = p_g - p_c \tag{1-7}$$

Given that the initial pressure of the free water is at p_g [Pa], it follows that the change in energy per volume of added free water is:

$$\psi = p_l - p_g = -p_c \tag{1-8}$$

Instead of defining the energy per volume of water, it can also be defined as the energy per weight of water, i.e. in terms of heads, h [m]. This definition of water potentials per weight is generally used in soil and groundwater hydrology. Given that the weight per volume of water is equal to the mass density of water, ρ_w [kg m^{-3}], multiplied by the gravitational acceleration g [m s^{-2}]. The matric potential head is related to ψ and the capillary pressure as (Hillel, 2004):

$$h = \frac{\psi}{\rho_w g} = -\frac{p_c}{\rho_w g} \qquad \text{1-9}$$

Gravitational Potential

The gravitational potential is the energy to move water (or air) from a reference level to a certain height z in a gravitational field. For water at elevation z, the gravitational potential energy per unit mass is gz. When the energy is divided by the volume, gravitation potential has units of pressure ($\rho g z$), and when expressed per unit weight, it has units of length (elevation head z) (Hillel, 2004).

1.3.1.2 Soil Hydraulic Properties

Capillary Pressure-Saturation Curve or Water Retention Curve

Increasing capillary pressure leads to air invasion in larger pores and decreasing water saturation (S_l) [-], while the water phase becomes confined to smaller pores that support larger air-water interface curvatures. The relation between capillary pressure and water saturation, $p_c(S_l)$, or its analogue, the relation between capillary pressure head and volumetric water content, $h(\theta)$, is a property of the porous medium that is related to the pore size distribution, the wettability of the solid particles, and the surface tension of the air-water interphase (Bear, 2014).

Permeability and Conductivity

Soil permeability, k_α [m^2] refers to the ability of the soil to transmit a fluid phase a, air or water, through pore spaces. It is defined as the volumetric fluid flux divided by the net force on the fluid per fluid volume and multiplied by the dynamic fluid viscosity, μ_α [Pa s]. When only one fluid is present, the permeability is the saturated or absolute permeability, k_s [m^2], which is a property of the porous medium and which does not depend on the fluid properties. When multiple phases are present, they can restrict each other's flow by occupying and blocking different pores and pathways (Fetzer, 2018). The relative permeability ($k_{r,a}$) [-] is a measure of the effective permeability of one phase and is defined as the ratio of the effective permeability (k_α) [m^2] to the saturated or absolute permeability (k_s) [m^2] (Levine & Cuthiell, 1986 in Ghanbarian et al., 2016):

$$k_{r,\alpha} = \frac{k_\alpha}{k_s} \tag{1-10}$$

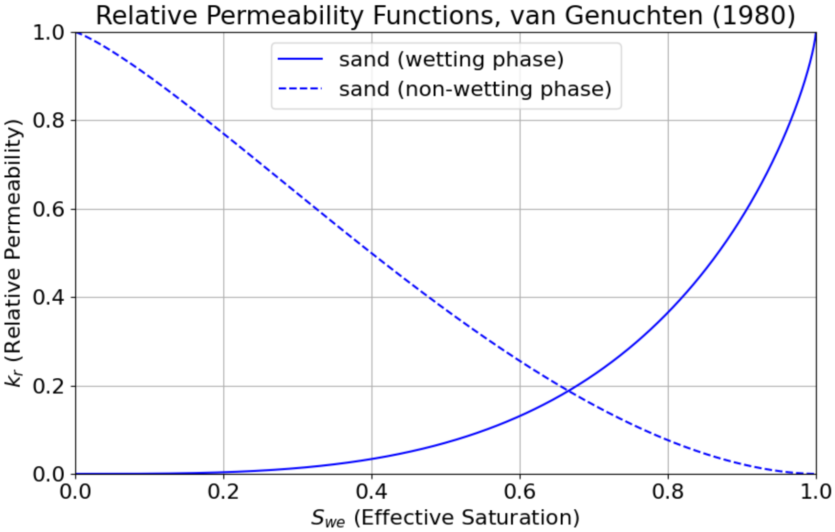

Figure 1-3: Relation between effective saturation and relative permeability of a sandy soil calculated according to van Genuchten (1980).

Hydraulic conductivity is proportional to the permeability and the proportionality factor depends on the fluid properties. One definition of hydraulic conductivity, K_a [m^2 Pa^{-1} s^{-1}] is the ratio of the volumetric fluid flux to the net force on the fluid per unit volume of the fluid:

$$K_\alpha = \frac{k_\alpha}{\mu_\alpha} \tag{1-11}$$

In another definition of K_a [m s^{-1}], which is used in soil hydrology, the volumetric flux is divided by the net force on the fluid per weight of water of the fluid volume (Bear, 2014):

$$K_\alpha = \frac{k_\alpha g \rho_w}{\mu_\alpha} \tag{1-12}$$

Similar to the permeability, the conductivity of a certain phase a when multiple phases are present is related to the conductivity when all pores are filled with that phase, i.e. the saturated conductivity, $K_{s,\alpha}$ multiplied by a relative conductivity, $K_{r,\alpha}$, which is equal to the relative permeability, $k_{r,a}$. $K_{r,\alpha}$ and $k_{r,a}$ are related to the effective wetting phase saturation, S_{we} (Hillel, 2004):

$$K_\alpha\left(S_{we}\right) = K_{s,\alpha}\, k_{r,\alpha}\left(S_{we}\right) \tag{1-13}$$

The relationship between conductivity and wetting phase saturation, $K_\alpha(S_{we})$, is another hydraulic property of the soil or porous medium that needs to be known in order to describe the flow of fluids as a function of the state variables. $K_\alpha(S_{we})$, depends on the pore size distribution, the pore connectivity, the tortuosity of the flow paths, and on the fluid properties. It also depends on the distribution of the fluid in the pores compared to the distribution of the other fluid, which depends on whether the fluid is the wetting or non-wetting fluid. Therefore, two $K_\alpha(S_{we})$, or two $k_{r,a}(S_{we})$, relations, i.e., one for the wetting phase and one for the non-wetting phase, need to be defined.

1.4 Van Genuchten-Mualem Model

One of the most used models for describing soil hydraulic properties is the van Genuchten-Mualem (vGM) model, it combines the van Genuchten (1980) empirical equation for the soil water retention curve and the Mualem theoretical model relating the retention curve to hydraulic conductivity (Mualem, 1976).

1.4.1 Soil-Water Retention Curve

The connection between h and θ, which is also known as the water retention curve, in soil can be described empirically by the following equation (van Genuchten, 1980):

$$\theta(h)=\begin{cases}\theta_r+\dfrac{\theta_{sat}-\theta_r}{\left[1+\left|\alpha_{vG}h\right|^{n_{vG}}\right]^{m_{vG}}}, h<0\\ \theta_{sat}, h\geq 0\end{cases} \quad 1\text{-}14$$

where a_{vG} [m^{-1}] is an empirical shape parameter inversely related to the air-entry pressure, which is the minimum matric suction at which air can enter and the soil starts to dry (Tehrani et al., 2019). m_{vG} [-] is the pore-size distribution index and n_{vG} [-] the curve shape parameter, both are empirical van Genuchten parameters. The soil-water retention can also be expressed as a function of saturation (van Genuchten, 1980 in Dourado Neto et al., 2011):

$$S_{we}=\frac{S_w-S_{wr}}{1-S_{wr}-S_{nr}}=\left[1+\left(\alpha_{vG}p_c\right)^{n_{vG}}\right]^{-m_{vG}}, \quad 1\text{-}15$$

here the van Genuchten parameter a_{vG} [Pa^{-1}] is pressure based.

1.4.2 Unsaturated Hydraulic Conductivity and Permeability

Mualem (1976) proposed a model that assumes that pores of different radii are randomly connected to each other and that the length of a pore is proportional to its radius. It relates hydraulic conductivity to the soil-water retention curve, which describes the water content and the matric potential. Van Genuchten (1980) later used the conceptual model of Mualem to develop analytical expressions for the hydraulic conductivity based on soil-water retention parameters:

$$K_l\left(S_{we}\right)=K_{s,l}S_{we}^{0.5}\left[1-\left(1-S_{we}^{\frac{1}{m_{vG}}}\right)^{m_{vG}}\right]^2 \quad 1\text{-}16$$

$$K_g\left(S_{we}\right)=K_{s,g}\left(1-S_{we}\right)^{0.5}\left(1-S_{we}^{\frac{1}{m_{vG}}}\right)^{2m_{vG}} \quad 1\text{-}17$$

with

$$m_{vG} := 1 - \frac{1}{n_{vG}} \qquad \text{1-18}$$

The Mualem model essentially predicts the liquid and gas phase conductivities as a function of effective wetting phase saturation, accounting for pore connectivity through $l = 0.5$ and the shape of the water retention curve through parameter m_{vG}.(Mualem, 1976).

A disadvantage of the vGM model is that it represents the pore space as connected cylindrical tubes or capillaries, that are either completely filled with water or with air. But at low water contents, film flow along particle surfaces and vapor diffusion through air-filled pores become the primary water transport mechanism. These flow and transport processes are not represented by vGM model making it less reliable for low water contents. Moreover, the θ_r parameter is typically obtained by curve-fitting to experimental data, which rarely extends to very dry conditions. This means θ_r values are often extrapolated, leading to unreliable predictions in dry soils.

In this context, the concept of the residual water content θ_r is seen critically. Nevertheless, it remains useful as it represents a threshold below which liquid water movement becomes severely restricted, and film flow and vapor transport dominate. This transition point effectively marks where water loses its ability to respond to hydraulic gradients in liquid form (Weber et al., 2024).

1.4.3 Handling Dry Conditions

As written in Chapter 1.4.2, the van Genuchten (vG) model uses θ_r as an artificial lower limit at a finite matric potential head to which a soil can dry, it should represent the immobile water, but in reality, soils continue to lose water slowly even at very high matric potential heads. Hence, the vG model underestimates water loss in very dry soils. This limitation is illustrated in Figure 1-4. After capillary drainage, the curve approaches θ_r, implying no further drying regardless of increasing h (black curve in Figure 1-4). Several extensions of retention models have been proposed to represent soil drying beyond the capillary domain. While differing in their physical assumptions, these models exhibit similar behavior at very high h. As soon as water transport is dominated by film flow along particle surfaces and vapor diffusion through air-filled pores, θ decreases approximately linear with h. For a better understanding, a representative linear dry extension is shown in Figure 1-4 to illustrate the characteristic decrease of θ with $ln(|h|)$.

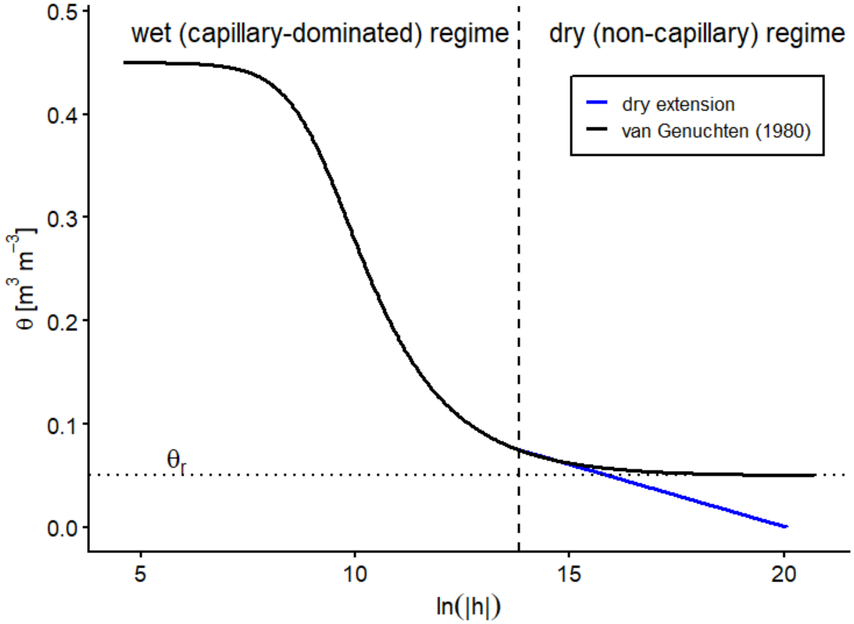

Figure 1-4: A generalized van Genuchten retention curve (black) with a representative linear dry extension (blue) to account for soil water behavior in the dry (non-capillary) regime.

Early examples include the Campbell power law formulation and its extensions, which allow retention to continue toward zero water content at finite matric suction (Campbell, 1974). Later approaches, such as the extended van Genuchten model of Fayer and Simmons (1995), account for adsorptive water by allowing the residual water content to vary with matric suction.

Rudiyanto et al. (2015) refined hydraulic conductivity predictions near the wilting point by introducing film flow and pore connectivity factors into his model. This approach showed an improved accuracy when tested against measured data from sandy loam soils under extreme drying conditions. Weber et al. (2019) proposed a continuous function approach that smoothly transitions between wet and dry regions without any artificial breakpoints. They incorporated vapor diffusion processes and accounted for temperature effects on water retention.

The Peters-Durner-Iden (PDI) model was developed to better represent soil hydraulic properties (water retention and hydraulic conductivity) across the full moisture range, especially for dry soil conditions (Peters et al., 2021). The PDI model addresses the limitation of the vG model by incorporating adsorptive water retention mechanisms that become important in dry soils when capillary forces are no longer the primary retention mechanism. Moreover, it provides a smooth transition between capillary dominated and adsorption dominated water retention regions. It is also using a film component to account for water films that form on soil particles in dry conditions (Peters et al., 2024).

Current soil models still face challenges and limitations regarding modeling dry soil. Most models need parameterization, which limits their practical use in field scale modeling (Arthur et al., 2014; Tuller & Or, 2005). Moreover, the temperature dependency of soil-water retention under dry conditions is often oversimplified, especially in models that need to function across a wide temperature range. Also, many models inadequately represent hysteresis effects in very dry soils, where scanning curves become increasingly important.

1.4.4 Pedotransfer Functions

Direct measurements of SHPs, especially at large scales, are often expensive, time intensive, invasive, and dependent on both the user and the method employed (Vereecken et al., 2010). Pedotransfer functions (PTFs) provide a method for relating SHPs to more easily measurable soil properties, such as soil texture, bulk density, and organic matter content. They are made to convert structural and compositional data of soils into functional information that characterizes soil behavior (Van Looy et al., 2017). Accurate estimation of unsaturated hydraulic properties is essential for reliable prediction and management of water flow and solute transport in soils, as errors in these estimates can significantly affect the quality of simulated soil hydrological fluxes and states (Montzka et al., 2011).

The majority of PTFs predict parameters of the Brooks-Corey or the vGM hydraulic conductivity model (Weber et al., 2024). The vGM model is one of the most used PTFs (Eq. 1-4) and implemented in a wide range of soil modeling tools (Kroes et al., 2017; Šimůnek et al., 2016; Van Looy et al., 2017; Weber et al., 2024).

Fatichi et al. (2020) applied a parameterization to include biotic soil-structural features into soil hydraulic functions as PTFs rely mostly on soil texture but overlook the critical role of soil structure originating by soil biophysical activity. They tested their parameterization against common PTF parameters on a local and a global scale. Including the soil structure can change the partitioning between infiltration, runoff and drainage on a local scale. This effect is especially visible in wet, vegetated regions and in fine-textured soil. On a global scale they concluded that the current modelling frameworks may lack sufficient resolution or representation of processes (e.g., convective rainfall, lateral flow, macropore flow, land surface heterogeneity) to translate soil structure effects into detectable climate impacts. Their results demonstrated that both hydrological and vegetation dynamics can be significantly influenced with the choice of PTFs. It affects simulated fluxes and the stored water content in the water profile consequently.

Weihermüller et al. (2021) investigated how the choice of PTFs affect simulation results of soil water balance fluxes using the HYDRUS-1D software to simulate water fluxes under different conditions. They tested 12 soil textural classes and 13 PTFs across those classes for 7 different scenarios (homogeneous layers, layered soils, groundwater table fluctuations). They found out that using different PTFs causes substantial variability in predicted fluxes causing differences in modelled water balance. Based on their analysis, they suggest that for the vGM model SHPs the PTFs by Rosetta are most robust. They emphasized the importance of harmonizing the choice of PTFS when different models are compared to avoid uncertainties in results due to PTFs.

Sobaga et al. (2023) examined how well the land-surface model ISBA (Interactions between Soil-Biosphere-Atmosphere) simulates soil hydrology, in particular soil water drainage. They tested four different soil hydraulic parameterizations (Brooks-Corey retention + Brooks-Corey conductivity, van Genuchten retention + van Genuchten / Mualem conductivity, van Genuchten retention + Brooks-Corey conductivity and van Genuchten retention + a modified hydraulic conductivity curve based on Iden et al. (2015)) to smooth conductivity near saturation and compared them to lysimeter data. They also tested the impact of accounting for vertical heterogeneity in soil hydrodynamic parameters and the use of in situ parameter estimation versus PTFs. Important findings were that vertically changing soil properties improve simulations of drainage dynamics compared to assuming homogenous profiles, especially retentions curve shapes mattered. The comparison of PTFs with in situ parameter estimates show that those differ from each other significantly, which highlights the risk of using default PTFs for deep soil profiles.

1.5 Experimental Methods Determining Evaporation

1.5.1 Lysimeters

One method to study evaporation processes in the soil is lysimeter experiments. Lysimeters are experimental tools used to study evaporation processes in controlled environments. These instruments allow researchers to study water and chemical fluxes through the soil by mimicking a small section of soil (soil monolith), capturing water that drains from it and measuring the amount that evaporates (Goss & Ehlers, 2009).

Weighing lysimeters provide the most accurate and realistic measurements of ET and precipitation, which are crucial for various inquiries in soil and atmospheric sciences (Peters et al., 2014). Large lysimeters help to understand processes taking place at the soil-plant-atmosphere interface. Lysimeters have been employed in agricultural research to assess groundwater recharge (Yang et al., 2000), track solute transport to groundwater (Schoen et al., 1999), and analyze water fluxes at the soil-plant-atmosphere interface (Meissner et al., 2007). They are also used in urban settings to investigate surface runoff (Nehls et al., 2011).

The early weighable lysimeters were equipped with lever-arm counterbalance systems (Aboukhaled et al., 1982) and continue to be in use today (Nolz et al., 2013). Measurement precision has improved and modern lysimeters utilize weighing cells that achieve resolutions as fine as 0.01 mm water equivalent (Von Unold & Fank, 2008). The precision makes modern weighing lysimeters the most accurate instruments available for measuring rainfall, actual evapotranspiration, and even dewfall (Meissner et al., 2007).

Weighable precision lysimeters allow the determination of drainage water quantity and quality, but also the estimation of the water fluxes at the soil-atmosphere interface (Schrader et al., 2013). Lysimeters have been used for quantifying precipitation in the form of rain, snow, dew, fog and rime and to determine actual evapotranspiration (Meissner et al., 2007; Young et al., 1996).

While calculating precipitation and evapotranspiration through simple water balance equations is theoretically straightforward, processing real-world data presents several challenges. These include data gaps, mechanical vibration noise, animal-caused outliers, mass offset after sampling, and temperature effects on scale readings (Peters et al., 2014). Despite these challenges, weighing lysimeters yield the most precise and realistic measurements for evapotranspiration (ET) and precipitation (P), which are crucial parameters for many soil and atmospheric science investigations (Doležal et al., 2018).

One lysimeter network which monitors changes in the hydrological cycle to observe climate change is the TERENO Project. The TERENO Project (TERrestrial ENvironmental Observatories) maintains 14 lysimeter sites across Germany, with a total of 132 installations (Zacharias et al., 2011). Part of TERENO is the SOILCan project, which represents a long-term, large-scale experiment designed to study the effects of climate and land management changes in terrestrial ecosystems, with particular focus on water, energy, and matter fluxes into groundwater and atmosphere (Pütz et al., 2016).

The TERENO-SOILCan lysimeter network operates at various experimental stations spanning different rainfall and temperature conditions. What makes this network exceptional is that intact soil monoliths, excavated locally at different experimental stations, were transported between sites to expose them to different climate regimes. This approach follows the "space-for-time substitution" method, enabling us to study how specific soil types respond to varying climatic conditions. By transferring the soil monoliths, scientists can simulate potential climate changes and compare their impacts on crop yields and soil water fluxes with observations from original locations (Groh et al., 2020).

1.5.2 Isotope Measurements

Measuring isotope profiles in soil water has evolved significantly over time. Traditional methods like cryogenic extraction and vacuum distillation were limited by their destructive nature and poor spatial resolution (Allison et al., 1987; Barnes & Allison, 1984). A breakthrough came with the development of gas-permeable membrane systems coupled with laser isotope analyzers (Rothfuss et al., 2013).

Rothfuss et al. (2015) published a particularly effective non-destructive method using gas-permeable polypropylene tubing connected to a cavity ring-down spectrometer. This experimental setup involved an acrylic glass column filled with sand, with membrane tubing installed at eight different depths. The membrane tubing is ideal for sampling soil water vapor without disturbing the soil as it prevents liquid water and soil particles from entering. The column was initially saturated with water of known isotopic composition, then allowed to evaporate for 290 days before being rewatered. Daily measurements of δ^2H and $\delta^{18}O$ values in the sampled soil water vapor were taken.

This setup made it possible to continuously monitor the evolution of soil water isotope profiles with unprecedented temporal resolution. The experiment demonstrated how the evaporation front receded into the soil over time, reaching approximately 6 cm depth after 290 days, and showed the increasing influence of atmospheric water vapor on surface soil layers as the soil dried.

Our simulations were set up to reproduce a soil-drying experiment of Rothfuss et al. (2015). The continuous and high frequency isotopologue dataset enables us to evaluate the simulation models can reproduce the isotopic fractionation dynamics during soil drying.

In the laboratory experiment, soil temperature, water content, and gas-phase of δ^2H and $\delta^{18}O$ values were measured at multiple depths (0.01, 0.03, 0.05, 0.07, 0.10, 0.20, 0.40, and 0.60 m) within an initially water-saturated soil column (inside diameter = 0.11 m, height = 0.6 m) filled with sand. Soil temperature was measured at each depth using type K thermocouples (Greisinger Electronic GmbH), while water content was measured using electric conductivity sensors (EC-5, Decagon Devices). Isotopic compositions of both liquid water and water vapor were analyzed with a cavity ring-down spectrometer (L1102-i, Picarro, Inc.) (Rothfuss et al., 2015).

In addition to soil measurements, atmospheric conditions 2 m above the column were monitored, this includes air temperature, relative humidity, and the concentration of the isotopologues in the gaseous phase and the evaporation rate. Air relative humidity and temperature were monitored with a relative humidity and temperature sensor (RFT-2, UMS GmbH), and isotope analysis was conducted by passively sampling laboratory air through stainless-steel tubing positioned 0.6 m above the soil surface.

With this method isotope compositions can be measured at very low soil water contents where traditional extraction methods would fail or require prohibitively large soil samples. Moreover, the isotope composition of tightly bound water at the soil surface, which would be difficult to extract with conventional vacuum distillation techniques can be measured.

1.6 Heavy Water Isotopologues as Tracers for Evaporation

Isotopologues are molecular species that have the same molecular formula but differ in their isotopic composition (Muller, 1994). And isotope of a given element differs from another isotope of the same element by the number of neutrons in its nucleus (Sharp, 2017).

Heavy stable isotopologue of water, namely $H_2^{18}O$ and ${}^1H\,{}^2HO$ (HDO), are well known tracers of water transport because they behave almost identically to H_2O in terms of chemical properties but differ in their physical properties during phase change and diffusion (Rothfuss et al., 2010). These small differences lead to fractionation effects. During evaporation, the heavier isotopologues tend to remain in the liquid phase while lighter ones are more likely to evaporate, which creates a distinct isotopic signature. The isotopic signature allows us to distinguish between water from different sources, track water movement in the soil, identify mixing between different water sources and determine which water sources plants are accessing. Isotopic signatures are also useful for understanding processes at the soil-atmosphere interface (Kiemle et al., 2023; Rothfuss et al., 2010; Zundel et al., 1978).

Generally, isotopologue concentrations are expressed by the isotopologue ratio R_α^i [-] of species i in phase α. The isotopic ratio is expressed as the ratio between the number of moles of the rare species (heavier isotopologue) n_α^i [mol] and the number of moles of $H_2^{16}O$ (more abundant lighter isotopologue) (Braud et al., 2005):

$$R_a^i = \frac{n_\alpha^i}{n_\alpha^{H_2O}} \qquad \text{1-19}$$

Because of the small values of R_α^i, they are typically expressed as relative differences to a standard expressed as a delta value δ_α^i [‰] (Braud et al., 2005):

$$\delta_\alpha^i = \frac{R_\alpha^i - R_{VSMOW}}{R_{VSMOW}} \times 1000‰ \qquad 1\text{-}20$$

R_{VSMOW} is a reference value given by the Vienna Standard Mean Ocean Water (VSMOW). The value for $R_{VSMOW}$is given by (Gonfiatini, 1978):

$$R_{VSMOW} = 311.52 \cdot 10^{-6} \quad for\ HDO \qquad 1\text{-}21$$

$$R_{VSMOW} = 2005.2 \cdot 10^{-6} \quad for\ H_2^{18}O \qquad 1\text{-}22$$

For transport simulations, isotopologue concentrations, which are calculated from isotopologue ratios, are used but with mass spectrometers, isotope ratios are measured. For $H_2^{18}O$, the isotopologue ratio is equal to the isotope ratio. For calculating the delta value of HDO, the reference isotopologue ratio is twice the isotope ratio (approximately while neglecting the H atoms in HDO molecules), but the δ_α^i values derived from isotope are equal to those derived from isotopologue ratios.

1.7 Isotope Fractionation

1.7.1 Equilibrium Fractionation

There are two types of fractionation, equilibrium and kinetic fractionation. Equilibrium isotope fractionation (α_{eq}^i [-]) refers to the process by which isotopes of an element distribute between different substances or phases in a system at equilibrium due to differences in their physical or chemical properties. It is equal to the ratio of the molecular isotopic ratios in the gas and liquid phases (Braud et al., 2005):

$$\alpha_{eq}^i = \frac{x_g^i / x_g^{H_2O}}{x_l^i / x_l^{H_2O}} \qquad 1\text{-}23$$

While isotopes of the same element share identical electron configurations and fundamental chemical behaviors, their mass differences create subtle but significant variations in bond energies and reaction kinetics. Lighter isotopes tend to form weaker bonds and are more likely to occupy higher energy states, while heavier isotopes form stronger bonds and prefer lower energy states (Sharp, 2017).

The degree of fractionation is inversely proportional to temperature for many common isotope exchange reactions, particularly those involving liquid-vapor phase transitions; fractionation effects are more pronounced at lower temperatures and diminish as temperature increases in these systems. The corresponding equation for the equilibrium fractionation factor is given by Majoube (1971):

$$\alpha_{eq}^{i} = \exp\left(-\left[\frac{a}{T^2} + \frac{b}{T} + c\right]\right) \tag{1-24}$$

For HDO and $H_2^{18}O$, the values of the coefficients are:

$$\begin{cases} a = 24844K^2 \\ b = -76.248K \quad for\ HDO \\ c = 0.052612 \end{cases}$$

$$\begin{cases} a = 1137K^2 \\ b = -0.4156K \quad for\ H_2^{18}O \\ c = 0.0020667 \end{cases}$$

It is important to note that this temperature relationship can vary depending on the specific physical process involved (such as ice formation, mineral precipitation, or adsorption), where different mechanisms may yield different temperature dependencies.

The equilibrium fractionation relationship based on mass fraction can be written as (Kiemle, 2019):

$$\frac{x_l^i}{x_l^{H_2O}} \cdot \alpha_{eq}^{i} = \frac{x_g^i}{x_g^{H_2O}} \tag{1-25}$$

1.7.2 Non-Equilibrium Fractionation

The first theoretical model explaining isotopic composition of water vapor during evaporation (non-equilibrium system) processes was proposed by Craig and Gordon (1963). The Craig-Gordon (CG) model estimates the isotopic composition of water vapor by considering two distinct layers: a laminar layer directly above the air-water interface, where transport occurs primarily through molecular diffusion, and a turbulent layer above the laminar layer, where transport is dominated by turbulent diffusion (Dar et al., 2020).

Kinetic isotope fractionation arises because isotopes of the same element have different masses, which affect their behavior during chemical reactions or physical processes. Lighter isotopes have higher diffusion coefficients than heavier isotopes, allowing them to move more rapidly through media. This difference in mobility leads to mass dependent transport rates; lighter isotopes generally react faster than heavier isotopes because they diffuse more quickly and form weaker bonds that break more easily. Unlike equilibrium fractionation, kinetic fractionation occurs in systems that are not at equilibrium, such as during evaporation or diffusion, and is characterized by unidirectional mass transport.

Mathieu and Bariac (1996) introduced a general formulation proposed by Merlivat and Jouzel (1979) of the kinetic fractionation factor. In this formulation the kinetic fractionation factor is dependent on the ratio of the isotopic vapor diffusion coefficient D_v^i [m^2 s^{-1}] and the vapor diffusion coefficient D_v [m^2 s^{-1}] and on turbulent (r_{aT} [s m^{-1}]) and molecular (r_{am} [s m^{-1}]) resistances to water vapor transfer (Braud et al., 2005).

$$\alpha_{iK} = \frac{\left[\left(\frac{D_v}{D_v^i}\right)^{n_K} + \frac{r_{aT}}{r_{am}}\right]}{1+\frac{r_{aT}}{r_{am}}} \tag{1-26}$$

where n_K [-] is the kinetic exponent. The ratio of turbulent to molecular resistance in water vapor transfer depends on the flow regime. Brutsaert (1982) formulated different approaches for smooth and rough surfaces based on wind tunnel experimental data. The classification of surfaces as smooth or rough is determined using the surface Reynolds number, which relates internal to viscous forces near the surface (Braud et al., 2005; Kiemle, 2019). The equations for resistance are:

$$\begin{cases} r_{am} = 13.6\left(\frac{v}{D_v}\right)^{n_K} \; for \left(\frac{u \cdot z_{om}}{v}\right) \leq 1 \; and \; with \; n_K = \frac{2}{3} \\ r_{am} = 7.3\left(\frac{u \cdot z_{om}}{v}\right)^{1/4}\left(\frac{v}{D_v}\right)^{n_K} \; for \left(\frac{u \cdot z_{om}}{v}\right) \geq 1 \; and \; with \; n_K = 1/2 \end{cases} \tag{1-27}$$

For smooth (laminar) and rough (turbulent) surfaces, respectively. With u [m s^{-1}] as the friction velocity, z_{om} [m] as the roughness length for momentum, v [m^2 s^{-1}] as the air kinematic viscosity. An alternative approach is given by Stewart (1975), which is a simplification of the equation of Merlivat and Jouzel (1979) and combines turbulent and molecular resistance into one exponent n'_K (Braud et al., 2005):

$$\alpha_{iK} = \left(\frac{D_v}{D_v^i}\right)^{n'_K} \tag{1-28}$$

The exponent is defined as (Mathieu & Bariac, 1996):

$$n'_K = \frac{(\theta_{sat} - \theta_r)n_a + (\theta_{sat} - \theta_{sur})n_s}{(\theta_{sat} - \theta_r)} \tag{1-29}$$

where θ_{sur} [m^3 m^{-3}] is the soil surface volumetric water content. Due to the dependence of n'_K on θ_r, the residual water content influences isotopologue fractionation processes. At very low water contents, the exponent is large and kinetic effects become more pronounced. Mathieu and Bariac (1996) used n_a=0.5 and n_s=1 leading to n'_K= 0.5 for a saturated soil and n'_K = 1 for a dry soil (Braud, Bariac, Gaudet, & Vauclin, 2005).

1.8 Soil Water Isotope Profile

From soil water isotope profiles, it is possible to receive quantitative information about soil evaporation flux, locate evaporation fronts and root water uptake depths (Rothfuss et al., 2010). The characteristic profile shape for a drying soil can be seen in Figure 1-5. The shape is caused by isotope fractionation.

The isotope ratios in the sublayer are constant at greater depth of the soil profile. It is characterized by liquid water and water vapor flow. Towards the drying front, heavy isotopes are enriching exponentially. Until a maximum of heavy isotope enrichment is reached. The position of the maximum heavy isotope enrichment coincides with the location of the drying front. Liquid water moves upward through capillary forces to the drying front, where the phase change from liquid to vapor predominantly occurs.

Several processes are important to create the characteristic maximum in heavy isotope enrichment. This includes equilibrium and kinetic fractionation. That leaves the remaining liquid water increasingly enriched in heavy isotopes. The position of the maximum heavy isotope enrichment is the result of the interaction between advective and diffusive processes: the upward movement of liquid water, the downward molecular diffusion of liquid water with heavy isotope enrichment, vapor diffusion transporting vapor depleted in heavy isotopes upward and back-diffusion of atmospheric water vapor. The sharp peak forms because below this point, liquid water connectivity allows for relatively rapid transport and mixing, while above this point, the soil is too dry for liquid water movement, restricting transport primarily to vapor phase diffusion. The steepness of the heavy isotope enrichment gradient approaching the maximum is controlled by the evaporation rate, soil hydraulic properties, and the residence time of water at the drying front. Higher evaporation rates typically produce more pronounced heavy isotope enrichment.

Above the drying front is the soil relatively dry and soil water is depleted in heavy isotopes. Here, water transport is dominated by water vapor. The depletion of heavy isotopes is due to diffusive mixing of soil water which is enriched in heavy isotopes and the atmospheric water vapor, which is depleted in heavy isotopes, leading to a gradient in the isotope profile (Kiemle, 2019; Rothfuss et al., 2010).

Above the soil surface within the laminar boundary layer, the water vapor is depleted in heavy isotopes primarily through two processes: equilibrium fractionation during the initial evaporation and kinetic fractionation due to the different diffusion rates of the isotopes while passing through the boundary layer. As vapor diffuses upward, the lighter isotopes move more quickly through the laminar boundary layer, creating additional abundance of light isotopes. In the turbulent layer, the water vapor is mixed with atmospheric vapor. The position and shape of the isotope profile is not static but responds dynamically to changing environmental conditions such as temperature, humidity, and precipitation events, which can shift the location of the drying front and alter the intensity of heavy isotope enrichment and depletion zones.

Soil water isotope profiles are commonly reported in δ notation based on isotope ratios. Because δ values are derived from these ratios, the profiles can also be expressed in terms of isotopologue ratios, as δ values calculated from isotope ratios are equal to those calculated from isotopologue ratios when referenced to the same standard (see Chapter 1.6). Consequently, δ based isotope profiles also reflect isotopologue fractionation along the soil-atmosphere continuum.

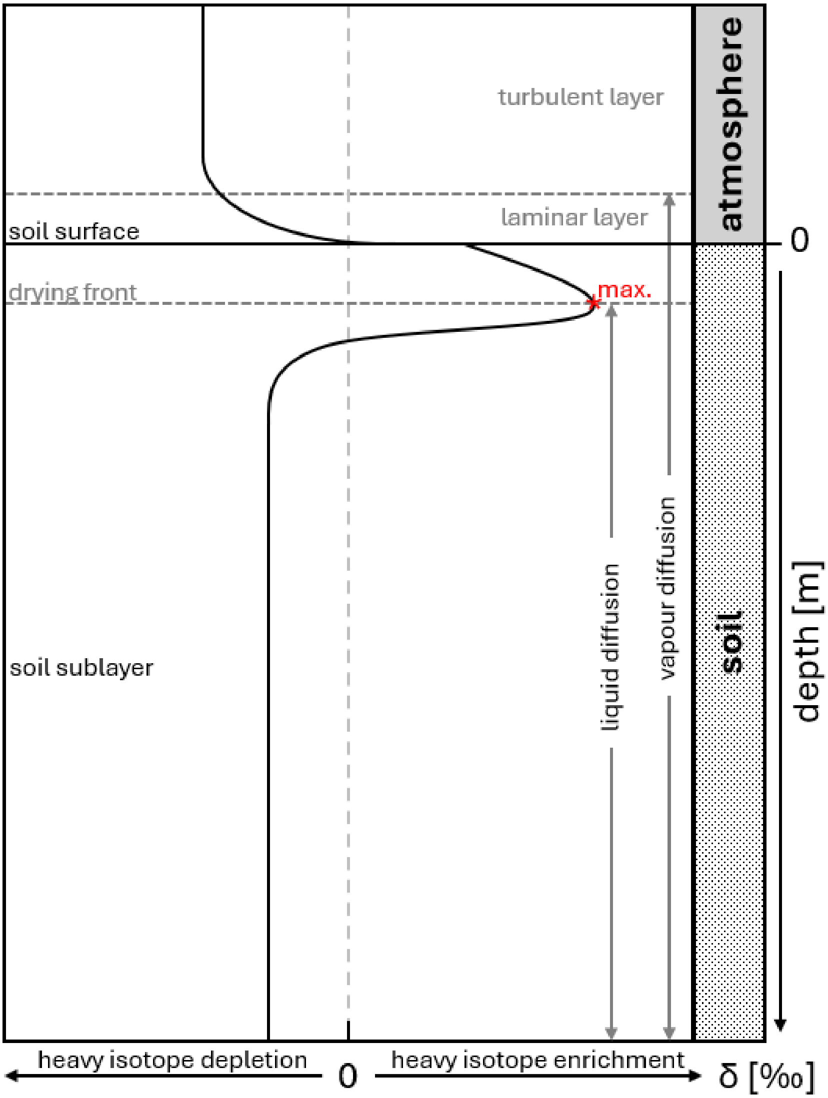

Figure 1-5: Schematic profile of heavy isotope enrichment in a drying soil. While water is depleted in heavy isotopes in depth, enrichment increases toward the drying front due to isotopic fractionation processes. The highest enrichment of heavy isotopes occurs at the drying front, gradually decreasing toward the soil surface because of back diffusion from atmospheric air, which is depleted in heavy isotopes.

1.9 Modeling Evaporation

Generally, various model approaches in varying accuracies are available to estimate evaporation. In the following models to solve the water balance, energy balance, and coupled water and energy balance are briefly described.

1.9.1 Water Balance

The water balance method helps to understand the movement and distribution of water within a defined volume over a specific period of time. It accounts for all water inputs, outputs, and changes in storage within a system. The basic water balance equation of a soil volume of a unit area and given depth for determining bare soil evaporation is written as (Burt et al., 2005; Imukova et al., 2016):

$$E = P + I - \Delta S - SR - T_r \qquad \text{1-30}$$

Where E [mm d^{-1}] is evaporation, P [mm d^{-1}] precipitation, I [mm d^{-1}] irrigation, ΔS [mm d^{-1}] change in soil water storage, SR [mm d^{-1}] denotes surface runoff losses and T_r [mm d^{-1}] transpiration (Burt et al., 2005).

1.9.2 Energy Balance

The energy balance method for estimating evapotranspiration relies on the concept that the energy required for water to evaporate comes from the net radiation available on the Earth's surface. This approach represents energy-limited evaporation (stage-I), where the process is constrained by available energy rather than by water content in the soil. In this method, the total incoming energy (net radiation) is balanced by the energy partitioned into different fluxes, including the outgoing latent heat flux LE [W m^{-2}] (evapotranspiration), the incoming net solar radiation R_N [W m^{-2}], the sensible heat flux H [W m^{-2}], and the soil heat flux Q_g [W m^{-2}] (Figure 1-6). The net solar radiation R_N includes both shortwave radiation from the sun and longwave radiation exchanges between the surface and atmosphere. The general surface energy balance equation is written as (Xu et al., 2005):

$$LE = R_N - Q_g - H \tag{1-31}$$

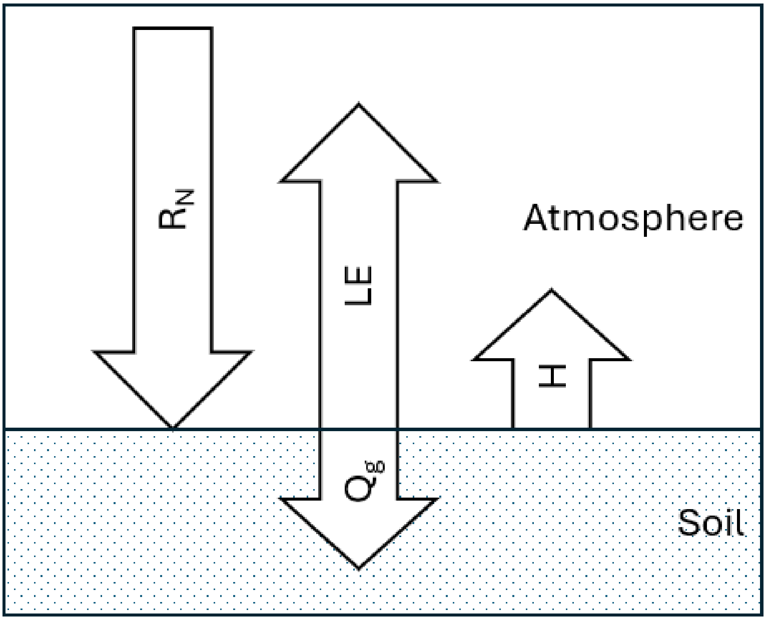

Figure 1-6: Vertical energy balance of a soil surface. Showing the total incoming net solar radiation R_N, the outgoing latent heat flux LE (evapotranspiration), the sensible heat flux H, and the soil heat flux Q_g.

Penman-Monteith Equation

One of the widely used energy balance methods is the Penman-Monteith (PM) equation (Allen et al., 1998):

$$\lambda ET_0 = \frac{\Delta\left(R_N - Q_g\right) + \left[\dfrac{\rho_a c_a\left(e_{sat}^0 - e_a\right)}{r_{av}}\right]}{\Delta + \gamma\left(1 + \dfrac{r_s}{r_{av}}\right)} \tag{1-32}$$

With ρ_a [kg m^{-3}] the air density, c_a [J kg^{-1} K^{-1}] the specific heat of dry air at constant pressure, e_{sat}^0 [kPa] saturation vapor pressure of the ambient air at 2 m height, r_{av} [s m^{-1}] the bulk surface aerodynamic resistance for water vapor, e_a [kPa] the mean daily ambient vapor pressure, R_N [J m^{-2} s^{-1}] the net radiation and r_s [s m^{-1}] the canopy resistance, Δ [kPa K^{-1}] the slope of the saturation vapor pressure curve, γ [kPa °K^{-1}] psychometric constant. λ [J g^{-1}] is the latent heat of vaporization and taken as $2.45 \cdot 10^6$ J kg^{-1}. Evapotranspiration, ET [kg m^{-2} s^{-1}], is therefore obtained as a mass flux of water (Zotarelli et al., 2010). The PM equation was developed to estimate evapotranspiration by closing the surface energy balance using meteorological measurements taken in the free atmosphere above the soil surface, thereby avoiding the need for direct measurements at the surface itself. With the exception of the soil heat flux, which is either assumed to be negligible when energy fluxes are averaged over longer time scales (e.g., daily) or estimated empirically as a fraction of the net radiation, all remaining terms are derived from atmospheric variables. Soil surface variables that influence the energy balance, such as surface temperature and surface vapor pressure, are eliminated through linearization of the relationship between saturation vapor pressure and temperature, allowing them to be expressed in terms of measurable air temperature and humidity.

The equation was updated by the FAO (Allen et al., 1998) using the FAO-56 PM equation (Eq. 1-33). In this approach, the equation is simplified by assuming constant canopy and aerodynamic parameters for a clipped grass reference crop. In reality, canopy resistance varies with stomatal conductance, leaf area index (LAI), and crop height, while aerodynamic resistance also depends on crop height and LAI. Furthermore, net radiation depends on the albedo of the canopy. All of these parameters vary over time and between different crops, and stomatal conductance additionally depends on plant water potential, which is related to soil water content.

To overcome this complexity, a hypothetical reference surface representing a well-watered grass vegetation was introduced with fixed reference parameters: a crop height of 0.12 m, a surface resistance of 70 s m^{-1}, and an albedo value of 0.23. By introducing this reference surface, which corresponds to a well-watered grass canopy, the PM equation is expressed in FAO-56 form using fewer variables and constant factors. It should be noted that these factors are calculated rather than empirical; however, they are derived under the assumption that the other variables in the equation have specific units. The units of the variables are given below:

$$ET_0 = \frac{0.408\left(R_N - Q_g\right) + \gamma \frac{900}{T+273} u_2 \left(e_{sat}^0 - e_a\right)}{\Delta\gamma\left(1+0.34u_2\right)} \tag{1-33}$$

In particular, net radiation (R_N) and soil heat flux (Q_g) are expressed in MJ m^{-2} d^{-1}, air temperature (T) in °C, vapor pressure (e) in kPa, wind speed (u_2) in m s^{-1} measured at 2 m height, and reference evapotranspiration (ET_0) in mm d^{-1}. The units of the variables used in the FAO-56 formulation are summarized below. For bare soils the PM equation is only applicable for the mainly energy driven stage-I evaporation but not for stage-II evaporation where evaporation is constrained by the soil hydraulic properties. For stage-II evaporation, a soil evaporation reduction coefficient K_r [-] must be used. K_r equals one as long as the surface remains wet (stage-I evaporation) as soon as the water content in the upper soil becomes limiting, K_r decreases linearly until it reaches zero. A K_r value of zero corresponds to a dried-out topsoil, where all water available for evaporation has evaporated (Allen et al., 1998).

Energy Balance by Priestly and Taylor

Priestly and Taylor (1972) (PT) developed a simplified energy balance approach for modeling reference evapotranspiration. The model assumes that evapotranspiration processes are only energy limited and that there is an optimal partitioning of the energy between sensible and latent heat:

$$ET_0 = \alpha\left(R_N - Q_g\right)\frac{\Delta}{\Delta+\gamma} \tag{1-34}$$

where α is the Priestley-Taylor coefficient [-], Δ [kPa °C^{-1}] is the slope of the saturation vapor pressure curve. The PT method is widely used in hydrologic and crop models to calculate reference evapotranspiration under conditions of sufficient water availability (Su & Singh, 2023).

1.9.3 Coupled Water and Energy Balance

Coupled water and energy balance methods are employed to model the interactions between water and energy fluxes in natural systems, such as soil, vegetation, and the atmosphere. These methods consider both water movement (via processes like evaporation and infiltration) and energy exchange (through mechanisms like radiation, sensible heat, and latent heat flux). Models based on coupled water and energy balance simulating their dynamics at different scales are for example, APSIM (Agricultural Production Systems Simulator) (Keating et al., 2003) or HYDRUS-1D (Šimůnek et al., 1998). These models simulate soil moisture movement, runoff, infiltration and evapotranspiration, using hydrological parameters. They also simulate energy exchange processes, including radiation, sensible heat, and latent heat fluxes. Hence, these models can predict crop yield, water availability and land use impacts.

1.9.3.1 Isothermal One Component One Phase Equation, Richards Equation

The Richards equation describes water movement within the unsaturated soil in the vadose zone. In the mass balance equation by Richards the net flow rate into the volume equals the increase rate of the water plus the source term in a control volume (Zha et al., 2019). The one-dimensional form of Richards equation can be expressed as:

$$\frac{\partial \theta}{\partial t} = \frac{\partial}{\partial z}\left[K_{l,h}\left(\frac{\partial h}{\partial z}+1\right)\right] \qquad \text{1-35}$$

where t [s] is the time; $K_{l,h}$ [m s^{-1}] is the isothermal hydraulic conductivity for liquid flow and h [m] is the pressure head of the liquid phase. To solve Richards equation, appropriate boundary conditions need to be specified for example exchanges between the soil and the atmosphere are represented through these boundary conditions, such as a prescribed flux boundary for infiltration or evaporation.

The HYDRUS-1D model, used in our lysimeter study (Chapter 2), models the movement of water, heat, and solutes in one-dimensional, variably saturated media using the Richards equation for water flux and convection-dispersion equations for heat and solute transport (Šimůnek et al., 1998).

The Richards equation does not consider the effects of vapor diffusion, vapor flow within the porous medium, and temperature gradients on flow and transport processes (Lehmann et al., 2008; Shahraeeni & Or, 2010; Vanderborght et al., 2017). Neglecting vapor-related processes can lead to inaccuracies under dry conditions, where vapor transport becomes significant. Similarly, the assumption of isothermal conditions may affect water movement, as temperature variations influence viscosity, density, surface tension, and vapor pressure, and can induce thermal gradients that drive additional flow. To address vapor transport while maintaining isothermal conditions Milly (1984) proposed the Isothermal One Component “One-and-a-Half” Phase model.

1.9.3.2 Isothermal One Component “One-and-a-Half” Phase Equation

Milly (1984) developed an Isothermal One Component, “One-and-a-Half” Phase model based on the soil water movement model of Philip and de Vries (1957). Philip and de Vries (1957) described water and heat transport in unsaturated soils considering liquid water and vapor movement, temperature gradients and coupled heat and mass transfer processes. Milly (1984) made several assumptions resulting in the so called “One-and-a-Half” flow equation. The “half” phase refers to the gas phase, in which flow is not considered but diffusive transport of components is. The “one” phase represents the liquid phase where both flow and diffusion are taken into account.

The assumptions Milly (1984) made, include isothermal conditions, focusing on liquid water movement and the neglection of the vapor flow caused by temperature gradients. The assumption of neglecting vapor flow is valid if water fluxes are considered over longer periods of time (1 month) and the temporal average of the temperature gradients cancels out because of diurnal variations in temperature (Vanderborght et al., 2017). This means the isothermal vapor diffusion flux (due to Kelvin effect) is higher than thermal vapor diffusion flux (due to vapor pressure dependence on temperature) of water transport near the soil surface. The model makes several key simplifications:

Firstly, that the gas phase pressure (p_g [Pa]) remains constant and equal to atmospheric pressure, which means it is independent from the liquid phase pressure and any dynamic effects, since no flow is assumed in the gas phase. The assumption can be made due to the gas phase viscosity being smaller in magnitude than the liquid phase viscosity (factor 50) (Vanderborght et al., 2017).

The second assumption relates to the interaction of water and air in both phases. The vapor concentration in this model is not influenced by the dry air concentration. This assumption can be made because the mass fraction of water in the liquid phase is close to one ($X_l^{H_2O} \approx 1$) and vapor concentration in the gas phase can be determined independently using the ideal gas law, without accounting for the presence of dry air (Vanderborght et al., 2017). Since the gas phase pressure is assumed constant (atmospheric pressure), the vapor pressure in the gas phase is determined by equilibrium conditions with the liquid phase. This equilibrium is governed by capillary pressure, which represents the pressure difference between the gas and liquid phases. Because we know the gas phase pressure is constant, the capillary pressure directly depends on the liquid phase pressure (Vanderborght et al., 2017). The final assumption is that liquid water is assumed incompressible over the considered pressure range, consistent with the assumption of constant temperature (Vanderborght et al., 2017). The equation can be written as follows:

$$\frac{\partial \theta_v}{\partial t} + \frac{\partial \theta_l}{\partial t} = \frac{\partial}{\partial z}\left[\left(K_{l,h} + K_{v,h}\right)\frac{\partial h}{\partial z} + K_{l,h}\right] \qquad \text{1-36}$$

Where $K_{v,h}$ [m s^{-1}] is the isothermal hydraulic conductivity for vapor transport. However, Millys (1984) simplification of neglecting temperature gradients are less valid in arid environments, near the soil surface where large temperature gradients exist and in very dry soil where liquid water films are discontinuous.

1.9.3.3 One Component, “One-and-a-Half” Phase Equation

The isothermal equation introduced by Milly (1984), can be extended to include temperature effects on water movement.

This results in an elemental equation describing non-isothermal liquid water flow and water vapor transport in soils (Vanderborght et al., 2017):

$$\frac{\partial \theta_l}{\partial t}+\frac{\partial \theta_v}{\partial t}=\frac{\partial}{\partial z}\left[\left(K_{l,h}+K_{v,h}\right)\frac{\sigma(T)}{\sigma\left(T_{ref}\right)}\left.\frac{\partial h}{\partial z}\right|_{T_{ref}}+K_{l,h}\right]+\frac{\partial}{\partial z}\left(K_{l,T}+K_{v,T}\right)\frac{\partial T}{\partial z}$$

1-37

where θ_v [m^3 m^{-3}] is the water vapor content expressed in equivalent volume of liquid water per volume of bulk soil, $K_{l,x}$ and $K_{v,x}$ are the hydraulic conductivities for liquid and vapor flow, respectively, $K_{x,h}$ [m s^{-1}] and $K_{x,T}$ [m^2 K^{-1} s^{-1}] are the isothermal and thermal hydraulic conductivities, respectively, σ [N m^{-1}] is the surface tension of the gas-fluid phase, T [K] is the temperature and $h|_{T_{ref}}$ [m] is the pressure head of the liquid phase at the reference temperature T_{ref}.

The One Component, “One-and-a-Half” Phase equation is implemented in the SiSPAT-Isotope model, which is used to analyze isotopologues in Chapter 3. Additionally, SiSPAT-Isotope was also used to simulate the temperature profiles necessary for understanding the non-isothermal effects on water movement.

A limitation of the one-component, “one-and-a-half” phase formulation is that vapor transport is treated as a dependent process rather than a fully coupled gas phase flow. Because no explicit gas phase continuity equation is solved, the approach cannot represent advective vapor transport driven by airflow or air pressure gradients, and it assumes local thermodynamic equilibrium between liquid water and vapor. Consequently, vapor pressure gradients that arise from non-equilibrium conditions cannot be captured explicitly.

In addition, heat transport is only indirectly represented and not solved simultaneously with the moisture and vapor equations, which can lead to an underestimation of latent heat effects during evaporation.

1.9.3.4 Fully Coupled Heat and Water Flow

To fully understand how water and vapor move through soil, we need to describe the flow of the liquid and gas phase $\{l, g\}$ through the soil and how the components water and air $\{H_2O, a\}$ are transported in each phase.

This can be modeled using an extended version of Darcy's law that works for multiple fluid phases in combination with a mass and energy balance (Kiemle et al., 2023; Vanderborght et al., 2017). For each component $\{\kappa\}$ the following mass balance equation is given (Kiemle et al., 2023). Eq. 1-38 is only valid for binary diffusion:

$$\sum_{\alpha\in\{l,g\}}\left(\phi\frac{\partial\left(\rho_\alpha X_\alpha^\kappa S_\alpha\right)}{\partial t}+\frac{\partial}{\partial z}\left(\upsilon_\alpha\rho_\alpha X_\alpha^\kappa\right)+\sum_\kappa\frac{\partial}{\partial z}\left(D_{pm,\alpha}^\kappa\rho_\alpha\frac{\partial X_\alpha^\kappa}{\partial z}\right)\right)=0 \tag{1-38}$$

where, ρ_α [kg m^{-3}] is the mass density of phase α, X_α^κ [kg kg^{-1}] is the mass fraction of component κ in phase α, $D_{\alpha,pm}^\kappa$[m^2 s^{-1}] is the effective binary diffusion coefficient of component κ in phase α in the porous medium and the fluid phase velocity is determined by Darcy's law (Kiemle et al., 2023):

$$\upsilon_\alpha=-\frac{k_{r,\alpha}}{\mu_\alpha}k_i\left(\frac{\partial p_\alpha}{\partial z}-\rho_\alpha g\right) \tag{1-39}$$

where $k_{r,\alpha}$ [-] is the relative permeability of phase α, k_i [m^2] is the intrinsic permeability, μ_α [Pa s^{-1}] is the dynamic viscosity of phase α, p_α [Pa] is the phase pressure, g [m s^{-2}] is the gravity term.

For accurate prediction of evaporation fluxes in porous media, we need to consider the temperature conditions within the medium itself. The complexity of heat transfer between different phases (gas, liquid, and solid) can be simplified by assuming they are in local thermal equilibrium. This means we can use a single energy balance equation rather than tracking temperatures separately for each phase (Kiemle et al., 2023; Vanderborght et al., 2017):

$$\sum_{\alpha\in\{l,g\}}\left(\phi\frac{\partial\left(\rho_\alpha u_\alpha S_\alpha\right)}{\partial t}+\frac{\partial}{\partial z}\left(\rho_\alpha h_\alpha \upsilon_\alpha\right)\right)+\left(1-\phi\right)\frac{\partial\left(\rho_s c_s T\right)}{\partial t}-\frac{\partial}{\partial t}\left(\lambda_{pm}\frac{\partial T}{\partial z}\right)=0 \tag{1-40}$$

where u_α [J kg^{-1}] is the internal energy of phase α, ρ_s is the mass density of the solid phase, h_α [J kg^{-1}] is the specific enthalpy, c_s [J kg^{-1} T^{-1}] is the specific heat capacity, λ_{pm}[J m^{-1}s^{-1} K^{-1}] is the effective thermal conductivity. The energy balance equation (Eq. 1-40) accounts for heat storage in both the pore space and solid matrix, heat consumption or production by phase changes, convective heat transport by fluid flow, and heat conduction through the porous medium.

With the fully coupled heat and water flow model, we can solve heat and water transport simultaneously and account for latent heat effects, which influence temperature and water content near the soil surface. The model incorporates conductive and convective heat fluxes leading to better predictions of evaporation rates.

The above mentioned fully coupled heat and water flow is implemented in the open-source simulation environment DuMu^x, which is applied in Chapter 3 for the simulation of isotopologue transport.

1.10 Modeling Stable Isotope Transport

Isotope transport within the soil was first studied and modeled for free water surfaces (Craig & Gordon, 1965). This model was adapted by Zimmermann et al. (1967) for saturated and evaporating soils under steady-state conditions. A significant advancement came from Barnes and Allison (1984), who extended the model to unsaturated soils and later incorporated non-isothermal conditions with soil temperature as a function of depth. Shurbaji and Phillips (1995) developed the first model describing non-steady state conditions and time-evolving atmospheric forcing, based on Philip and de Vries'(1957) heat and water transport model. They introduced a depth dependent transition factor that accounted for both hydrological and isotope parameters, including the equilibrium fractionation factor, the isotope specific diffusion coefficients for the vapor and liquid phase, and a smaller vapor phase diffusivity of heavy isotopes. This allowed their model to more accurately capture the evolution of soil-water isotope profiles. However, their model still relied on measured boundary conditions, including soil surface temperature and humidity.

A simplified approach of solving the surface energy balance was considered by Mathieu and Bariac (1996) under constant potential evaporation and prescribed soil temperature profiles. This approach was further used and extended to variable climatic conditions and to fully coupled heat, water and isotope transport with surface energy budget calculations by Mélayah et al.(1996). This model is very sensitive to the initial isotope profile and changes in liquid water convective transport. Based on the approach by Mélayah et al. (1996). Braud et al. (2005) addressed and corrected inconsistencies in the derivations presented by Melayah et al. (1996). Based on this framework, several isotope transport models have been developed, including SiSPAT-Isotope (Braud et al., 2005) and Soil-Litter-Iso (Haverd & Cuntz, 2010).

The SiSPAT-Isotope model is forced by climatic data (air temperature and humidity, wind speed, incoming solar and long wave radiation and precipitation). Soil temperature and water matric potential are the independent variables. Upper boundary conditions of the soil module are provided by the solution of the energy balance and the continuity of mass transfer at the soil surface, connecting the surface and the atmosphere (Braud et al., 2005).

Based on Braud et al. (2005), Zhou et al.(2021) enhanced the HYDRUS-1D model with an isotope module that simulates isotope processes while accounting for evaporation fractionation. The HYDRUS-

1D isotope module offers improved computational efficiency compared to SiSPAT-Isotope. HYDRUS-1D's approach for higher efficiency is to simulate only water flow in isothermal systems, whereas SiSPAT-Isotope computes both water flow and heat transport regardless of whether the system is isothermal. By eliminating heat transport calculations in isothermal conditions, the HYDRUS-1D isotope module achieves higher numerical efficiency.

With the above mentioned models, only 1D processes within the unsaturated zone and interface region can be simulated. All of them account for atmospheric conditions through evaporation boundary conditions and parameterizations to describe kinetic fractionation. However, the influence of atmospheric variables (e.g., wind conditions, humidity, and temperature) on fractionation processes can only be simulated under certain conditions with suitable parameterizations.

Kiemle et al. (2023) developed a more comprehensive model that includes the influence of atmospheric flow on isotopic fractionation processes in the porous-medium domain with thermodynamic consistency. This was achieved by explicitly accounting for flow and transport in the free-flow domain (atmosphere) and coupling it to the porous-medium domain (soil). Unlike traditional approaches, this model resolves the kinetic fractionation process at the interface region without relying on parameterizations. It successfully captures evaporation dynamics for both $H_2^{16}O, HDO$ and $H_2^{18}O$ under varying atmospheric conditions, including both turbulent and laminar flows.

By resolving and coupling both domains at the representative elementary volume (REV) scale, the model enables detailed analysis of isotopologue transport and evaporation processes across the free-flow, interface, and porous-medium regions (Kiemle et al., 2023). The numerical simulation environment DuMu^x was used for implementing and solving the isotope model.

The SiSPAT-Isotope model using the One Component, "One-and-a-Half" Phase Equation to solve the water balance is later on used and compared to the model of Kiemle et al. (2023) which is solving the fully coupled mass balance and tested against isotopologue measurements (see Chapter 3). With this comparison we can study which model simplifications are appropriate for the evaporation process and which methods predict measurements more reliably.

1.11 Isotopic Evaporation Flux

The interface between the atmosphere and the soil surface describes the upper boundary condition for the isotopic evaporation flux in the soil. At this interface, the evaporation process and the subsequent fractionation of water isotopologues are influenced by the mechanisms within the soil system as well as by atmospheric dynamics including turbulence, humidity gradients, and advection in free-flow conditions.

The surface isotopic flux (E^i[kg m^{-2} s^{-1}]) is controlled by diffusion and can be assumed to be proportional to the isotopic concentration gradient between the soil surface (C_v^{is} [kg m^{-3}]) and the atmosphere (C_v^{ia} [kg m^{-3}]) (Braud et al., 2005):

$$E^i = \frac{C_v^{is} - C_v^{ia}}{r_i} \qquad 1\text{-}41$$

The resistance to isotopic species transport r_i [s m^{-1}] can be written as (Barnes & Allison, 1984):

$$r_i = r_a \alpha_{iK} \qquad 1\text{-}42$$

r_a [s m^{-1}] is the aerodynamic resistance to heat and water transfer.

1.11.1 Isotopic Evaporation Flux Based on Isotopic Ratios

The isotopic evaporation rate as a function of isotopic ratios (R_l^{is}, R_v^{ia}) can be written as (Kiemle, 2019):

$$E^i = \frac{M^i}{M^{H_2O}} \frac{\rho_\alpha}{r_a \alpha_{iK}} \left(q_s R_l^{is} \alpha_{eq}^i - q_a R_v^{ia} \right) \qquad 1\text{-}43$$

Where $q_s$and q_a [kg kg^{-1}] are the specific humidities at the soil surface and atmosphere, respectively. M^i and M^{H_2O} [g mol^{-1}] are the molar mass of the heavy isotopologue and H_2O, respectively. For the final expression it is assumed that the liquid fraction is in equilibrium with the overlying vapor (Braud et al., 2005). In this form, the isotopic evaporation rate is defined in SiSPAT-Isotope.

1.11.2 Isotopic Evaporation Flux Based on Mass Fractions

The concentration of the isotopic species is defined by the mass of the isotopic species (m^i [kg]) and the total volume (V_{total} [m^3]) of the respective phase:

$$C_\alpha^i = \frac{m^i}{V_{total}} \cdot \frac{m_{total}}{m_{total}} = \rho_\alpha X_\alpha^i \qquad \text{1-44}$$

This definition applies to both liquid and vapor phases. Using the total mass (sum of all component masses), isotopic concentration can be expressed in terms of mass fraction (Braud et al., 2005):

$$m_{total} = \sum_i M^i n^i \qquad \text{1-45}$$

By incorporating Equation 1-44 into Equation 1-41, we derive the mass-fraction-based isotopic evaporation flux (Kiemle, 2019):

$$E^i = \rho_\alpha \frac{\left(\alpha_{eq}^i X_l^{is} X_v^{H_2O,s} - X_v^{ia}\right)}{r_a \alpha_{iK} M^{H_2O}} \qquad \text{1-46}$$

The fraction-based isotopic fractionation flux is implemented in DuMu^x.

1.12 Research Objectives and Scientific Questions

The previous introduction (Chapter 1.1) emphasized the critical role of measuring and estimating evaporation for effective water management. Two experimental methods, lysimeters (Chapter 1.5.1) and isotope measurements (Chapter 1.5.2), for quantifying evaporation were introduced. Both methods provide detailed long term data sets to research evaporation processes and can be used to test hydrological models and evaluate models regarding evaporation processes. The different model approaches use varying degrees of simplification for the different system components, meaning that predictions from these models have limited capabilities depending on which model approach is chosen (Chapter 1.9).

According to Smits et al. (2015), numerical models of heat and mass transfer often oversimplify or neglect many complexities of the transport processes. This is partly because existing theories have not been thoroughly tested or refined, largely due to a lack of data with sufficient temporal and spatial resolution.

One limitation in research about evaporation stems from the availability of both field and laboratory data, which are crucial for testing and refining energy and mass transfer theories (Smits et al., 2011). Li et al.(2019) compared three numerical models which are used to describe the water flow and heat transfer in soil. They compare the models with data from wind tunnel experiments and concluded that all model approaches and corresponding top boundary conditions have different limitations and no model is appropriate for every tested scenario. The choice of the model should depend on the research focus and efficiency and availability of the data set. They mention the need for detailed experimental measurements which include all kinds of soil textures and atmospheric conditions to improve the predictions of models across scales.

Feng et al. (2023) took existing satellite driven ET/heat flux algorithms and performed an analysis of six existing soil evaporation algorithms to identify how to use soil moisture or precipitation data to represent soil water stress and decide which algorithm works best under alpine barren conditions. Based on that, they built two improved versions of process-based land surface ET/heat fluxes algorithms, one was using normalized surface soil moisture, the other using the ratio of cumulative antecedent precipitation to cumulative equilibrium evaporation as moisture constraints. The study improves estimation of soil evaporation in an extreme environment (Tibetan Plateau) by integrating more realistic limitations (soil moisture and precipitation) and remote sensing data showing that data based constraints make a difference.

This supports the idea that empirical data (soil moisture, precipitation, evaporation observations) are crucial to test, refine and improve heat mass transfer models. Feng et al. (2023) points out that even with modern remote sensing and modelling, there is still a need for more high-quality ground data (field measurements) especially for remote, barren or extreme environments.

Direct flux measurements are difficult to obtain, particularly when capturing diurnal variations. This has led researchers like Steenpass et al. (2010) or Dimitrov et al. (2015) to employ indirect methods, measuring surface water contents and temperatures to derive fluxes through inverse modeling. While eddy covariance techniques can measure fluxes, the large region from which they receive data makes measurements easily influenced by variations in surface properties surrounding the station, as demonstrated in work by Graf et al. (2012). Laboratory studies face other complications, for example in wind tunnel experiments where the properties of the wind field cannot be precisely controlled. Additionally, the small scale of surfaces investigated in these experiments means results are heavily influenced by changing lateral conditions (Coltmann, 2024).

Despite the progress of the last years, significant gaps remain in modeling and monitoring the dynamic interactions of heat, water, and vapor transport between soil and atmosphere. Existing numerical models often oversimplify these processes due to limited high-resolution datasets and reliance on parameterizations. Controlled experiments and improved datasets are needed to refine models and strengthen theoretical understanding of heat and water transfer in soils.

We have the possibility to work with two unique data sets to test and compare evaporation models. The first data set is from the TERENO SoilCan project. The TERENO SoilCan network of 132 lysimeters installed at 14 experimental field sites across four observatories in Germany. These lysimeters sample soil in grassland and arable ecosystems with standardized crop rotations under different management regimes. The project monitors a wide range of variables and data sets have been collected, for weather parameters, matter flux and water balance data at the lysimeter sites. The data sets are unique as they have a high temporal and spatial resolution with measurement intervals in minute to 10-minute intervals at several depths (dependent on sensor). The lysimeters contain undisturbed soil cores capturing realistic soil hydrologic behavior. SoilCan was intentionally built to be long term and because it includes many sites and years, it captures variability across climates, soil types, land uses, and management practices (Pütz et al., 2016).

The other data set is from the experiments of Rothfuss et al. (2015) introduced in Chapter 1.5.2. The study measured daily profiles of $\delta^2 H$ and $\delta^{18} O$ in soil water for 290 days and accordingly, gives continuous, non-destructive time series. It was the first experiment to validate the gas permeable tubing method over a year under drying and wetting cycles. As the methods even work for low water contents and receive isotope information without disturbing the soil, they were able to track the evaporation front moving through the soil. They map the depth of the evaporation front each day, showing how it gradually moved down. Because the data are continuous and vertically resolved, it allows detailed testing of models using isotope transport. With those two very unique data sets we wanted to test evaporation models, which exist with different degrees of complexity, from the Richards equation to fully coupled heat and water flow models (Chapter 1.9) to evaluate how reliable various simplifications are.

Simpler models like the Richards equation neglect processes such as vapor diffusion, air flow, and non-isothermal conditions that are important under dry soil conditions. In this context, we asked ourselves:

1. To what extent can a Richards equation-based model accurately reproduce observed evaporation processes? Can we simplify the complex evaporation process while maintaining accuracy? How does the Richards equation perform across: (a) multiple temporal scales (hourly to monthly), and (b) varying saturation levels (from saturated to very dry conditions)?

We hypothesize that simpler models (e.g., Richards equation) will perform adequately under conditions of high soil moisture and minimal temporal temperature gradients. It will show a decreasing accuracy at finer temporal scales (hourly) compared to coarse scales (daily or monthly) due to its limited ability to account for temperature fluctuations. We expect that the impact of temperature fluctuations on model accuracy will be larger under very dry conditions when evaporation processes are mainly driven by vapor diffusion compared to saturated conditions. Neglecting vapor transport will introduce substantial errors when soil moisture drops below field capacity during periods of soil warming. Furthermore, ignoring the effect of temperature on vapor concentrations in the soil will lead to an underestimation of vapor concentrations and consequently of evaporation. The magnitude of these errors is expected to increase progressively as the soil becomes drier and soil temperature increases. Beyond a certain temporal threshold, the impact of diurnal temperature fluctuations on evaporation estimates will be negligible, making the Richards equation models more suitable for long term predictions. More complex models (e.g., fully coupled heat and water flow models) will be necessary for accurately capturing evaporation processes during stage-II and III evaporation and under conditions with significant diurnal temperature fluctuations.

PTFs are an effective tool for predicting SHPs. But as described in Chapter 1.4.4 hydrological dynamics in models can be significantly influenced by the applied PTFs. The variability can result in deviations in ET. Hence, we wanted to know:

2. How adequate are current methods for estimating SHPs in the context of evaporation modeling? What impact does the usage of PTFs have on simulated evaporation rates compared to directly measured soil properties? To what extent do uncertainties in SHPs cause uncertainties in modeled evaporation under different moisture conditions?

We hypothesize that evaporation models using PTFs will show greater deviations from observed evaporation rates compared to models using directly measured SHPs, with increasing deviations as the soil proceeds to dry out.

To address these questions, we will use the data set of the TERENO SoilCan network, providing measurements under natural outdoor conditions in natural undisturbed soils for three years with different climatic conditions. The use of our unique high resolution lysimeter data set allows us to directly observe actual soil evaporation rates at a fine temporal scale, providing a strong basis to test and compare different modeling approaches. With this data set we try to assess under which conditions evaporation rates could be predicted using the FAO Penman-Monteith method (Chapter 1.9.1) combined with soil water flow simulations based on the Richards equation. Soil hydraulic properties will be estimated using either ROSETTA PTFs (Schaap et al., 2001), in situ measured soil hydraulic properties, or soil surface water content measurements through inverse modeling (Dimitrov et al., 2015).

A second set of research questions focuses on the potential of isotope measurements and modeling approaches. Isotope measurements have been used to study evaporation, as described in Chapter 1.6, and have high potential for investigating evaporation mechanisms such as the evaporation front and different stages of evaporation with high temporal resolution (here: daily), which leads to the question:

3. What is the potential of daily heavy stable water isotope measurements for identifying specific evaporation related processes such as the development of an evaporation front?

We hypothesize that daily measurements of heavy stable water isotope profiles will provide sufficient temporal resolution to detect the formation and movement of the evaporation front, characterized by a distinct peak in isotopic enrichment. We assume that the observation of Rothfuss et al.(2015), that the evaporation front is located at the depth of the maximal gradient between δ^i values, can be confirmed. Isotopic signatures should be detectable even when changes in bulk soil moisture content are below the detection limit of conventional soil moisture sensors, demonstrating the value of isotope measurements for evaporation processes in dry soil.

Different models with different approaches for simulating isotopologue transport exist (Chapter 1.10). The models which were introduced are SiSPAT-Isotope, a one component, “One-and-a-Half” phase model, and DuMu^x a fully coupled heat and water flow model.

The effect of the level of detail in process descriptions and how it impacts the accuracy of the isotopologue simulations has not been investigated yet. In this context we wanted to study:

4. How do the one component, “One-and-a-Half” phase (SiSPAT-Isotope) and the fully coupled water and energy model (DuMu^x) differ in simulating isotopologue transport in a drying, unsaturated porous medium? How does the implementation of boundary conditions affect isotopologue transport simulation results? In particular, what is the impact of residual water content on simulated isotopologue transport, considering the differences between the vGM model used in SiSPAT-Isotope versus the approach used in DuMu^x in the dry regime? What insights about evaporation processes can be gained by comparing these different modeling approaches?

We hypothesize, that the fully coupled DuMu^x model will differ from the one component, “One-and-a-Half” phase approach (SiSPAT-Isotope) primarily in its treatment of the gas phase and porous medium-free flow interface processes. While both models account for temperature effects, DuMu^x’s explicit modeling of gas phase dynamics will lead to differences in predicted vapor transport, especially during stage-II and III evaporation. The differences in how residual water content is handled between the models (vGM approach in SiSPAT-Isotope versus a fully dry out of the soil in DuMu^x) will lead to different predictions of isotope transport in very dry conditions.

By comparing these two modeling approaches against experimental data, we expect to identify which simplifications in the one component, “One-and-a-Half” phase are justified, and which lead to significant deviations from observed isotope patterns during soil drying. We will use high frequency experimental isotope data from Rothfuss et al. (2015) and combining these data with the DuMu^x and SiSPAT-Isotope model to analyze isotopologue transport and compared both models' performance against the isotopologue measurements.

1.13 Thesis Outline

This thesis consists of two main parts, each based on published manuscripts.

Chapter 2 uses lysimeter data from the TERENO SOILCan network to evaluate whether evaporation rates can be predicted from weather data using the FAO Penman-Monteith method, combined with soil water flow simulations based on the Richards equation. Four soil types with different textures (ranging from sandy loam to silt loam) were tested. The study focuses on the importance of accurate soil hydraulic property (SHP) estimation methods for improving evaporation predictions, particularly under water-limited conditions, and emphasizes the need for modeling temperature-dependent vapor transport to replicate diurnal evaporation rates.

Chapter 3 explores the use of heavy stable water isotopologues to better understand evaporation processes, including the identification of the evaporation front under very dry soil conditions. Two models SiSPAT-Isotope and DuMu^x are compared for simulating isotopologue transport in a drying unsaturated porous medium. Measured isotope data are compared with simulations from both models. The effect of boundary layer thickness on evaporation and heavy isotopologue enrichment, as well as the influence of residual water content, is studied. The DuMu^x model is used to investigate the evaporation front in drying soil and compare it to the measurements from Rothfuss (2015).

The study highlights the importance of properly simulating diffusive transport and the effects of residual water to accurately model evaporation fronts and isotopic ratio profiles in drying soils.

Finally, Chapter 4 presents the main conclusions of this thesis and offers recommendations for further research.

2 Prediction of Soil Evaporation Measured With Weighable Lysimeters Using the FAO Penman–Monteith Method in Combination With Richards Equation

This chapter is adapted from: Schneider, J., Groh, J., Pütz, T., Helmig, R., Rothfuss, Y., Vereecken, H., & Vanderborght, J. (2021). Prediction of soil evaporation measured with weighable lysimeters using the FAO Penman–Monteith method in combination with Richards equation. Vadose Zone Journal, 20(1), e20102.

Changes were made in the abstract (Chapter 2.1) to describe the main results. Additional information about the ANOVA was added in Chapter 2.3.2.3 and Annex A.3. In Chapter 2.3.3 information about the effect of soil color on the calculated potential evaporation was added. Information about the vertical soil profile on evaporation rates was added in the Annex A.1. Annex A.2 gives additional information about measured and calculated net radiation. Additionally, a conclusion (Chapter 2.6) was added. Throughout the whole Chapter 2 minor additions for a better understanding are given.

2.1 Abstract

Multiannual data (2016-2018) from 12 weighed lysimeters (four soil types with textures ranging from sandy loam to silt loam, three replicates) of the TERENO SOILCan network were used to evaluate if evaporation (E) rates could be predicted from weather data using the FAO Penman-Monteith (PM) method combined with soil water flow simulations using the Richards equation. Soil hydraulic properties (SHPs) were estimated either from soil texture using the ROSETTA pedotransfer functions, from in situ measured water retention curves, or from soil surface water contents using inverse modeling.

In all years, E was water limited and the measured evaporation rates (E_m) surprisingly did not vary significantly among the four different soil types. When SHPs derived from pedotransfer functions were used, simulated evaporation rates of the finer textured soils overestimated the measured ones considerably. Better agreement was obtained when simulations were based on in situ measured or inversely estimated SHPs. The SHPs estimated from pedotransfer functions represented unrealistically large characteristic lengths of evaporation (L_c), and L_c was found to be a useful characteristic to constrain estimates of SHPs. Also, when soil evaporation was water limited and E_m rates were below potential evaporation (E_{pot}) (PM evaporation scaled by an empirical coefficient), the diurnal dynamics of E_m followed those of E_{pot}. The Richards equation that considers only isothermal liquid water flow did not reproduce these dynamics caused by temperature dependent vapor transport in the soil. Measured E_m showed diurnal signatures that the isothermal Richards model could not reproduce even with optimised SHPs. Overall, the results show that (i) the PM + Richards approach can reproduce long term (seasonal/ monthly) cumulative evaporation (E_{cum}) if SHPs are chosen correctly, (ii) PTFs may be inadequate for prediction in finer soils without further constraint, and (iii) inclusion of vapor transport mechanisms should be considered when short-term (hourly/diurnal) dynamics are important.

2.2 Introduction

Bare soil evaporation (E) is a critical component of the water cycle at local and global scales. The process of mass transfer across the soil–atmospheric interface is fundamental (Davarzani et al., 2014). Evaporation in arid or semiarid areas can amount to more than half of evapotranspiration (Huxman et al., 2005). Or and Lehmann (2019) estimated that E contributes up to 15% of the total evapotranspiration losses globally and found that this fraction is relatively constant for different climates and biomes. Processes of E are generally well studied, but it has been a challenge to represent E in simulation models (Seager et al., 2007). E is mediated by a set of processes such as flow of liquid water, and transport of water vapor and heat in the porous medium that are coupled with heat and vapor transport in the atmosphere, also referred to as free flow, and driven by absorbed radiation (Fetzer et al., 2017). The E process can be split up into two stages: an energy limited E (stage-I) and a water limited E (stage-II). During stage-I, E is determined by the energy available (radiant energy absorbed at the surface, soil heat flux, sensible and latent heat flux between the soil surface, and the free flow). During stage-II, E is limited by water transfer from the soil to the evaporation surface.

There are several approaches of different complexity to model E, and a systematic review of the processes and their simplifications is given by Fetzer et al. (2017). Fetzer et al. (2017) compared these approaches using simulation studies and highlighted differences and similarities between them. To model accumulated evaporation rates (i.e., cumulative evaporation [E_{cum}]) over a longer period, simpler approaches can be used. E rates during stage-I can be estimated using the standardized FAO Penman-Monteith (FAO-PM) approach (Allen et al., 1998). The FAO-PM estimates E rates using the PM equation that solves the surface energy balance for standardized properties of a reference surface representing a well-watered uniform grass surface, linearizes the relation between saturated vapor pressure and temperature, and approximates the soil heat flux as a function of the absorbed radiation. To simulate the transition between stage-I and II, simpler models use a threshold surface water potential that is fixed and used as a constant potential boundary condition during stage-II. The evaporation rate during stage-II is obtained by solving the Richards equation, which describes isothermal liquid water fluxes in the unsaturated soil, for this constant boundary condition. Despite the fact that this approach decouples the evaporation rate during stage-II from the surface energy balance, heat, and vapor fluxes in the soil, it provided similar estimates of E_{cum} as more comprehensive process models (Fetzer et al., 2017). However, diurnal dynamics of E simulated by the more comprehensive approaches could not be reproduced by the simpler FAO-PM–Richards equation approach due to neglected vapor fluxes and heat flow in the porous medium (Fetzer et al., 2017). Li et al. (2019) compared three different model concepts to determine E: the Richards equation only considering isothermal liquid water flow (Richards model), a model based on the Richards equation that considered vapor transport (Richards vapor model), and a nonequilibrium two-component two-phase model (Non 2-2 model). They mentioned that predictions of E during stage-II by models based on Richards equation depend on the accuracy of chosen top boundary conditions like the critical water pressure. Rianna, Reder, and Pagano (2018) tested four models and their ability to predict measured evaporation (E_m) by comparing them with E rates from lysimeters. The models tested did not solve the Richards equation directly to represent soil water movement but used different metamodels of the soil water balance: the Aydin (1998) and Allen et al. (1998), Boesten and Stroosnijder (1986), and Ritchie (1972) (also known as the FAO-56 dual K_c approach) models. They stated that these E models with soil hydraulic parameters based on lysimeter data reproduce E losses accurately.

In addition to selecting a process model, which fits best to given environmental conditions, soil hydraulic properties (SHPs) must be known in order to predict E. When only liquid flow in the soil is considered, the unsaturated hydraulic conductivity and water retention function must be available. In most studies that estimate soil water fluxes at regional and global scales, water retention and hydraulic conductivity functions are derived from soil texture information using pedotransfer functions (PTFs; (Fatichi et al., 2020; Or & Lehmann, 2019). These PTFs have been derived from empirical relations between soil properties (e.g., soil texture) and parameters of functions that describe the water retention and hydraulic conductivity curve (Schaap et al., 2001).

Parameters of functions that are fitted to retention curves and that are estimated from other soil properties using PTFs are not constrained directly by processes, such as E. This may lead to a large overestimation of evaporation when SHPs with these parameters are used in the Richards equation to estimate evaporation (Lehmann et al., 2020). Lehmann et al.(2020) used a characteristic length for evaporation (L_c) to identify hydraulic parameter sets that would lead to unrealistic high evaporation losses. Especially soils with an intermediate texture were found to be susceptible to overestimation of E. Soil hydraulic properties are also affected by soil structure, which is related to the presence of larger pores and the connectivity of smaller pores between soil aggregates (An et al., 2018; Assouline & Narkis, 2019; Carminati, Kaestner, Ippisch, et al., 2007; Shokri et al., 2010).Especially in agricultural soils, the structure of the surface layer during bare soil periods may deviate significantly from that of the deeper soil layers due to tillage practices, which change bulk density and soil structure. The impact of soil structure on soil water fluxes has been associated mainly with (preferential) infiltration. However, also for E, soil structure may play an important role (Dimitrov et al., 2015; Haghighi & Or, 2015; Schwartz et al., 2010; Tran et al., 2019).

In vadose zone research, weighable lysimeters are an established method to investigate E and to calibrate and test models (Dijkema et al., 2018; Mutziger et al., 2005; Pütz et al., 2018).By measuring soil water storage changes and seepage water losses with high temporal resolution and precision with weighable lysimeters, diurnal dynamics of E fluxes can be directly calculated giving a closer look into the processes controlling E (Hoffmann et al., 2016; Peters et al., 2017; Pütz et al., 2018). Lysimeters are used to observe and compare soil E fluxes under natural conditions for soils with different hydraulic properties, different tillage, or under different climate conditions (Dijkema et al., 2018; Marek et al., 2016; Quinn et al., 2018).

Dijkema et al. (2018) compared lysimeter data from a desert site with simulations using a model including non-isothermal liquid and vapor transport. They showed that under dry conditions, the model underestimated measured E rate, which they attributed to underestimations of the vapor transport process through the upper dry soil layer and underestimation of the hydraulic conductivity of the dry soil that was estimated using a capillary bundle model. Recent studies emphasize the importance of appropriately choosing the lysimeter's boundary conditions that reflect surrounding (natural) environmental conditions in order to achieve a reliable reproduction of the natural system (Benettin et al., 2019; Groh et al., 2018, 2020; Heinlein et al., 2017; Kohfahl et al., 2019; Teuling, 2018; Trigo et al., 2018).

The mimicking of a natural system also implies the use of undisturbed or monolithic soil cores or blocks in lysimeters. Our overarching objective was to compare lysimetric-based measurements and estimates of E to simulations using an FAO-PM–Richards equation based approach. Subobjectives were to examine (a) how SHPs that are derived from PTFs or from direct in situ measurements perform in the prediction of E; (b) whether the characteristic length for evaporation (L_c) can be used an indicator of parameter sets that generate unrealistic estimates of E, and (c) the (diurnal) dynamics of evaporation during stage-II, which are influenced by temperature dependent vapor fluxes.

Although bare soil evaporation is a key component of the water cycle, it remains difficult to represent accurately in simulation models, especially during water-limited (stage-II) evaporation, when heat and vapor transport processes become important. Many large-scale studies rely on soil hydraulic properties (SHPs) estimated from pedotransfer functions (PTFs) based on soil texture, but these SHPs are not constrained by evaporation processes and may therefore produce unrealistic or greatly overestimated evaporation rates when used with models such as the FAO Penman-Monteith method combined with the Richards equation. Additionally, the influence of soil structure, especially in the tilled surface layer, is often not captured in such models. Aim is to evaluate whether evaporation measured with high-precision lysimeters can be accurately predicted using the FAO Penman-Monteith approach combined with Richards equation simulations, and to determine how the choice of soil hydraulic properties and soil structure influences the accuracy of these predictions.

2.3 Material and Methods

2.3.1 Study Site

Experiments were performed at the Selhausen TERENO field (50°52'7'' N, 6°26'58'' E; 104 m asl), which is located in the Eifel/Lower Rhine Valley Observatory of TERENO in Germany (Bogena et al., 2018; Pütz et al., 2016; Zacharias et al., 2011). It is characterized by a temperate humid climate with a mean annual temperature of 11.8 (± 0.58) °C

(2000–2018). From 2000 to 2008, annual precipitation ranged between 480 mm in 2018 and 829 mm in 2001 with an average of 702 (± 90.3) mm (Knaps, 2019).

The Selhausen site is part of the TERENO-SOILCan network of lysimeters (Pütz et al., 2016). The objective of this long-term lysimeter monitoring program is to capture the effects of climate change and various management methods on water, energy, and matter fluxes between soil and atmosphere using the space-for-time concept (Ineson et al., 1998; Lipman & Waynick, 1916).

2.3.2 Lysimeter Installation

Two lysimeter clusters (SE3 and SE4), managed as arable land, were used in the present study. At each cluster, six lysimeters were arranged in a hexagonal pattern (Figure 2-1).

Figure 2-1: The lysimeters arranged in a hexagonal pattern at site SE3 at the start and end of the bare soil observation period for the years 2016–2018.

Each lysimeter cylinder, made of stainless steel with a surface area of 1.0 m^2 and a depth of 1.5 m (Pütz et al., 2016), is placed in a porous concrete ring. The gap between lysimeter and the concrete housing was closed with a synthetic resin collar, which was filled with surrounding soil. The small (0.01 m) remaining gap between the collar and the lysimeter was closed with silicone rubber sheet to ensure that soil temperature dynamics reflect those of the surrounding. Water content is measured by time domain reflectometry probes (TDR100, Campbell Scientific) at 10-, 30-, and 50-cm depth. The weight of the lysimeters is recorded in 1-min intervals. The matric potential is measured with matric potential sensors in 0.1 m depth (MPS-1, Decagon Devices); at other depths, tensiometers are installed (TS1, METER Group). The lysimeters' weighing systems have an accuracy of 0.01 mm (Hannes et al., 2015).

The seepage water of a lysimeter is collected in a weighable tank with a resolution of 1 g, which corresponds to 0.001 mm (Pütz et al., 2016). The matric potential near the bottom of the lysimeter (1.4 m depth) is adapted to the measured matric potential in the surrounding field at the same depth by water pumping out or in through the suction rake, which consists of five parallel suction cups, at the bottom of the lysimeter. If the matric potential in the lysimeter increases compared to the field, water is pumped out of the lysimeter into the seepage water tank and vice versa when the matric potential decreases in the lysimeter. This allows downward and upward vertical water fluxes across the lysimeter bottom and ensures that the water potential dynamics at the bottom of the lysimeter are as observed in the surrounding field (Karimov et al., 2014; Luo & Sophocleous, 2010). The adaptation of the matric potential to the surrounding conditions is based on the space-for-time concept of the TERENO SOILCan project.

A weather station (WXT510, Vaisala Oyj) next to each lysimeter station monitors meteorological parameters: wind speed, air temperature, relative humidity, barometric pressure at 2 m height, and precipitation at 1 m height (OTT Pluvio2, OTT HydroMet). Net radiation sensors (LP Net07, Delta OHM) above one lysimeter of each cluster and cameras document the state of the lysimeters (Pütz et al., 2016). Meterological parameters were measured in 10-minute intervals.

The 12 lysimeters were filled with undisturbed soil originating from the four sites within the SOILCan network in Germany: Bad Lauchstädt (BL), Dedelow (DD), Sauerbach (SB), and Selhausen (SE) (for information related to these stations, see Groh et al. (2016)). Hence, for each of the four soil types, there are three replicate lysimeters. The soil types and textures are listed in Table 2-1, and more detailed profiles are described in Annex A.1 (supplemental material).

Table 2-1: Soil types and soil texture of the top soil layers of the different lysimeters in the different hexagons and from different origins (Pütz, et al., 2016).

FAO soil type	Texture sand/silt/clay	Origin[a]
	%	
Cutanic Luvisol	16/66/18	SE
Haplic Chernozem	5/73/22	BL
Haplic Cambisol	13/62/25	SB
Haplic Luvisol	58/31/11	DD

[a] SE, Selhausen; BL, Bad Lauchstädt; SB, Sauerbach; DD, Dedelow

Soil surrounding the lysimeters was treated in the same manner as the lysimeters. Soil evaporation was monitored in the arable land lysimeters for three consecutive years (2016 - 2018) between harvest and sowing when there was no or a little vegetation and E was dominated by bare soil characteristics. During each bare soil period, the soil was tilled twice. In 2017, herbicides were sprayed due to the growth of weeds. From 14 Aug. 2017 until 1 Sept. 2017, minor plant growth was observed on the lysimeters. From 2016 to 2018, 256 d of bare soil observations were available. For each year, there were 91 d of bare soil data available except for 2016, when 72 d were available. Dates of start and end of the monitor periods, of crop harvest and sowing, and of tillage and herbicide applications are given in Table 2-2.

In addition, in each year, a different crop was grown on the lysimeters before the bare soil period, which influenced the initial conditions of the bare soil period due to preceding evapotranspiration. In 2016 winter barley (*Hordeum vulgare* L.; ET = 367 ± 26 mm), in 2017 winter rye (*Secale cereale* L.; ET = 448 ± 22 mm), and in 2018 oat (*Avena sativa* L.; ET = 339 ± 21 mm) were cultivated (Groh et al., 2020).

Table 2-2: Selected periods and surface treatments during the observed time period for analyzing evaporation (E) of bare soil for stations SE3 and SE4 in Selhausen.

Surface treatment	2016	2017	2018
Harvest	8 July 2016	21 July 2017	24 July 2018
Initial date of E monitoring	20 Aug. 2016	1 Aug.2017	1 Aug.2018
Application of herbicides	13 Aug. 2016	1 Sept. 2017	–

First tillage treatment	25 Aug. 2016	19 Sep. 2017	30 Aug. 2018
Second tillage treatment	11 Oct. 2016	25 Oct. 2017	12 Sep. 2018
Sowing	11 Oct. 2016	15 Mar. 2018	5 Nov.2018

The observation period in 2018 was characterized by dry conditions with only 119 mm of precipitation during the bare soil period and a mean net radiation of 57.7 W m^{-2}, contrasting with 2017 with 180 mm of precipitation and a mean net radiation of 54.6 W m^{-2}. The year 2016 showed intermediate values between 2017 and 2018 regarding precipitation, radiation, and average temperatures Table 2-3).

Table 2-3: Climatic conditions during the bare soil periods from August until October for the years 2016-2018.

Parameter	Year	Mean net radiation [W m^{-2}]	Precipitation [mm]	Mean temperature [°C]
Total	2016	63.1	132	15.5
	2017	54.6	156	15.4
	2018	57.7	119	16.0
August	2016	95.5	33	18.9
	2017	86.0	96	18.3
	2018	81.3	30	20.2
September	2016	71.5	25	18.0
	2017	53.6	64	14.4
	2018	64.2	59	15.6
October	2016	22.6	74	9.6
	2017	24.0	21	13.4

Parameter	Year	Mean net radiation [W m^{-2}]	Precipitation [mm]	Mean temperature [°C]
	2018	27.6	30	12.0

2.3.2.1 Bare Soil Evaporation Measurements and Statistical Analysis

2.3.2.2 Data Processing

The distinction of precipitation and E from lysimeter mass changes needs a suitable data preprocessing and postprocessing to reduce the effect of errors and noises on the water fluxes. Lysimeter and leachate tank weights were processed in the following manner: (a) the raw data were corrected by adjusting systematic errors and outliers, (b) random errors and noise were smoothed, (c) E and precipitation fluxes were calculated, and (d) data were checked for plausibility and data gaps were filled in a postprocessing step (Schrader et al., 2013).

Steps i and ii: Error Correction and Smoothing.

A distinction was made between measurement noise (e.g., induced by external sources such as wind) and outliers (defined as singular disturbances or technical malfunctions) (Peters et al., 2017). In some cases, outliers and noise could be removed by automated plausibility controls or suitable filter schemes; in other cases, manual corrections were required (Schrader et al., 2013).

To smooth the time series of mass measurements obtained with 1-min resolution and avoid smoothing errors on the estimation of precipitation and evapotranspiration, the adaptive window and adaptive threshold filter method (AWAT filter) developed by Peters et al. (2014); Peters et al. (2016); and Peters et al. (2017) was used. To manage time-variable noise levels, the filter uses an adaptive threshold (δ) and adaptive averaging window width (ω) (Peters et al., 2016). For our calculations, δ varied between 0.02 (0.02 kg) and 0.2 mm (0.2 kg), and ω between 3 and 31 min. An intermediate output of the filter algorithm is a step function of lysimeter weights. This step function is subsequently interpolated using spline functions to produce a time series with 1-min temporal resolution of noise-removed and interpolated lysimeter weights. Further information and an extensive validation of this method can be found in Hannes et al. (2015) and Peters et al. (Peters et al., 2014, 2016, 2017).

Step iii: Calculation of Evaporation and Precipitation. E and precipitation were calculated from time series of lysimeter (WL) and seepage tank weights (WT) obtained in Step ii as in Schrader et al. (2013), assuming no simultaneous E and precipitation during a 1- min time interval:

$$P_t = \begin{cases} WL_t - WL_{t-1} + WT_t - WT_{t-1} \\ for\, WL_t - WL_{t-1} + WT_t - WT_{t-1} > 0 \\ 0\, for\, WL_t - WL_{t-1} + WT_t - WT_{t-1} \leq 0 \end{cases}$$

$$E_t = \begin{cases} -\left(WL_t - WL_{t-1} + WT_t - WT_{t-1}\right) \\ for\, WL_t - WL_{t-1} + WT_t - WT_{t-1} < 0 \\ 0\, for\, WL_t - WL_{t-1} + WT_t - WT_{t-1} \geq 0 \end{cases} \quad 2\text{-}1$$

where P_t [kg] and ET_t [kg] are the precipitation and evapotranspiration amounts during the time interval t. Time series of P and E were subsequently aggregated to hourly values.

Step iv: Postprocessing. The obtained E rates were tested for plausibility. For times with missing data, three cases were considered to fill the data gaps. In case data were missing in one or two of the three replicate lysimeters (2.9% of the dataset), the mean E rate of the other lysimeters with the same soil profile was taken to fill the data gap. In case data were missing in the three lysimeters of the same soil type for a period shorter than 6 h (0.31% of the dataset), fluxes were assumed to be constant during this period and estimated from the weights at the end and beginning of the time period. If data gaps exceeded 6 h (0.05% of the data set), E fluxes were set equal to E rates of the other lysimeters.

2.3.2.3 Statistical Analysis

A multivariate nested ANOVA was carried out to evaluate the variability in E flux among the different soil types and within lysimeter replicates (i.e., filled with a given soil type). For this, 33 d with gap-filled data were excluded from the analysis. The considered factors in the ANOVA analysis were soil type, time, and lysimeter. The lysimeter factor was treated as a random factor nested within each soil type. The daily E rate was the investigated dependent variable and expressed as:

$$E_{d,s,l} = \bar{E} + D_d + S_s + (DS)_{d,s} + L_{l,s} + \varepsilon_{d,s,l} \qquad \text{2-2}$$

The ANOVA model predicts evaporation at day d from a certain lysimeter l, taken from a soil s, $E_{d,s,l}$ [mm d^{-1}], as the sum of the overall average E ($\bar{E}$ and four additive 'effects': the effect of the day D_d, the effect of the soil S_s on E, the effect of the interaction between the soil and day $(DS)_{d,s}$, and the effect of the lysimeter$L_{l,s}$ (mean difference between the E in lysimeter k and the mean E of all three lysimeters of soil S, and $\varepsilon_{d,s,l}$ is the error term. Since only one measurement was done in one lysimeter for a given time, the statistics of the error term had to be derived from the lysimeter-time interaction effect (the difference between the interaction between the lysimeter and time effect and the average interaction effect of the soil and the time). The ANOVA analysis was carried out with the MATLAB (Mathworks, 2019) anovan function. The same ANOVA model was used to evaluate the soil moisture content measurements in the different lysimeters and soils.

The time effect is related to the meteorological conditions, rainfall and potential evaporation, that vary over time and influence the evaporation. The effect of the soil on evaporation is expressed by both the mean soil effect S_s and the interaction between the soil and time $(DS)_{d,s}$, which expresses to what extent the variation of the evaporation with time differs between different soils. This additive model is not perfect since it assumes that the lysimeter effect is constant in time and it neglects the interaction between the lysimeter effect and time. The observed interaction is considered as the random error $\varepsilon_{d,s,l}$ in the model, which is assumed to be uncorrelated over time.

To assess the impact, an additional analysis was conducted (Annex A.3) The data indicate that a correlation exists over a period of approximately five days. Ignoring this correlation, as was done in the present analysis, affects the calculated significance levels. Using a subset of the data with measurements taken every five days, the significance levels were slightly lower in this case, the overall conclusions of the study remained unchanged.

2.3.3 Computation of Potential Evaporation

Reference evapotranspiration, ET_0 [mm d^{-1}] was estimated with the PM method (Allen et al., 1998):

$$\lambda ET_0 = \frac{\Delta\left(R_N - Q_g\right) + \left[\frac{\rho_\alpha c_\alpha \left(e_{sat}^0 - e_a\right)}{r_{av}}\right]}{\Delta + \gamma\left(1 + \frac{r_s}{r_{av}}\right)} \qquad \text{2-3}$$

where λ [MJ kg^{-1}] is the latent heat of evaporation, R_N [MJ m^{-2} d^{-1}] is the net radiation, Q_g [MJ m^{-2} d^{-1}] is the soil heat flux, $(e_{sat}^0 - e_a)$ [kPa] is the vapor pressure deficit, ρ_a [kg m^{-3}] is the air density at a constant pressure, and c_a [J kg^{-1} C^{-1}] is the specific heat of the air. The slope of the saturation vapor pressure temperature relationship is expressed as Δ [kPa °C^{-1}], whereas γ [kPa °C^{-1}] is the psychometric constant. Aerodynamic and surface bulk resistance are denoted by r_{av} and r_s [s m^{-1}], respectively. R_N was measured about one lysimeter at each lysimeter hexagon, hence two data sets for R_N are available. As the soils are very similar, the two data sets for R_N, plotted against each other, scatter around the 1:1 line (Annex A.2). A brief explanation why we chose measured over calculated R_N can be found in Annex A.2. It should be noted that the net radiation that is measured over a soil surface may deviate from the net radiation of the reference surface that is used to calculate ET_0. When the actual evaporation from the surface is smaller than the reference evaporation, the surface will be warmer and the measured net radiation smaller than the net radiation of the reference surface. To assess this difference, we compared measured net radiation with the net radiation that is calculated according to the FAO approach (see Annex A.2). The close agreement between the two R_N datasets, indicate that potential differences in surface albedo (e.g. due to soil color) were negligible.

The aerodynamic resistance is derived from the wind speed considering a logarithmic wind profile. For calculating the evapotranspiration of a reference grass surface, the surface resistance represents the stomatal resistance and is defined to be r_s = 50 s m^{-1} for daytime and r_s = 200 s m^{-1} for nighttime periods (Allen et al., 2005). The soil heat flux Q_g [MJ m^{-2} d^{-1}] is calculated from the net radiation and put equal to $0.1R_N$ during daytime and $0.5\,R_N$ during nighttime (Allen et al., 1998). To obtain the potential bare soil evaporation E_{pot} [mm d^{-1}], the calculated reference ET_0 [mm d^{-1}] was scaled by an empirical coefficient (Allen et al., 2005):

$$E_{pot} = 1.15ET_0 \tag{2-4}$$

Note that ET_0 determined with Equation 2-3 accounts for a reference grass surface using a surface resistance r_s that accounts for stomatal resistance. When we calculated E_{pot} using r_s = 0 in Equation 2-3, we found very similar values as E_{pot} obtained with Equation 2-4.

2.3.4 Simulation of Soil Water Flow

E_{pot} values reflect situations when the soil surface is water saturated, and E is energy controlled (stage-I; (Idso et al., 1974)). When the E_m rate becomes less than E_{pot}, E is soil controlled (i.e., movement of water to the soil surface is a limiting factor [stage-II]).

In order to simulate the periods when the E takes place at a potential rate (stage-I), the HYDRUS-1D soil water flow model based on the Richards equation was used that simulates the temporal evolution of the surface soil water content so that time periods when the surface is sufficiently wet to maintain the E_{pot} rate can be identified. In a second instance, the model was used to simulate the evaporation rate

(E_{sim}) during stage-II when the flux of soil water to the surface is limiting the E rate.

To describe the dynamics and vertical distribution of the soil water content and water fluxes in the soil profile, the Richards equation was used. The Richards equation simplifies the two-phase (liquid and gas) two-component (dry air and water) flow and transport, which are coupled to the heat transport, to an isothermal (no coupling to heat transport in the soil) one-component (only water) and one-phase (only liquid) equation (Vanderborght et al., 2017).

It thereby assumes that the effect of the air phase on the liquid flow is minor, that flow due to thermal gradients can be neglected, and that transport of water vapor in the gas phase can be neglected compared with the transport of water by the liquid flow (Li et al., 2020).

The one-component, one-phase Richards model for one-dimensional vertical flow in a soil profile without plants given by Šimůnek et al. (2013):

$$\frac{\partial \theta}{\partial t} = \frac{\partial}{\partial x}\left[K\left(\frac{\partial h}{\partial x} + 1 \right) \right] \qquad \text{2-5}$$

where h [m] is the water pressure head, θ [m^3 m^{-3}] the volumetric water content, t [s] the time, x the vertical spatial coordinate (m, positive upward), and $K(h, \theta)$ [m s^{-1}] the hydraulic conductivity function, which depends on pressure head or water content. The soil water retention and hydraulic conductivity function complete Equation 2-5. To solve Equation 2-5, boundary conditions at the soil surface and the bottom of the lysimeter must be defined. A common approach is to define so-called “atmospheric” or mixed boundary conditions (Šimůnek et al., 2013; Vanderborght et al., 2017) . During stage-I and during precipitation events, the E_{pot} flux (Equation 2-4) and the precipitation rate define the flux boundary condition. These flux boundary conditions are used as long as the water pressure head at the surface stays above or below a critical threshold pressure head for evaporation or infiltration conditions, respectively. When the threshold pressure head is reached, the boundary condition is shifted to a pressure head boundary condition. For the minimum allowed pressure head at the soil surface, a critical pressure head of -1,000 m was used. The periods when the pressure head boundary condition is used correspond with stage-II periods and the calculated water fluxes at the soil surface with the stage-II E rates. This approach to estimate stage-II E rates is based on the idea that these rates are predominantly limited by liquid water fluxes in deeper soil layers (Salvucci, 1997).

Assuming that thermal and vapor fluxes have a low impact, the so calculated fluxes were found by Assouline et al. (2013).; Assouline et al. (2014); and Assouline and Narkis (2019) to reproduce quite well the stage-II E rates.

However, simulations by Fetzer et al. (2017)demonstrated that these assumptions may not hold true during daytime, when water transport through the dried out and heated up surface layer is mainly due to vapor transport. The higher temperatures during the day increase the vapor pressure in the soil resulting in higher vapor concentration gradients and vapor transport. This incomplete description of the subsurface vapor diffusion and evaporation dynamics is also described by Shahraeeni and Or (2010, 2012a,2012b); Shokri et al. (2010); and Or et al. (2013).

2.3.4.1 HYDRUS-1D Model Setup, Soil Hydraulic Properties, and Initial Conditions

To solve the Richards equation, we used the HYDRUS-1D code. HYDRUS-1D is an established model that has been applied successfully for the simulation of various hydrologic processes and problems in the vadose zone (Šimůnek et al., 2018). The model domain consisted of a 1,5 m soil profile that was discretized into 1 cm finite elements. For estimating the unsaturated hydraulic conductivity function in terms of soil water retention parameters, the description by van Genuchten-Mualem (vGM) was chosen (van Genuchten, 1980):

$$\theta(h)=\begin{cases}\theta_r+\dfrac{\theta_{sat}-\theta_r}{\left[1+\left|\alpha_{vG}h\right|^{n_{vG}}\right]^{m_{vG}}}, h<0\\ \theta_{sat}, h\geq 0\end{cases} \tag{2-6}$$

$$K_l\left(S_{we}\right)=K_{s,l}S_{we}^{0.5}\left[1-\left(1-S_{we}^{\frac{1}{m_{vG}}}\right)^{m_{vG}}\right]^2 \tag{2-7}$$

where a_{vG} [m^{-1}] is related to the inverse of the air entry value, n the pore size distribution, l the pore connectivity, h [m] the matric potential head and m_{vG} is defined as $m_{vG} = 1 - 1/n_{vG}$, where $n_{vG} > 1$. S_{we} is the effective saturation, and θ_{sat} [m^3 m^{-3}] and θ_r [m^3 m^{-3}] are the saturated and residual water contents, respectively.

Two sets of hydraulic parameters were used in this study: a first set for the vGM model were estimated from soil texture (Groh et al., 2016) using the ROSETTA PTF implemented in HYDRUS-1D (Schaap et al., 2001) (Figure 2-2). Values for θ_{sat} were derived from measured maximal soil water contents in 2016, 2017, and 2018 (I). A second set of SHP parameters was derived by fitting the water retention curve (Equation 2-6) to measurements of water content and water potentials in the lysimeters at the 10-, 30-, and 50-cm depth with the SoilHyP R- package (Table 2-4, II). Comparing texture dependent SHP (I), there is a difference between the two different soil types, silty loam (BL, SB, and SE), and sandy loam (DD) (Figure 2-2). The fitted SHPs (II) are very similar for all soils and do not show differences that can be related to difference in texture (Figure 2-2).

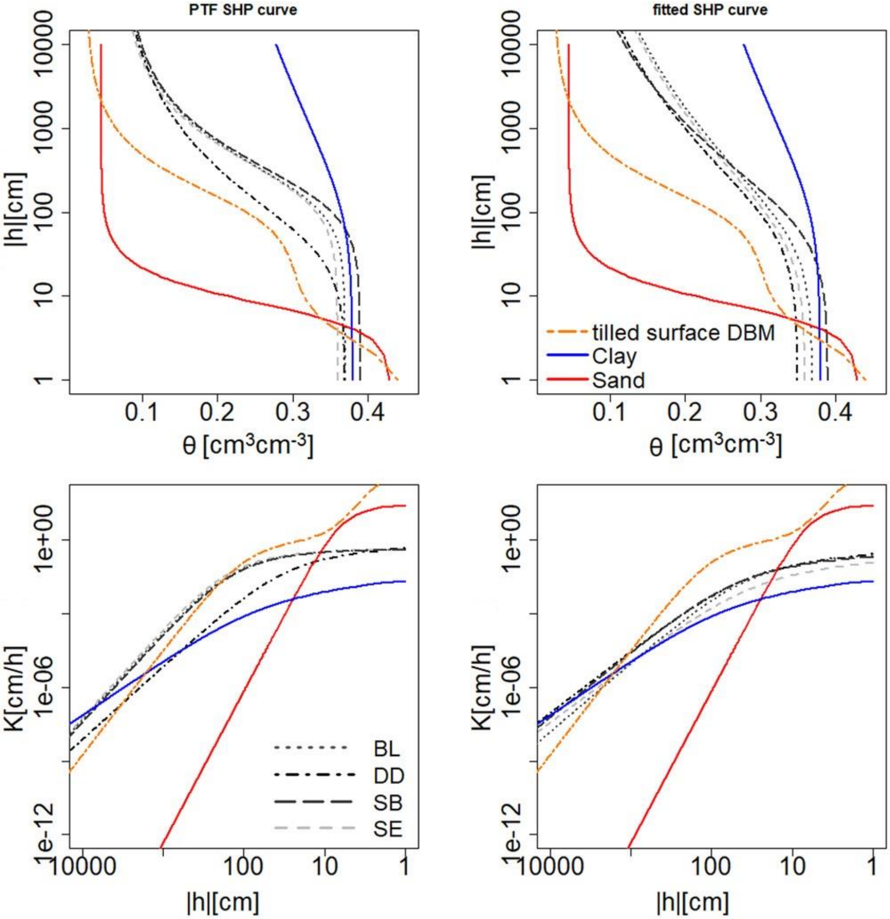

Figure 2-2: Hydraulic conductivity (K) plotted against the pressure head (h, bottom) and the water retention curve (top) for the four different soil types: Selhausen (SE), Bad Lauchstädt (BL), Sauerbach (SB), and Dedelow (DD). As a reference, curves for clay and sand defined by the ROSETTA database were added. Pedotransfer function (PTF) soil hydraulic property (SHP) presents texture-based van Genuchten-Mualem parameters, and the fitted SHPs are derived from in situ measurements of water contents and pressure heads. Parameters for the tilled surface (DBM) are given by radiometer measurements as described in (Dimitrov et al., 2015). θ is the volumetric water content.

Table 2-4: The hydraulic parameters of the van Genuchten - Mualem model (vGM) for the different soils estimated from soil texture using ROSETTA pedotransfer functions implemented in HYDRUS-1D (Groh et al., 2016; Schaap et al., 2001) (PTF SHP).

	θ_r	θ_{sat}	α_1	n_1	K_s	τ	w_2	α_2	N_2
	$cm^3\ cm^{-3}$		cm^{-1}		cm d^{-1}			cm^{-1}	
PTF SHP									
Bad Lauchstädt (BL)	0.0737	0.37	0.0053	1.6290	10.8	0.5			
Dedelow (DD)	0.0566	0.37	0.0210	1.3924	18.4	0.5			
Sauerbach (SB)	0.0737	0.39	0.0056	1.6305	10.8	0.5			
Selhausen (SE)	0.0685	0.36	0.0048	1.6576	10.8	0.5			
Fitted SHP									
BL	2.0×10^{-10}	0.37	0.0170	1.1800	10.8	0.5			
DD	5.0×10^{-08}	0.35	0.0140	1.2100	18.4	0.5			
SB	0.01	0.39	0.0120	1.2600	10.8	0.5			
SE	2.6×10^{-08}	0.36	0.0170	1.1800	10.8	0.5			
Tilled soil SE	0.025	0.45	0.0085	1.9	1,200	0.5	0.35	0.425	2.57

Note. The saturated water content (θ_{sat}) is taken from maximum field values. Also, the soil hydraulic parameters estimated from fits of the retention curve to water content and pressure head measurements in the lysimeters (fitted SHP) are shown. For the Selhausen soil, parameters of the Durner bimodal hydraulic functions that were obtained by inverse modeling of surface soil moisture and account for the impact of the changed structure of the surface soil layer of a tilled plot (Dimitrov et al., 2015) are also shown. θ_r is the residual water content, θ_s is the saturated water content, α and n are shape parameters, K_s is the saturated hydraulic conductivity, w [kg kg^{-1}] represents the weight of the pore domain to total pore volume, and τ is the tortuosity parameter in the conductivity function. θ_{sat} values were derived from field measurements.

As mentioned before, during each bare soil period, the soil was tilled twice, hence we wanted to know if the tillage has a considerable effect on evaporation rates.

Therefore, for one soil, SE, a third set of hydraulic parameters was considered. These parameters were derived from L-band brightness temperatures, which are related to the soil moisture content of the surface soil layer and which were measured using a tower-based L-band radiometer that looked on three plots with different soil surface structure: a compacted, harrowed and tilled soil plot (Dimitrov et al., 2015). Parameters of the surface soil layer were estimated using inverse modeling with a radiative transfer model that was coupled with the Richards equation. In order to represent the effect of the soil structure changes due to soil surface management, the bimodal model of Durner (DBM) was used to represent the SHP of the tilled surface layer (Durner, 1994; Priesack & Durner, 2006).

The tilled surface layer was assumed to be 5 cm thick, which corresponds with the common tillage depth of the lysimeters. The SHP parameters of the soil below the tilled surface layer were derived from the soil texture using the ROSETTA PTF. The effect of tillage on the SHP was assumed to be nondynamic or static. In reality, tillage is done each growing season, and rainfall events after tillage might change SHP. Further information about the estimation of the hydraulic parameters is provided by (Dimitrov et al., 2014).

The tilled surface layer had a larger saturated hydraulic conductivity (K_s) than the undisturbed soil (Figure 2-2). For more negative h, K_{tilled} is smaller than that of the nondisturbed soil representing the impact of the empty interaggregate pores and the hydraulic disconnection of the aggregates.

Initial conditions were set up by interpolation of soil moisture contents measured at 10-, 30-, and 50-cm depth at the beginning of each observation period. There were neither sensors at the surface nor bottom of the lysimeter. Hence, the value of the shallowest sensor at 10 cm in the lysimeter was considered instead, whereas saturation was considered to prevail at 1.50-m depth as initial condition. “Atmospheric” boundary conditions were defined at the upper boundary, and a variable pressure head boundary condition was determined at the bottom boundary.

2.3.5 Characteristic Length of Evaporation

We defined the characteristic length of evaporation, L_c, as the depth to which a wet soil dries out during stage-I evaporation. In order to define this depth, we calculated the amount of water that can be evaporated during stage-I, $E_{cum,I}$ [m]. This amount was divided by the change in water content in the dried-out soil layer, which was approximated by $(\theta_i - \theta_{sur})/2$:

$$L_c = 2\frac{E_{cum,I}}{\theta_i - \theta_{sur}} \tag{2-8}$$

where $\theta_i$is the initial water content and θ_{sur} is the water content at the soil surface. $E_{cum,I}$ was derived from the soil “desorptivity” (S_{evap}, m d$^{-0.5}$) and the potential evaporation rate (E_{pot}), which was taken to be 4 mm d^{-1}, using the time compression analysis (Fetzer et al., 2017). The time compression analysis assumes that the maximal evaporation rate that can be supplied at a certain time from a soil profile, which was initially at a uniform water content θ_i, only depends on the amount of water that evaporated since the start of the evaporation process. Considering a virtual evaporation process in which the surface soil moisture at the start of the evaporation process is instantaneously decreased to the surface soil moisture θ_{surf}, and neglecting the impact of gravity on the water flow, the evaporation rate at the soil surface can be described as:

$$E = \frac{S_{evap}}{2\sqrt{t}} \tag{2-9}$$

and the time at which E_{pot} is reached in this process, t_{pot}, is:

$$t_{pot} = \frac{S_{evap}^2}{4E_{pot}^2} \tag{2-10}$$

The cumulative amount of water that evaporates until E reaches E_{pot}, which is according to the time compression analysis equal to the amount of water that can be evaporated during phase I of an evaporation process with an initially constant evaporation rate E_{pot}, $E_{cum,I}$, can be described as:

$$E_{cum,I} = \frac{S_{evap}^2}{2E_{pot}} \qquad \text{2-11}$$

So that

$$L_c = \frac{S_{evap}^2}{\left(\theta_i - \theta_{sur}\right) E_{pot}} \qquad \text{2-12}$$

$S_{evap}^2$was derived from the hydraulic conductivity and the water retention curve according to (Parlange et al., 1985):

$$S_{evap}^2 = \frac{8}{3} \int_{h_s}^{h_i} \left[\theta\left(h_i\right) - \theta\left(h\right)\right] K\left(h\right) dh \qquad \text{2-13}$$

where h_i is the initial pressure head and h_s is the pressure head at the soil surface. θ_{sur} was set equal to the residual water content, θ_r and h_s to -15,000 cm [at this pressure head $\theta(h) \approx \theta_r$]. The initial water content was defined as the water content at h_i = -10 cm.

2.3.6 Evaluation of Model Performance

Deviations of predictions and observations were evaluated by using the $RMSD$. The $RMSD$ can be divided into the unsystematic difference $RMSD_u$ and the systematic difference $RMSD_s$, which are defined as (Willmott et al., 1985; Wilmott, 1982):

$$RMSD_s = \left[n^{-1} \sum_{i=1}^{n} \left(\hat{y}_l - x_i\right)^2 \right]^{0.5} \qquad \text{2-14}$$

$$RMSD_u = \left[n^{-1} \sum_{i=1}^{n} \left(y_i - \hat{y}_l\right)^2 \right]^{0.5} \qquad \text{2-15}$$

$$RMSD = \left(RMSD_s^2 + RMSD_u^2\right)^{0.5} \qquad \text{2-16}$$

where x_i refers to E_m and y_i is $E_{SHP/PTF/tilled}$, and $\widehat{y_l}$ is calculated from the ordinary least-squares (OLS) linear regression between $E_{SHP/PTF/tilled}$ and E_m.

Dividing the RMSD helps to understand whether model performance can be improved through recalibration (reducing $RMSD_s$) or if it's limited by inherent randomness ($RMSD_u$).

2.4 Results

2.4.1 Potential and Measured Evaporation: Total Amounts, Monthly and Daily Averages

In Figure 2-3 E_{pot}, E_m from the different soils, and the precipitation (P_i), are shown for the monitoring periods in the three different years. For all years, $E_m < E_{pot}, E_{pot} > P_i$, and E_m does not differ considerably among the soil types. The difference between E_{pot} and E_m was the largest in 2018 and the smallest in 2017, whereas precipitation was the largest in 2017 and the smallest in 2018. Despite the fact that $E_{pot} > P_i, E_m$ was smaller than the precipitation in all years so that there was an infiltration surplus in all years that wetted up the soil profile. The infiltration surplus was largest in 2016. Since the timing and duration of the monitoring period in 2016 is different from that in the other two years, a direct comparison of the values for this year with the other two years is difficult.

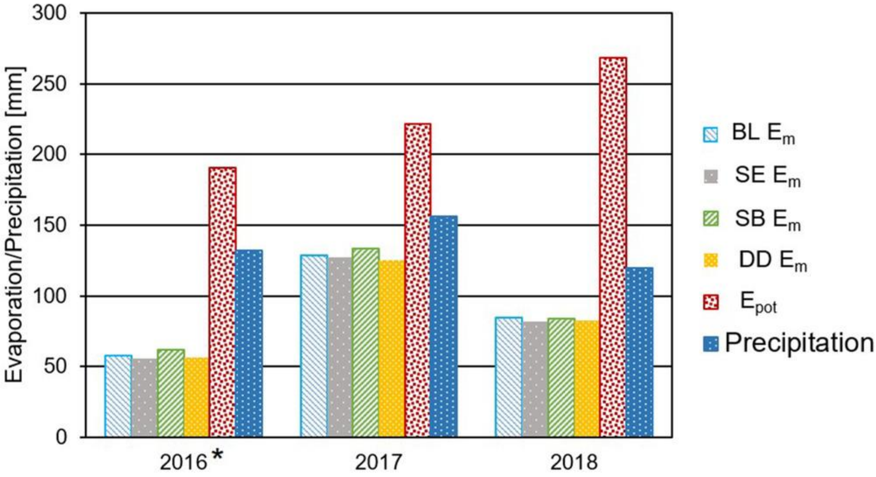

Figure 2-3: Comparison between measured evaporation (E_m) for the Bad Lauchstädt (BL), Selhausen (SE), Sauerbach (SB), and Dedelow (DD) soils, potential evaporation (E_{pot}), and precipitation.*In 2016, bare

soil evaporation was monitored over a 72-d period vs. the 91-d period for 2017 and 2018.

According to the ANOVA analysis, the difference in time-averaged E_m among soil types was not significant (Table 2-5). The time-averaged E rates of the 12 different lysimeters were significantly different independently from the soil type. Their rates varied too much within a given soil type to observe significant soil effects on the time-averaged E, and consequently cumulative E. The standard deviation of the soil effect was 0.014 mm d^{-1}, whereas the standard deviation of the time-averaged E rates from the different lysimeters was 0.027 mm d^{-1}. In other words, the soil effects (Table 2-6) were too small compared to the variation of the E between the different lysimeters. The soil–time interaction effects were significant. This means that despite the nonsignificant differences between the time-averaged E rates of the different soils, the temporal variations of the E rates varied significantly between the different soils. It should be noted that the analysis was carried out using daily averaged E rates. Therefore, the analysis does not provide information about differences in evaporation rates between soils and individual lysimeters at a higher temporal resolution (e.g., diurnal variation in E). The day-to-day “unexplained variation” or “model error” was 0.09 mm d^{-1} (Table 2-5) and represents the standard deviation of the difference between the E rate at a given day of a single lysimeter, which is corrected for its average lysimeter effect, and the average rate of lysimeters from the same soil at that day. The time effects were strongly significant (i.e., average E rates in the different lysimeters of the different soils varied significantly over time compared with the “unexplained” variation).

Table 2-5: ANOVA analysis showing the significance of differences caused by time, soil, lysimeters and the unexplained error.

Source	**Sum of squares**	**df**	**Mean square**	***F***	**Prob > *F***	**SD effect**
						mm d^{-1}
Time	1,118.419	222	5.037	626.608	0	0.647
Soil	0.364	3	0.121	0.738	0.557	0.014
Lysimeter(soil)	1.316	8	0.164	20.473	6.99×10^{-30}	0.027
Time × soil	17.700	666	0.026	3.305	2.98×10^{-88}	0.094
Error	14.279	1,776	0.008			0.089
Total	1,152.081	2,675				

Table 2-6: Coefficients table: overall mean evaporation $\bar{E}$ and soil effects (S_s) of the four different soils: Bad Lauchstädt (BL), Selhausen (SE), Sauerbach (SB), and Dedelow (DD)

Parameter	**Value**
	mm d^{-1}
Overall mean $\bar{E}$	1.020
Soil effect, S_s	
BL	0.006
SE	0.005
SB	0.009
DD	-0.02

2.4.2 Monthly Mean Diurnal Variation of Potential and Measured Evaporation

Figure 2-4 presents the monthly mean diurnal variation of the $E_{pot}$and E_m in the four soils. In all cases, the peak of the mean diurnal E_m was less than that of E_{pot}. In months when E_m was significantly less than E_{pot} (August 2016 and 2018, September and October 2018), the peak of the mean diurnal E_m flattened off. The mean diurnal evaporation values show that water-limited or stage-II evaporation occurred during all months. E_m values during stage-II depend on the SHPs (Mosthaf et al., 2014). We therefore expected to observe differences in the E rates between the different soils in these months, especially between the DD soil with a sandier texture and the other soils. But the mean diurnal E_m variation was very similar for the different soil types.

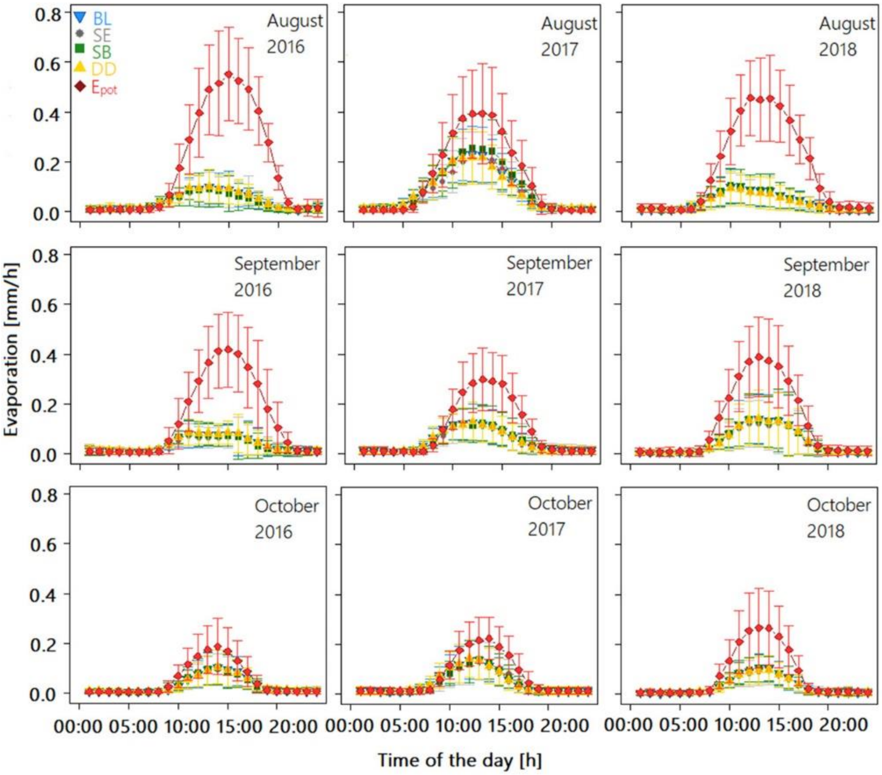

Figure 2-4: Monthly mean diurnal variation of potential and actual evaporation rates in each soil for the three different observation periods (2016, 2017, and 2018). BL, SE, SB, and DD are the different soil types: Bad Lauchstädt, Selhausen, Sauerbach, and Dedelow, respectively. E_{pot} describes the potential evaporation. The vertical bars represent the standard deviation of the day-to-day hourly evaporation rate at a given hour.

2.4.3 Water Content

Temporal dynamics in soil water content (θ) were stronger in shallow layers (10- and 30-cm depths) than at 50 cm, regardless of the investigated bare soil period (Figure 2-7). The driest soil conditions were observed in 2018: although the θ_{10cm} value was ~0.25 m^3 m^{-3} at the beginning of the monitoring period in August in 2017 and 2016, it was only ~0.12 m^3 m^{-3} in 2018. θ_{30cm} and θ_{50cm} were around 0.3 m^3 m^{-3} at the beginning of August in 2016 and were considerably larger than in 2017 and 2018 (~0.2 m^3 m^{-3}). In 2016, the soils remained wet at 30- and 50-cm depth. Compared with 2016 and 2018, 2017 was a relatively wet year when several drying and rewetting periods could be observed in the first 10 cm. In 2018, due to the initially dry soil conditions in the upper soil, precipitation was not sufficient to wet up the soil at 30 and 50 cm. In summary, with each year, a different scenario was observed. During the observation period in 2016, climate conditions were dry and the soil, especially in the deeper soil layers, was wet (Figure 2-5). In 2017, climate conditions were relatively wet, as was the soil. The opposite conditions occurred in 2018, when the climate was dry, as well as the soil .

A systematic difference in water content at a given soil depth among the different soil types was not detected in the ANOVA analysis (i.e., it was systematically smaller than the difference in water content at the considered depth among lysimeters of the same soil type). The standard deviation of the lysimeter effects on soil moisture measurements in a certain soil was between 0.023 m^3 m^{-3} at 10- and 30-cm depth and 0.03 m^3 m^{-3} at 50-cm depth, whereas the standard deviation of the soil effect on soil moisture was only 0.011 m^3 m^{-3} at 10-cm depth, 0.019 m^3 m^{-3} at 30-cm depth, and 0.021 m^3 m^{-3} at 50-cm depth. The unexplained error in the ANOVA model was 0.023, 0.024, and 0.019 m^3 m^{-3} at 10-, 30-, and 50-cm depth, respectively.

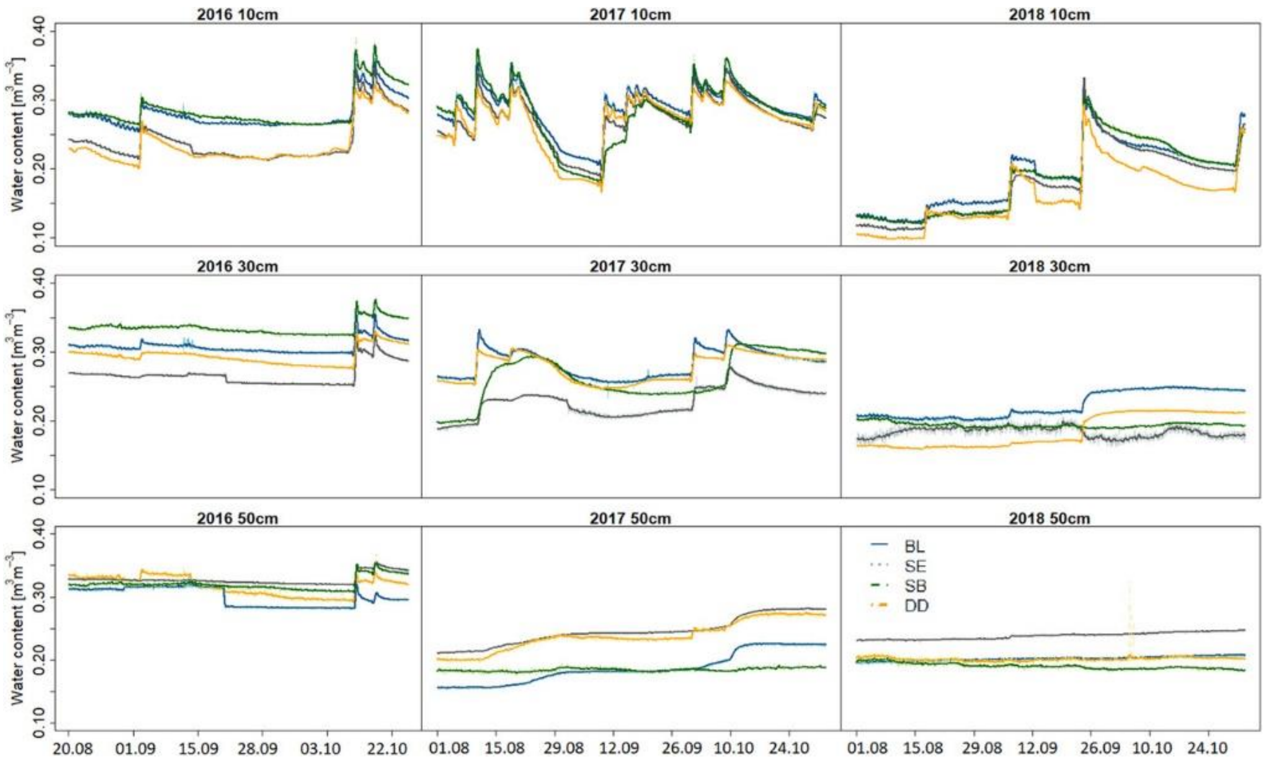

Figure 2-5: Water contents in m^3 m^{-3} at different soil depths (10, 30, and 50 cm) for August - October 2016 - 2018. BL, SE, SB, and DD are the different soil types Bad Lauchstädt, Selhausen, Sauerbach, and Dedelow, respectively.

2.4.4 Model Results

2.4.4.1 Cumulative Evaporation Rates

Simulations using SHPs that were derived from soil texture with PTFs highly overestimated evaporation. Although there was barely any difference in E_{PTF} between the silty loam soils (BL, SB, and SE), the sandy loam soil (DD) E_{PTF} rates were less in comparison with BL, SB and SE in all years. Although $E_{PTF} >> E_m$, differences between textures can be seen in simulations contrary to observations. The highest E_{PTF} rates were simulated for 2016 with $E_{sim} \approx E_{pot}$ for the silty loam soils. The lowest overestimation by E_{PTF} was in 2018 for the DD soil (+35.5 mm).

Using SHP parameters obtained from fits to in situ measurements of water content and pressure heads led to better estimates of E (E_{SHP}) compared with E_{PTF} (Figure 2-8). For all years and soils, $E_{SHP} < E_{PTF}$ and E_{SHP} corresponded better than E_{PTF} with E_m. E_{SHP} was smaller for the silty loam BL and SE soils than for the silty loam SB and the sandy loam DD. For the latter two soils, E_{SHP} was still larger than E_m, especially in 2016.

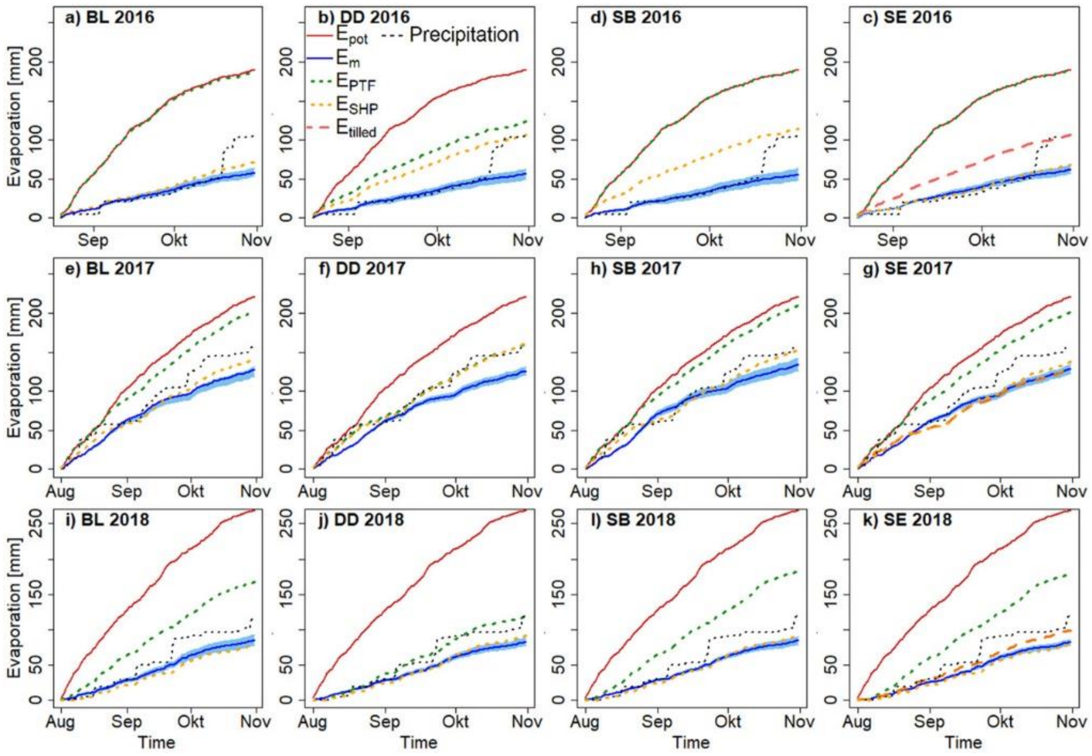

Figure 2-6: Comparison of cumulative precipitation (P), potential (E_{pot}), measured (E_m), and simulated evaporation for the different soils in different years. Simulations using hydraulic parameters obtained from pedotransfer functions (E_{PTF}) and from in situ measurements of water content and pressure heads (E_{SHP}) are shown. For the SE soil, simulations using parameters obtained from surface soil moisture measurements and inverse modeling are also shown (E_{tilled}). Shaded areas show the range in evaporation of lysimeters filled with the same soil. BL, SE, SB, and DD are the different soil types Bad Lauchstädt, Selhausen, Sauerbach, and Dedelow, respectively.

Further simulations with HYDRUS-1D were carried out for the SE soil using SHPs that were estimated from surface soil moisture measurement of a tilled soil plot, E_{tilled}. Due to tillage, the hydraulic properties of the upper layer showed similarities to those of a coarse textured layer (Carminati et al., 2007).

A coarser layer on top of the soil profile accelerates the decrease in hydraulic connectivity of the soil surface with the soil profile, which reduces the duration of stage-I and causes a rapid transition towards stage-II and much smaller E rates during stage-II (Assouline et al., 2014). This was also observed indirectly in the tilled plots that were monitored by Dimitrov (2015)at the SE site. Observed surface temperature differences between the tilled and compacted plots corroborated the differences in simulated evaporation fluxes between both plots that resulted from the different SHPs of the plots due to the different structure of the surface layer. Implementing the tilled layer in HYDRUS-1D resulted in $E_{tilled} < E_{pot}$, in contrast with the simulation for a homogeneous soil profile using the PTF-derived SHPs, which predicted $E_m \approx E_{pot}$ for the silty loam (BL, SB, and SE) in 2016 (191 mm). The tilled surface layer limited E_{tilled} to 107 mm, which is closer to the observations (58 mm). A reduced E_{tilled} compared with E_{PTF} was also simulated in 2018 (99 mm), and in 2017, $E_{tilled} = E_m$ (Figure 2-8).

For a more detailed analysis of this system and the influence of a tilled layer on E rate dynamics, more field information is needed (e.g., detailed measurements above 10-cm depth, near-surface atmospheric conditions, tillage, etc.). Note again that a tilled layer of 5-cm thickness is an assumption and using a thicker or thinner surface layer may have an impact on the E_{tilled} rates.

2.4.4.2 Characteristic Lengths of Evaporation

The soil water retention curves that are obtained for the different soils using PTFs, using in situ measurements of soil water contents and pressure heads, or using inverse modeling show important differences (Figure 2-2). For instance, the water retention curves derived using PTFs suggest a narrower pore size distribution than the retention curves that were measured in situ, which is reflected in the smaller n_1 values of the in situ measured curves. These differences are translated in the soil hydraulic conductivity curves. For the same saturated hydraulic conductivity, the Mualem model predicts considerably smaller unsaturated hydraulic conductivities when the n_1 parameter decreases. The hydraulic conductivity curves that are based on the in situ measured soil water retention curves resemble the unsaturated hydraulic conductivity of a clay soil. Also, the unsaturated hydraulic conductivity of the tilled surface layer is considerably smaller than the unsaturated hydraulic conductivity that was derived from PTFs. How these differences in soil hydraulic properties translate into differences in simulated soil evaporation can be characterized using the characteristic length of evaporation (L_c,Table 2-7). Soil hydraulic parameters that are derived from soil texture using PTFs corresponded for the silty loam soils with very high characteristic lengths (i.e., around 300 cm). The large overestimation of E_m by E_{PTF} demonstrates that large characteristic lengths do not represent the evaporation properties of these soils. This confirms the argument of Lehmann et al. (2020) that estimates of SHPs should best be constrained by characteristic lengths of evaporation. Soil hydraulic parameters that were derived from fitting the water retention curve to in situ measured water content and pressure head measurements corresponded with smaller L_c (10–50 cm) and better predicted E_m. Additionally, the tilled surface layer had a smaller L_c. It should be noted that the ranking of L_c reproduced well the ranking of the simulated E in the different soils and different years. L_c can therefore be considered as a good characteristic that translates SHPs to evaporation properties of a soil.

Table 2-7: Characteristic lengths of evaporation calculated from soil hydraulic parameters (SHPs) that were derived from soil texture using pedotransfer functions (PTFs) ($L_{c,PTF}$), from in situ measured soil water contents and pressure heads ($L_{c,SHP}$), and from soil surface water contents in a tilled soil using inverse modeling ($L_{c,tilled}$) in the different soils

Soil[a]	$L_{c,PTF}$	$L_{c,SHP}$	$L_{c,tilled}$
	cm		
SB	359	32	
SE	291	10	43
DD	55	29	
BL	308	10	

[a] SB, Sauerbach; SE, Selhausen; DD, Dedelow; BL, Bad Lauchstädt.

Since the measured cumulative evaporation rates were reproduced the best by the simulations that used hydraulic parameters derived from in situ measured retention curves, E_{SHP}, we evaluated the simulated daily evaporation rates only for E_{SHP}. The overall difference between daily E_m and E_{SHP} is quantified by the root mean square difference $[RMSE = (RMSD_s^2 + RMSD_u^2)^{0.5}]$.

In Figure 2-7, the scatter plots for E_{SHP} show us frequent under- and overestimation of evaporation. In 2016, the overestimation of the cumulative E_m in the DD and SB soils by E_{SHP} is reflected in the large $RMSD_s$. The $RMSD_s$ is small for 2018 when cumulative E_m was predicted well in all soils. The nonstructural error between the daily E_m and E_{SHP} varied between 0.41 mm d^{-1} in 2018 and 0.69 mm d^{-1} in 2017. This error represents the day-to-day error between the model and measurements that cannot be removed after a linear transformation of the simulation results. It is considerably larger than the day-to-day "unexplained variation" of the daily evaporation rates among lysimeters of the same soil, (0.09 mm d^{-1}, Table 2-5). This indicates that the nonstructural error must be attributed to model uncertainty or errors rather than to measurement errors. In 2017, the good fit of E_{cum} is achieved due to under- and overestimations of *E*, which are canceling out each other. Compared with 2016 and 2018, 2017 has more days where $E_{SHP} < E_m$. A closer inspection revealed that the period in 2017 when $E_{SHP} < E_m$ was before the pesticide application on 1 September, and during this period, the soil surface was not completely bare and the measured water loss from the lysimeter could represent transpiration by weeds.

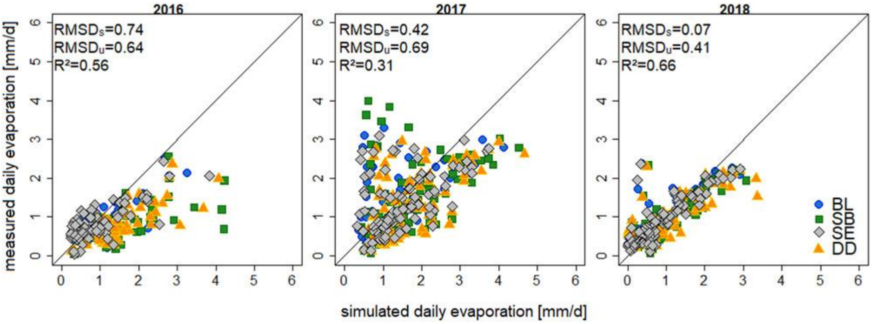

Figure 2-7: Scatter plots of measured daily (E_m) versus simulated (E_{SHP}) using soil hydraulic parameters estimated from in situ measured retention curves. The systemic ($RMSD_s$) and unsystemic ($RMSD_u$) RMSD values are mean values for the Bad Lauchstädt (BL), Dedelow (DD) Sauerbach (SB), and Selhausen (SE) soil in each year; individual values for each soil can be found in Annex A.1 (supplemental material). In 2017, dates of high underestimation are not considered for calculating $RMSD_s$, $RMSD_u$, and R^2, as completely bare soil conditions are not given in this timeframe.

We can identify three main cases for daily E rates: (a) $E_{SHP} > E_m$ during stage-II as seen in 2018 (Figure 2-8 a), (b) $E_{SHP} < E_m$ during stage-II (August 2018) (Figure 2-8 b), and (c) $E_{pot} = E_m = E_{SHP}$, which is mostly the case in early stage-I (Figure 2-8 d). This leads to the following conjectures: at an intermediate soil wetness (θ = 0.15–0.3), E_m decreases to<E_{pot} faster than E_{SHP} does (Figure 2-8 a). This faster decrease is due to an overestimation of the unsaturated conductivity for an intermediate wetness or due to E_{pot} overestimating stage-I evaporation. Under dry conditions, vapor transport and liquid film flow play important roles but are not taken into account in the hydraulic conductivity function used (Or et al., 2013) Figure 2-8 b), which may lead to an underestimation of E_m. The role of vapor transport during dry conditions was also apparent from the course of the diurnal E_m rate, which followed the typical course of the E_{pot} but at a lower rate (Figure 2-8 a, b). Another indication for vapor flow is the increase of daily E_m when E_{pot} increases during stage-II (Figure 2-8). The diurnal course of E_m and the increase of E_m with E_{pot} during stage-II cannot be reproduced by a model that only considers liquid flow, uses a pressure head threshold upper boundary condition, and does not account for an increase of vapor transport due to higher vapor concentrations and concentration gradients in the surface soil layer when the soil surface heats up (Fetzer et al., 2017).

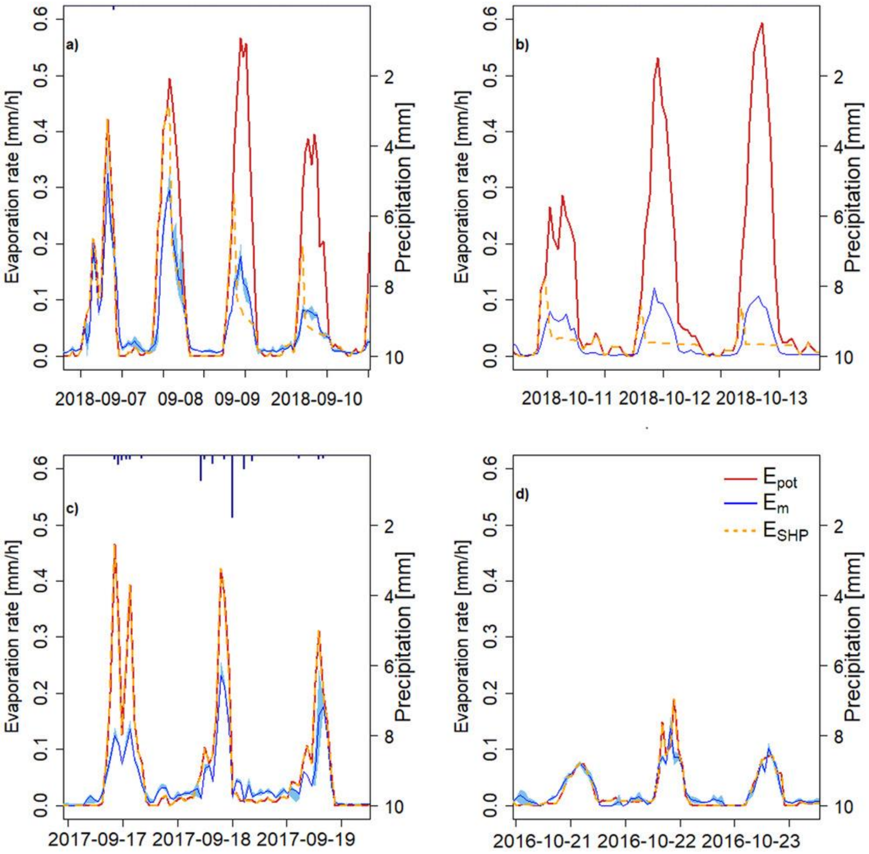

Figure 2-8: Examples highlighting three differences between measured and simulated evaporation: (a) overestimation of evaporation by the Richards equation during stage-II, (b) underestimation of evaporation rates during stage-II, (c) evaporation rate underestimated by the model during nighttime due to an underestimation of the potential evaporation, and (d) measured and simulate evaporation equal to the potential evaporation. Shaded areas show the range in evaporation rates of lysimeter replicates.

Having a closer look at diurnal dynamics, we can also identify a fourth case relevant for hourly E rates: (d) $E_m > E_{pot}$ and $E_{SHP} \leq E_m$ by night (Figure 2-8 a,c), which is especially relevant for wet soils as in 2017. Large differences were especially visible during nighttime, when

E_m is mainly driven by wind speed (Figure 2-8 c);(Groh et al., 2019). Recent investigations highlight that water losses during night are of relevance at the global scale(Padrón et al., 2020). Also, non-rainfall water such as dew might play a role for larger E_m, which can make up 2-7 mm per month of E on grassland lysimeters (Brunke et al., 2019).

2.5 Discussion

During all three observation periods, daily potential evaporation (E_{pot}) was never reached by daily measured evaporation (E_m), even under wet conditions as in 2017. Even though evaporation was water limited, no differences in E_m were observed between different soils. This does not agree with findings of Merlin et al. (2016) and Tolk et al.(2015), who found clear effects of soil texture on evaporation fluxes and of the soil type on evaporation rate during stage-II. We can assume that a lack of differences in E is due to small differences in soil texture and soil hydraulic properties in our lysimeters in combination with the impact of a disturbed surface layer. Additionally, it must be considered that E_{pot} is much smaller in this study than experienced by Tolk et al. (2015).

Three model approaches with different SHPs were compared with each other. Using SHPs that were estimated from soil texture using the ROSETTA PTFs resulted in a considerable overestimation of the measured evaporation, especially for the silty loam soils (BL, SB, and SE). This suggests that the hydraulic conductivity of the fine soils was overestimated.

For one soil, SHPs were derived from surface measurements of soil moisture using inverse modeling (Dimitrov et al., 2015), and it was observed that the disturbance of a surface layer by, for instance, tillage affected the hydraulic properties of the surface layer. Loosening the soil surface disrupts the connection of the soil surface via fine capillaries with soil water in deeper soil layers. This reduces the amount of water that can be evaporated from a wet soil at a potential rate. Under unsaturated conditions, the hydraulic conductivity of a loosened aggregated soil layer can be much smaller than that of a less structured soil so that the loosened aggregated soil behaves as a soil with a coarser texture. Not considering this effect of soil loosening or soil structure on unsaturated soil properties could lead to an overestimation of E from finer textured soils, as was also demonstrated in a simulation study by Schlüter et al. (2012). In addition, the thickness of the loosened layer could have an effect on the evaporation, but this was not investigated further in our study, since we did not have information about this surface layer thickness. Assouline et al. (2014); Li et al.(2020); and Shokri et al. (2010)discussed the effect of soil layering on evaporation. They considered layers of different textures and quantified the effect of soil layering in terms of the unsaturated hydraulic properties of the soil layers, (i.e., the characteristic length; Lehmann et al.(2008)). These concepts could also be applied to layers with a different soil structure. Implementing a surface layer with different SHPs because of a change in soil structure due to soil loosening improved the simulation results, but except for 2017, E_{tilled} was larger than E_m.

A second set of SHP parameters were derived from in situ measurements of water content and soil water pressure heads. Even though the saturated hydraulic conductivity was still estimated from soil texture, using in situ measured water retention curves improved the estimation of the evaporation rates considerably. The in situ measured retention curves suggested a wider pore size distribution than the retention curves that were derived from PTFs. This resulted in lower estimates of the unsaturated hydraulic conductivity using the capillary model of Mualem (van Genuchten, 1980) and consequently in a lower simulated evaporation and a better agreement with the measured evaporation.

The simulated evaporation rates were very sensitive to the SHP used. In analogy to Lehmann et al. (2008), we derived a characteristic length of evaporation (L_c) from the soil hydraulic soil properties and found that L_c can be used to compare evaporation that is predicted for different SHPs. We also confirmed the conclusion by Lehmann et al. (2020) that SHPs derived from soil texture using PTFs may have unrealistically large L_c values for soils with a medium soil texture and consequently lead to overestimations of evaporation losses from these soils.

It must also be taken into account that the soil profiles in this study were assumed to be vertically homogeneous with respect to their hydraulic properties. In reality, natural soils often exhibit vertical heterogeneity due changes in texture and structure with depth. Such vertical variations in soil hydraulic properties can affect water flow and soil evaporation. Ignoring this heterogeneity may therefore contribute to discrepancies between simulated and measured evaporation. Consequently, the assumption of homogeneous soil profiles may have led to an overestimation of evaporation in our simulations. Besides the soil texture, the influence of soil color on albedo and how it affects soil temperature and evaporation should be considered as one interacting factor. Gascoin et al. (2012) used a land surface model and hourly meteorological data, to investigate the effect of coupling bare soil albedo with surface soil moisture on a moraine. One result is that implementing the effect of soil moisture on bare soil albedo importantly influences the surface fluxes at the monthly and annual scale.

The Richards equation considers only liquid flow in the soil and uses a pressure head boundary at the soil surface to simulate the evaporation when the water pressure head reaches a threshold value. The Richards equation simulated bare soil lysimeter evaporation losses quite well when appropriate SHPs were used, including how they were reduced compared with the potential evaporation losses, estimated with the FAO-PM method scaled by an empirical coefficient (Allen et al., 2005). The use of a threshold boundary condition in the Richards equation decouples simulated evaporation dynamics from the dynamics of evaporative forcing and heat fluxes during stage-II and forces the simulated evaporation rate to decrease monotonously over time when the soil dries out (Vanderborght et al., 2017). As was already shown using numerical simulations (Assouline et al., 2013; Fetzer et al., 2017) and is now further confirmed by measurements, this approach it is not able to reproduce diurnal dynamics when vapor transport in the porous medium is more important than liquid flow and vapor concentration in the soil increases during a day due to an increase in soil temperature. Neither can an increase in daily evaporation during stage-II, due to for instance a higher radiative forcing, be reproduced by this model. Other boundary conditions (e.g., using resistance terms that depend on surface soil moisture; van de Griend & Owe, (1994)) could be implemented to represent diurnal evaporation dynamics. Especially in loosened surface layers with large interaggregate pores, advective air flow may enhance vapor transport (Farrell et al., 1966; Ishihara et al., 1992; Kimball & Lemon, 1971; Maier et al., 2012; Scotter & Raats, 1969). Further research is needed to evaluate and quantify the impact of soil surface management practices, which influence soil structure and surface roughness and which aim at reducing soil evaporation losses.

Since the soil evaporation was in general smaller than E_{pot}, except during some nights, we could not test the FAO-PM approach to calculate the potential evaporation of a wet soil surface. An important assumption in the PM is that the soil heat flux at the soil surface can be approximated as a fraction of the net radiation. When fluxes are averaged or accumulated over a longer time, this approximation may provide quite accurate results. However, over shorter times, when soil heat fluxes can make an important contribution in the surface energy balance, a more accurate estimation of the soil heat flux may be required - for instance, to obtain better estimates of the variation in daily evaporation. In this case, if soil heat flux is of concern and a better estimate for diurnal variations in potential evaporation is needed, models as developed by Evett et al. (2012) can give estimates that are more accurate.

2.6 Conclusion

Our study is evaluating a unique data set of measurements under natural outdoor conditions in natural undisturbed soil for three years with different climatic conditions. The comparison of the simulations shows that estimates of evaporation are sensitive to the choice of SHPs. SHPs derived from texture-based pedotransfer functions overestimated evaporation, especially in the silty loam, due to unrealistically high hydraulic conductivities and characteristic lengths of evaporation. Using in situ measured water retention curves improved simulations by giving more realistic estimates of unsaturated hydraulic conductivity. Incorporating a tilled surface layer with modified SHPs also improved simulations, which highlights the strong influence of soil structure and surface disturbance on evaporation dynamics.

The Richards equation reproduced cumulative evaporation losses reasonably well when appropriate SHPs were used but remained unable to capture diurnal variations or increases in stage-II evaporation driven by atmospheric forcing. This limitation arises from the use of a pressure head boundary condition that neglects vapor phase processes, thermal gradients and potential advective air flow in the surface layer.

Our work shows that accurate SHPs, preferably obtained from measurements, are important for reliable evaporation modeling; soil surface structure and management influence evaporation but are often neglected, and improved boundary conditions and vapor transport formulations are needed to capture diurnal dynamics and fully represent soil atmospheric interactions. Our findings underline the importance of accounting for both hydraulic and structural soil properties when predicting soil evaporation and provide a basis for improving models used in hydrological and agricultural applications.

With this study a data set is provided which can also be used for further studies and for the validation of more detailed models than the approach used in this research.

3 Analysis of Experimental and Simulation Data of Evaporation-Driven Isotopic Fractionation in Unsaturated Porous Media

This chapter is adapted from: Schneider, J., Kiemle, S., Heck, K., Rothfuss, Y., Braud, I., Helmig, R., & Vanderborght, J. (2024). Analysis of experimental and simulation data of evaporation-driven isotopic fractionation in unsaturated porous media. Vadose Zone Journal, 23(5), e20363.

Throughout Chapter 3 the terminology regarding isotopologues was improved and equations changed into 1-D formulations. Minor information was added for better understanding. In chapter 3.3.3 the R-VSMOW value was corrected, the correction does not have any impact on the results. The discussion and conclusion (Chapter 3.4) were complemented with information about the handling of the kinetic fractionation in DuMu^x and a paragraph about model preferences.

The **first authorship is shared**, Stefanie Kiemle contributed to this work with simulations using a multi-phase multi-component transport model that resolves flow through the near-surface atmosphere and the soil, and models transport and fractionation of the stable water isotopologueues using the numerical simulation environment DuMu^x.

As the **co-first author**, I (Jana Schneider) conducted all simulations using the SiSPAT-Isotope model, which simulates water and heat transfer in the soil-plant-atmosphere continuum and the movement and fractionation of water isotopes during processes like evaporation, condensation, and water transport through soil.

This collaborative approach allowed us to compare different modeling frameworks and develop a comprehensive understanding of evaporation driven isotopic fractionation in unsaturated porous media.

3.1 Abstract

Stable water isotopologues can add valuable information to the understanding of evaporation processes. The identification of the evaporation front from profiles of isotopic composition under very dry soil conditions is of particular interest. We compared two different models that describe isotopologue transport in a drying unsaturated porous medium, SiSPAT-Isotope and DuMu^x. In DuMu^x, the medium can dry out completely whereas in SiSPAT-Isotope, drying is limited to the residual water saturation. We evaluated the impact of residual water saturation on simulated heavy isotopologue enrichment. For a low residual water saturation, both models simulated similar heavy isotopologue enrichment. For high residual water saturation, SiSPAT-Isotope simulated considerably lower heavy isotopologue enrichment than DuMu^x. This is attributed to the buffering of changes in isotopologue composition by the residual water in SiSPAT-Isotope and an additional enrichment of heavy isotopologues due to evaporation of residual water in DuMu^x. Additionally, we present a comparison between high-frequency experimental data and model simulations. We found that diffusive transport processes in the laminar boundary layer and in the dried-out surface soil layer need to be represented correctly to reproduce the observed downward movement of the evaporation front and the associated peak of heavy isotopologue enrichment. Artificially increasing the boundary layer thickness to reproduce a decrease in evaporation rate leads to incorrect simulation of the location of the evaporation front and isotopic composition profile.

3.2 Introduction

Evaporation is a key variable in the global water cycle depending on the land surface type, soil evaporation makes up 10 % to 87 % of the total evapotranspiration (Rothfuss et al., 2021). Especially in dry regions, soil evaporation can account for up to 95 % of the total evapotranspiration (Kool et al., 2014; Wilcox et al., 2003). Soil evaporation is defined as the water loss from the soil surface that is not associated with carbon assimilation by the vegetation. Reducing the water loss caused by soil evaporation increases the amount of water that can be used for plant transpiration, which is linked with carbon uptake by vegetation. Consequently, this uptake leads to an increase in vegetation growth and crop growth, and finally to enhanced crop yields. Especially in dry regions and in terms of climate change, reducing soil evaporation is a key process to optimize water use management (Anderson et al., 2017; Boutraa et al., 2010; Kool et al., 2014; Milly et al., 2005; Oki & Kanae, 2006). Water-stable isotopologues ($^{1}H^{2}H^{16}O$ and $H_2^{18}O$) are powerful tracers for water flow in soil-plant-atmosphere systems (Braud et al., 2005; Dubbert & Werner, 2019; Rothfuss et al., 2021; Rothfuss & Javaux, 2017; Yakir & Sternberg, 2000), as their transport and gas-liquid exchange behavior differs from $H_2^{16}O$. This difference in transport behavior leads to a change in heavy isotopologue enrichment in the pore water that is related to evaporation rates. Furthermore, they can be used to infer how incoming water with a different isotopic signature than the water present in the soil pores intermixes and displaces pore water (Braud et al., 2005; Herczeg & Leaney, 2011; Rothfuss et al., 2010, 2015). Consequently, the variation in the ratio of soil water isotopes ($\delta^{2}H$, $\delta^{18}O$) provides information about flow, mixing within the unsaturated zone, the evaporation front, and interactions between atmosphere and soil. Especially for evaporation, measurements of isotope ratio profiles can be used to assess evaporation rates and the depth of the evaporation front in the soil profile, as evaporation processes at the soil surface and within the soil lead to an enrichment of the heavier water isotopologues in the liquid phase (Rothfuss et al., 2021).

Modeling the transport of isotopologues in the unsaturated zone can enhance the understanding of the influencing parameters of evaporation and can be used to assess water management strategies. There are several models available that can model isotopologue transport and fractionation for that purpose. State-of-the-art for water-stable isotopologue modeling is the Simple Soil-Plant-Atmosphere Transport model (SiSPAT-Isotope), which is a soil-vegetation-atmosphere transfer model including a module for isotopologue transport in the soil and within plants (Braud et al., 2005; Haverd & Cuntz, 2010). The liquid water flow and vapor transport model is based on the Philip and de Vries (1957) model. Another model based on the same physical processes is Soil-Litter-Iso (Haverd et al., 2011; Haverd & Cuntz, 2010), developed to be used on a regional scale based on Ross' fast solution to the Richards equation (Ross, 2006). Additionally, the HYDRUS-1D model can simulate isotopologue transport while accounting for evaporation fractionation (Zhou et al., 2021). The fractionation process is based on the same equations as the SiSPAT-Isotope module. Recently, Kiemle et al.(2023) presented a model for isotopologue transport in a coupled soil-atmosphere model within the framework of the numerical simulator DuMu^x (Koch et al., 2021).

As isotopologue fractionation mainly occurs at the evaporation front, that is, the interface between dry and wet soil, the model should be able to describe the drying of the unsaturated zone to dry soil conditions. Generally, when the soil dries out, capillary pressure rises. To describe that process on the continuum scale, commonly a relationship between capillary pressure and saturation is used (e.g., the van Genuchten relationship (van Genuchten, 1980)).

Under dry soil conditions, this relationship generally leads to large gradients and theoretically infinite capillary pressures, which makes the numerical modeling of these conditions particularly challenging. There are different possibilities to overcome these difficulties. One possibility is to regularize the capillary-pressure-saturation relationship after a certain threshold in water saturation is reached, which is the method that is used in DuMu^x. Another possibility, which is used in SiSPAT-Isotope, is to not allow complete drying of the soil but to keep a certain amount of water saturation immobile without further evaporation by setting a maximum capillary pressure that cannot be exceeded. If this maximum capillary pressure can be set sufficiently high so that the vapor pressure in equilibrium with this capillary pressure is lower than the minimum vapor pressure simulated or observed, then the fluxes from the porous medium to the soil surface can be matched to the fluxes in the free flow boundary layer, taking into account the flow and transport resistances in the porous medium and the boundary layer defined by their properties and states. However, when this maximal capillary pressure is reached in the simulation and kept constant, the vapor pressures at the soil surface cannot further drop so that fluxes through the boundary layer and evaporation rates would stay constant whereas the fluxes from the drying porous medium toward the soil surface decrease further. To avoid this discrepancy in a coupled simulation, the boundary layer thickness should be increased. These differences in the handling of very dry soil conditions, not only change simulated evaporation rates but also have implications for isotopologue transport and fractionation. One goal of this paper is to compare the isotopologue transport described in SiSPAT-Isotope with the implementation in DuMu^x, especially highlighting the differences that occur in dry soil with water saturation below residual water saturation. Further, we will present a comparison of the simulated isotope ratio profiles with the high-frequency experimental data from Rothfuss et al. (2015).

Since the experimental conditions in the laboratory experiments did not allow us to precisely define the surface boundary conditions, which are essential for modeling evaporation, we had to derive them from the measured evaporation rates. Therefore, the aim of our simulation study is not to simulate the evaporation (which we basically prescribe) but to simulate the evaporation-driven isotope fractionation, that is, the evolution in time and depth of the isotope ratioss in the soil profile.

A comparison of modeled isotopologue fractionation in the unsaturated zone with detailed experimental data is missing in the literature. Last, we will show that the evaporation front can be detected at the maximum gradient of isotope ratios.

3.3 Methods

In this section, we introduce the general mathematical concepts of DuMu^x and SiSPAT-Isotope to describe mass and energy transport within a porous medium.

3.3.1 Mathematical Concept

Note, that we use the following abbreviations to describe our systems. We use the components κ: water (H_2O), dry air (air), and stable water isotopologue (i, for all isotopologues). The phase (α) is either referred to as liquid (l) or gaseous (g) or solid (s). The abbreviation (ff) is used for the free-flow domain (atmosphere domain) and the abbreviation (pm) is for the porous-medium domain (soil domain). All processes are described on the representative elementary volume (REV)-scale.

Note, a detailed description of the assumptions for the mass and energy balance concepts used in DuMu^x and SiSPAT-Isotope can be found in Vanderborght et al. (2017).

3.3.1.1 Mass and Energy Transport in the Porous Medium

DuMu^x-Mass Balance

To describe non-isothermal, multi-component, multi-phase flow within a porous medium, DuMu^x implicitly solves a multi-phase Darcy's law in combination with a mass and energy balance. The component mass balance for all components κ can be described as follows:

$$\sum_{\alpha\in\{l,g\}}\left(\phi\frac{\partial}{\partial t}\left(\rho_\alpha X_\alpha^\kappa S_\alpha\right)+\frac{\partial}{\partial z}\left(v_\alpha\rho_\alpha X_\alpha^\kappa\right)-\frac{\partial}{\partial z}\left(D_{\alpha,pm}^\kappa\rho_\alpha\frac{\partial X_\alpha^\kappa}{\partial z}\right)\right)=q^\kappa\forall\kappa\in\{H_2O,air,i\}$$

3-1

Here, ϕ [-] is the porosity, ρ_α [kg m^{-3}] the mass density, X_α^κ [kg kg^{-1}] is the mass fraction, $D_{pm,\alpha}^\kappa$ [m^2 s^{-1}] is the effective diffusion coefficient, and q^κ [kg m^{-3} s^{-1}] accounts for the source/sink term. As we are regarding all processes on the REV-scale, we introduce an effective parameter, namely the phase saturation S_α [m^3 m^{-3}]. The sum of the saturation for all phases within a REV equals 1. The fluid-phase flux v_α [m s^{-1}] is described using the multi-phase Darcy's law:

$$v_\alpha=-\frac{k_{r,\alpha}}{\mu_\alpha}k_i\left(\frac{\partial p_\alpha}{\partial z}-\rho_\alpha g\right)$$

3-2

with the relative permeability $k_{r,\alpha}$ [-], the dynamic viscosity μ_α [Pa s], the phase pressure p_α [Pa], and the intrinsic permeability k_i [m^2]. The gravity is described by g[m s^{-2}].

The effective diffusion coefficient is defined as:

$$D_{pm,\alpha}^{\kappa} = \phi S_\alpha D_\alpha^{k,j} \tau \, . \qquad \text{3-3}$$

Here, τ [-] is the tortuosity factor and $D_\alpha^{\kappa,j}$ [m^2 s^{-1}] is the binary diffusion coefficient (of components κ and in phase α). Because of the low advection velocities and the high diffusion coefficient in the gaseous phase, dispersion is not considered in the model concepts. The same applies to the liquid phase because the liquid velocities are very low. Under these conditions molecular diffusion dominates over mechanical dispersion. If velocities were higher, dispersion would need to be included explicitly.

DuMu^x - Energy Balance

For energy transport, we assume a local thermodynamic equilibrium between the phases. Thus, for all phases, the energy balance is written as follows:

$$\sum_{\alpha \in \{l,g\}} \left(\phi \frac{\partial \left(\rho_\alpha S_\alpha u_\alpha \right)}{\partial t} + \frac{\partial \left(\rho_\alpha h_\alpha v_\alpha \right)}{\partial z} \right) + \left(1 - \phi \right) \frac{\partial \left(\rho_s c_s T \right)}{\partial t} - \frac{\partial}{\partial z} \left(\lambda_{pm} \frac{\partial T}{\partial z} \right) = 0$$

3-4

The energy transport is described by the specific internal energy u_α [J kg^{-1}], the specific enthalpy h_α [J kg^{-1}], and the temperature T [K]. Further, to account for the energy storage of the solid phase, we use the solid heat capacity c_s [J kg^{-1} K^{-1}] and the solid density ρ_s [kg m^3].

The heat conductivity is defined by using an effective thermal conductivity λ_{pm} [W m^{-1} K^{-1}] to account for the changes in thermal conductivity based on the saturation of the porous medium:

$$\lambda_{pm} = \lambda_{dry} + \sqrt{\left(S_l \right)} \left(\lambda_{wet} - \lambda_{dry} \right) \qquad \text{3-5}$$

with $\lambda_{wet} = \lambda_s^{(1-\phi)}\lambda_l^{\phi}$ and $\lambda_{dry} = \lambda_s^{(1-\phi)}\lambda_g^{\phi}$, where λ_s, λ_g, and λ_l [W m^{-1} K^{-1}] are the solid phase, gas phase, and liquid phase conductivities, respectively.

SiSPAT-Isotope - Mass Balance

The SiSPAT-Isotope model simulates the transport of heat, water, and its heavier stable isotopologue within the soil-plant-atmosphere continuum making a few simplifications compared to the full two-phase four-component approach used in DuMu^x. Coupled heat and water transfer equations within the soil, including the liquid and vapor transfer, are solved with the approach of Philip and de Vries(1957), modified by Milly (1982). SiSPAT-Isotope considers only vertical fluxes. The pressure in the gas phase is assumed to be constant and not influenced by flow in the gas or liquid phase so that the flow in the liquid phase is not coupled to flow in the gas phase. Considering only vertical fluxes, the gas velocity, v_g [m s^{-1}] at a certain depth is calculated from the change in volumetric gas content per unit of time that is integrated over depth from that depth to the bottom of the simulation domain assuming a no-flow boundary condition for the gas flow at the bottom of the simulation domain. Further, the advection in the liquid phase is not influenced by the pressures of the gas phase, and gradients in the liquid phase density are assumed to be negligible. The approach does not further consider a coupling between the transport of the water components and the dry air component, which is based on the approximation that the dry air component in the liquid phase can be neglected $\sum_{\kappa \neq \alpha} X_l^{\kappa} \approxeq 1$. Also, we assume that in equation (3-6), all water isotopologues are combined as one component $X_{\alpha}^{\mathrm{all}_{H_2O}}$. Assuming these simplifications for the multiphase flow equation, the following equation can be named as a 1-component, 1.5-phase equation, as water is regarded as the only component and (Vanderborght, Fetzer, Mosthaf, Smits, & Helmig, 2017):

$$\phi\frac{\partial\rho_g X_g^{all_{H_2O}} S_g}{\partial t}+\phi\frac{\partial\rho_l X_l^{all_{H_2O}} S_l}{\partial t}+\frac{\partial}{\partial z}\left(v_l\rho_l X_l^{all_{H_2O}}\right)+$$
$$\frac{\partial}{\partial z}\left(v_g\rho_g X_g^{all_{H_2O}}\right)-\frac{\partial}{\partial z}\left[\rho_g D_{pm,g}^{all_{H_2O}}\frac{\partial X_g^{all_{H_2O}}}{\partial z}\right]=0$$

3-6

SiSPAT-Isotope - Energy Balance

The basic heat equation used in SiSPAT-Isotope is taken from de Vries (1958):

$$\frac{\partial}{\partial z}\left[\left(D_{g,pm}^{H_2O}L_v\right)\frac{\partial\rho_g X_g^{H_2O}}{\partial z}+\lambda_{pm}\frac{\partial T}{\partial z}-v_g\rho_g c_g T-v_l\rho_l c_l T\right]$$
$$-\left(\phi S_g c_g\rho_g+\phi S_l c_l\rho_l+(1-\phi)c_s\rho_s\right)\frac{\partial T}{\partial t}-L_v\frac{\partial\rho_g X_g^{H_2O}}{\partial t}=0$$

3-7

Where c_α [J kg^{-1} K^{-1}] is the heat capacity of phase α and L_v [J kg^{-1}] is the latent heat of vaporization of liquid water. Compared to equation (3-4), the heat used during gas phase expansion is neglected.

3.3.1.2 Constitutive Relations for Modeling of Drying Within The Porous Medium Domain

In the unsaturated zone at equilibrium conditions, a pressure difference - capillary pressure, p_c [Pa] between the fluid phase (liquid, p_g [Pa]) and gas phase (gaseous phase, p_l [Pa]), is observed:

$$p_c=p_g-p_l \qquad 3\text{-}8$$

On the REV scale, capillary pressure depends on water saturation. A common method to describe the dependence of capillary pressure on saturation for two-phase systems is the van Genuchten model (van Genuchten, 1980). Here, the wetting phase saturation is expressed as a function of capillary pressure using empirically determined parameters:

$$S_{we} = \left[1 + \left(\alpha_{vG} p_c \right)^{n_{vG}} \right]^{-m_{vG}}, \tag{3-9}$$

with $m_{vG} = 1 - \frac{1}{n_{vG}}$ and $S_{we} = \frac{S_w - S_{wr}}{1 - S_{wr} - S_{nr}}$. $\alpha_{vG}, m_{vG},$ and n_{vG} are empirical parameters describing soil properties. Residual water saturation S_{wr} and residual gas saturation S_{nr} are empirical parameters expressing the saturation threshold where respectively the wetting or non-wetting phase becomes immobile. S_{we} denotes the effective wetting saturation. In SiSPAT-Isotope, the van Genuchten model describes the volumetric water content $\theta = \phi S_w$, using the residual water content $\theta_r = \phi S_{wr}$ and the saturated water content $\theta_{sat} = \phi(1 - S_{nr})$.

The relative permeability $k_{r,\alpha}$ likewise can be modeled as a function of saturation (Mualem, 1976; van Genuchten, 1980) with:

$$k_{r,l} = \left(S_{we} \right)^{0.5} \left[1 - \left(1 - S_{we}^{\frac{1}{m_{vG}}} \right)^{m_{vG}} \right]^2, \tag{3-10}$$

$$k_{r,g} = \left(1 - S_{we} \right)^{0.5} \left[1 - S_{we}^{\frac{1}{m_{vG}}} \right]^{2 m_{vG}} \tag{3-11}$$

As mentioned before, DuMu^x and SiSPAT-Isotope handle very dry soil conditions differently. During drying, before the residual water saturation is reached, both models calculate the relationship between capillary pressure and saturation with the van Genuchten model. Assuming chemical equilibrium in the porous medium, the vapor concentration in the gas phase is related to the capillary pressure using Kelvin's equation $p^{\kappa}_{sat,Kelvin}$ [Pa], and the saturated vapor pressure p^{κ}_{sat} (when $p_c = 0$) is related to the temperature:

$$p^{\kappa}_{sat,Kelvin} = p^{\kappa}_{sat} \exp\left(-\frac{p_c}{\rho_l RT} \right) \tag{3-12}$$

where R [J mol^{-1} K^{-1}] describes the universal gas constant. If vapor transport is considered, liquid water can be lost via vapor transport and water saturation may decrease to values lower than the residual saturation. Consequently, the capillary pressure-saturation relation can be extended between $S_l = S_{wr}$ and $S_l = 0$. Once the residual water saturation is reached, in DuMu^x, the capillary pressure-saturation curve is regularized to avoid infinite capillary pressures. This allows the fact that the water saturation can fall below residual water saturation, as drying due to evaporation and transport of water vapor in the gas phase is still possible. Advective transport in the liquid phase is not possible anymore, due to the relative permeability becoming zero once residual water saturation is reached (Figure 3-1). Using such regularization methods results in numerical stable solutions, which is discussed by Mosthaf et al.(2014).

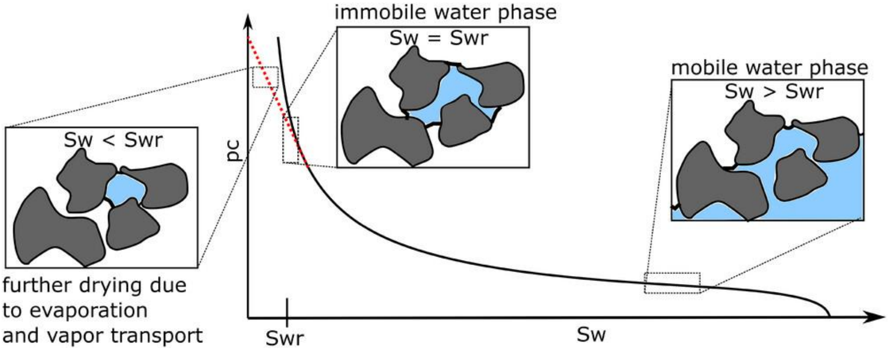

Figure 3-1: Capillary pressure-saturation relationship and its regularization (denoted with the red, dotted line) once residual water saturation is reached. The regularization in DuMu^x is described by a linear relation between capillary pressure and water saturation between $S_l = S_{wr}$ and $S_l = 0$.

In SiSPAT-Isotope, drying is limited by the residual water saturation. An approach describing the physical behavior of the capillary pressure–saturation relationship more accurately was also implemented in SiSPAT-Isotope but was not used in our simulations because of numerical instabilities. In this approach, the capillary pressure–saturation relation is described by a log-linear relation that was found to describe empirical observations well (Schneider & Goss, 2012). Other approaches to describe the capillary pressure-water saturation relation in dry soils can be found in, for example, Campbell et al. (G. Campbell & Schiozawa, 1992)and Fayer and Simmons (1995).

This difference in handling of porous media with very low water saturations not only leads to differences in the description of evaporation but also has implications for the fractionation of isotopologues as demonstrated in the following after introducing the processes leading to fractionation in general.

3.3.2 Physical Processes of Evaporation-Driven Stable Water Isotopologue Fractionation

3.3.2.1 Stable Water Isotopologue Fractionation in General - Equilibrium and Kinetic Fractionation

Natural stable water isotopologues move in the soil pore space both in the gaseous and liquid phases and exchange continuously between the two phases. Due to a difference in molecular weight of different isotopologues, the ratio of the thermodynamic equilibrium concentrations of an isotopologue in the two phases differs from the ratio of the H_2O molecule concentrations, which leads to a higher abundance of heavier isotopologues in the liquid phase and lower abundance in the gas phase, called equilibrium fractionation. Equilibrium fractionation can be expressed using the fractionation factor α_{eq}^{i} [-], which is equal to the ratio of the molecular isotopic ratios in the gas and liquid phases and related to the ratio of concentrations of the isotopologues in both phases as (Braud et al., 2005):

$$\alpha_{eq}^{i} = \frac{x_g^i / x_g^{H_2O}}{x_l^i / x_l^{H_2O}} = \frac{\rho_l}{\rho_g^{H_2O}} \frac{C_g^i}{C_l^i} = \exp\left(-\left(\frac{a}{T^2} + \frac{b}{T} + c\right)\right) \qquad \text{3-13}$$

where x_α^κ are the mole fractions [-] of $\kappa \in \{H_2O, i, air\}$ and $i \in \{{}^1H\,{}^2H^{16}O,\ {}^1H_2^{18}O\}$ in the phase $\alpha \in \{l, g\}$, ρ_l and $\rho_g^{H_2O}$ [kg m^{-3}] are the volumetric mass densities of the liquid phase and of the water vapor in the gas phase, respectively, and C_g^i and C_l^i [kg m^{-3}] are the concentrations of the isotopologue in the gas and liquid phases, respectively. The relation is approximate for the concentrations and is based on the assumption that the molar and mass fractions of the heavier isotopologues are negligible compared to the mass fraction of H_2O. The coefficients a, b, and c for the isotopologues ${}^1H\ {}^2H^{16}O$ and ${}^1H_2^{18}O$ are listed in Table A 4.

Table 3-1: Parameter for transport, hydraulic, and thermal properties.

Parameter	Values
Tortuosity τ	0.67 [-]
Porosity ϕ	0.44 [-]
Permeability, k	1.29*10^{-11}[m^2]
Residual water Saturation, S_{wr}	0.1364 [-]
Residual gas saturation, S_{nr}	0.1911[-]
van Genuchten parameter, n_{vG}	5.4 [-]
van Genuchten parameter, α_{vG}	0.00031 [Pa^{-1}]
Solid density, ρ_s	2650 [kg m^{-3}]
Solid thermal conductivity, λ_s	2.8 [W m^{-1} K^{-1}]
Solid heat capacity, c_s	507.53 [J kg^{-1} K^{-1}]

Due to the different transport behavior of isotopologues, that is, due to different binary molecular diffusion coefficients of isotopologues, vapor transport resulting from a gradient in vapor concentration and molecular diffusion will correspond with a greater flux of lighter than heavier isotopologues. The different binary molecular diffusion coefficients are listed in Table A 4.

This flux difference between lighter and heavier water isotopologues leads to kinetic fractionation. When vapor transport in the porous medium is described in the transport models, kinetic fractionation resulting from vapor fluxes in the porous medium emerges from the transport equations. The kinetic fractionation that results from the evaporation of water at the free-flow porous-medium interface is due to a slower molecular diffusive transfer of the heavier isotopologues through the boundary layer in the free flow (see Section 3.3.3 for more details).

3.3.2.2 Simulation of Isotopic Fractionation in the Drying Porous Medium

Isotopic fractionation in the porous medium is simulated by solving the component transport equations (or mass balance equations) in the different phases. In DuMu^x, this corresponds to solving mass balances for four components (Eq. 3-1): the components $H_2O, air, H_2^{18}O$

and ${}^{1}H\ {}^{2}H^{16}O$. In SiSPAT-Isotope, one mass balance equation for all water components in both liquid and gaseous phases is solved (Eq. 3-6). Since H_2O is the main component, it is assumed that the total water balance can be described using transport coefficients (diffusion in gas and liquid phases and relations between capillary pressure and water vapor pressures) of H_2O and is not influenced by the transport of the heavier water-stable isotopologues water components.

The transport of heavier water-stable isotopologues is described in SiSPAT-Isotope using a mass conservation equation with isotopologue-specific transport coefficients (diffusion coefficients and equilibrium fraction factors) (Braud et al., 2005; Melayah et al., 1996):

$$\frac{\partial}{\partial z}\left[D_{l,g}^{i}\frac{\partial \rho_l X_l^i}{\partial z}-v_{l,g}\rho_l X_l^i\right]-\frac{\partial\left[\Theta^i\rho_l X_l^i\right]}{\partial t}=0, \quad 3\text{-}14$$

$$\Theta^i=\phi\left[S_l+\left(1-S_l\right)\beta^i\right] \quad 3\text{-}15$$

$$v_{l,g}=\left(v_l+\beta^i v_g-D_{g,pm}^{i}\frac{\partial\beta^i}{\partial z}\right) \quad 3\text{-}16$$

$$D_{l,g}^{i}=\left(D_{l,pm}^{i}+D_{g,pm}^{i}\beta^i\right) \quad 3\text{-}17$$

where $\beta^i=\alpha_{eq}^{i}\frac{\rho_g^{H_2O}}{\rho_l}$, where α_{eq}^{i} is the equilibrium fractionation factor as defined in Equation 3-12 and Θ^i accounts for variations of β^i in time. Equation 3-14 is the same as Equation 3-1.

As mentioned before, the difference in the handling of very dry porous media, when water saturation reaches residual water saturation, can have a strong influence on isotopic fractionation, as depicted in Figure 3-2.

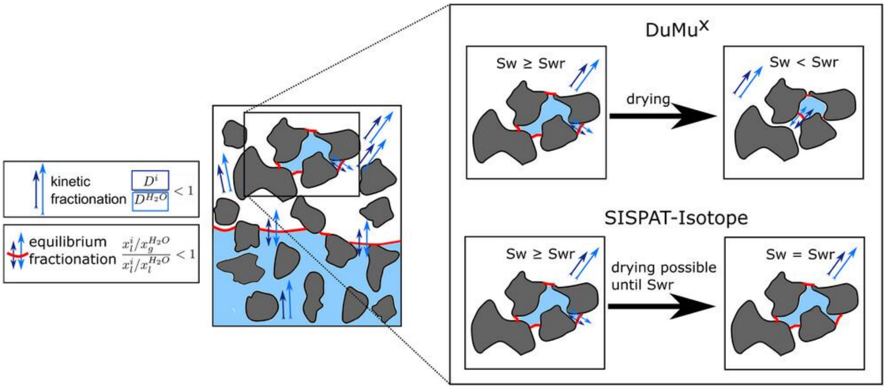

Figure 3-2: Left: Fractionation processes in the porous medium. Right: Drying and fractionation of isotopologues in DuMu^x and SiSPAT-Isotope under dry soil conditions.

In DuMu^x, water saturation can drop below residual saturation, which means that more water can evaporate leading to more diffusive transport, kinetic fractionation, and more enrichment of the heavier isotopologues. On the other hand, when all liquid water is evaporated, the capacity term in the isotopologue transport equation (i.e., Θ^i, Equation 3-14) becomes very small so that the isotopologue concentrations near the free-flow porous-medium interface can rapidly equilibrate with the lower isotopologue concentrations in the free flow.

3.3.3 Simulation Scenario

This section describes the simulation scenario of isotopic fractionation during soil drying. The simulations were set up to reproduce a soil-drying experiment (Rothfuss et al., 2015) in which stable water isotopes were monitored non-invasively and continuously at different depths in the soil column with a high frequency. The continuous and high-frequency isotope dataset allows us to test whether the simulation models can reproduce the observed dynamics of isotopic fractionation during soil drying. To our knowledge, our study is the first that compares numerical simulations of isotopic fractionation in drying soils against such high-frequency measurements.

In the following, we briefly present the experimental setup (Rothfuss et al., 2015) and how we set up the simulations accordingly (Figure 3-3).

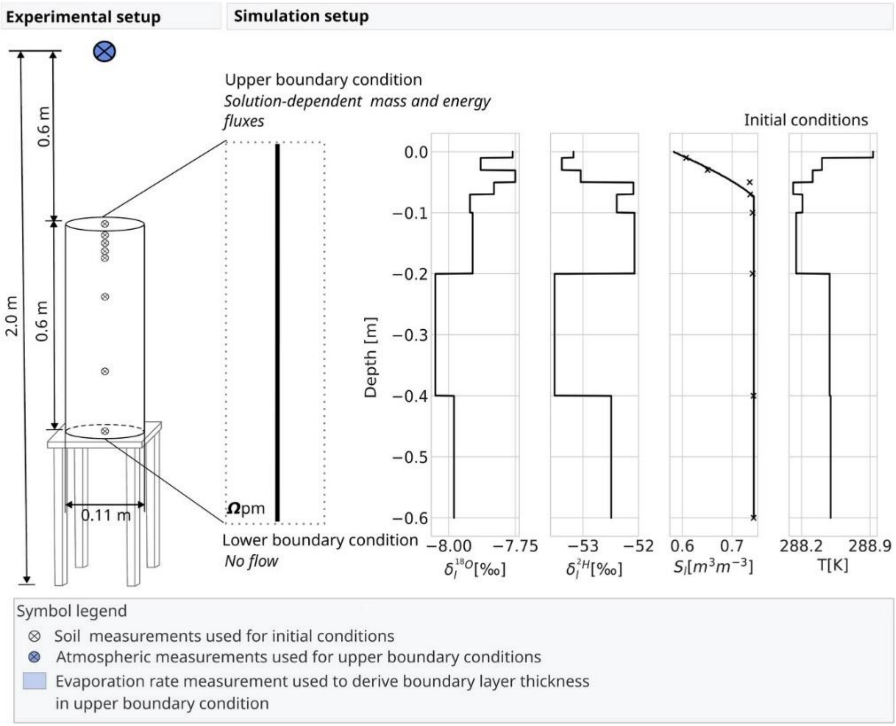

Figure 3-3: Schematic description of the experimental setup (left side) and its adaption for numerical simulations (right side). The three-dimensional experiment was reduced to a one-dimensional simulation setup for both simulators. The domain was discretized into 600 cells (0.001 m $cell^{-1}$) in DuMu^x (finite volume method) and into 289 nodes in SiSPAT-Isotope (finite difference method). In SiSPAT-Isotope, the discretization grid was additionally refined toward the top and the bottom of the domain (min. 0.000115 m $node^{-1}$, max. 0.0201 m $node^{-1}$).

During the experiment, which was carried out in a laboratory, soil temperature, water content, and the isotopic abundances in the gas phase (here:$\delta^{18}O$ and $\delta^{2}H$) were measured at different depths (0.01, 0.03, 0.05, 0.07, 0.10, 0.20, 0.40, and 0.60 m) inside an initially water-saturated sand (FH31) column (inside diameter = 0.11 m, height = 0.6 m) over a period of 290 days. Soil temperature was measured in each depth with a type K thermocouple (Greisinger Electronic GmbH). For soil water content measurements, electric conductivity sensors (EC-

5, Decagon Devices) were taken. Isotopic analysis of liquid water and water vapor was performed using a cavity ring-down spectrometer (L1102-i, Picarro, Inc.) (Rothfuss et al., 2015).

In addition to the soil measurements, the atmospheric conditions 2 m above the sand column (air temperature, relative humidity, and $\delta\ ^2H$, $\delta^{18}O$ in the gaseous phase) and the evaporation rate were monitored. Air relative humidity and temperature were monitored with a combined relative humidity and temperature sensor (RFT- 2, UMS GmbH). For the analysis of isotopes, laboratory air was sampled passively with a stainless-steel tubing at 0.6 m above the soil surface (Figure 3-3 "Atmospheric measurements").

The simulation setup was designed to describe the flow and transport of the components H_2O, air, $H_2^{18}O$, and $^1H\ ^2H^{16}O$ during evaporation from a column in one dimension (here: vertical direction, domain height = 0.6 m). The parameters of the transport, hydraulic, and thermal properties are listed in Table 3-1. The values for porosity, residual water saturation, and residual non-wetting saturation were derived from the experiment by Rothfuss et al. (2015). The other parameter values are taken from experiments conducted by Stingaciu et al. (2010).

The initial conditions were derived from the soil measurements. In Figure 3-3, the initial profiles for saturation, temperature, $\delta^{18}O$ and δ^2H are displayed. While temperature, $\delta^{18}O$ and δ^2H are initially given as block profiles, saturation is initially defined as a smooth profile. The gas pressure ($p_g = 10^5\ Pa$) is kept initially constant over the column height. The boundary conditions are described by Neumann conditions. At the bottom, we apply a no-flow condition and at the top, we use solution-dependent flux conditions. The mass transfer across the soil-atmosphere interface is described by evaporation fluxes E^κ [kg m^{-2} s^{-1}]:

$$E^\kappa = \rho_g D_g^{\kappa,air} \frac{\left[X_g^\kappa\right]^{pm} - \left[X_g^\kappa\right]^{ff}}{\delta z}, \kappa \in \left\{H_2O, i\right\}, \qquad 3\text{-}18$$

and the energy transfer across the soil-atmosphere interface is described by a heat flux H_g[J m^{-2} s^{-1}]:

$$H_g = \lambda_g \frac{[T]^{pm} - [T]^{ff}}{\delta z} \qquad \text{3-19}$$

To account for the correct impact of the atmosphere on the isotopologues in the soil profile, the atmospheric conditions (here: $\left[X_g^\kappa\right]^{ff}$ and $[T]^{ff}$) are prescribed through experimental data. The boundary layer thickness δ_Z [m] is kept constant in DuMu^x ($\delta_Z = 0.005$ m) and varies with time in SiSPAT-Isotope. In both cases, the measured cumulative evaporation rate fits this value. The derivation of the boundary layer thickness in both simulators is explained in Section A.6 in the Annex. At the interface, we assume that only molecular diffusion occurs. Therefore, the kinetic fractionation is considered through the isotope-specific binary diffusion coefficient, as presented in Barnes and Allison (1984). The fractionation processes within the porous medium are defined through the component description of the isotopologues. The binary diffusion coefficients and the vapor pressure of the isotopologues (the change in vapor pressure can be also expressed by the equilibrium fractionation factor, which is explained in Section 3.3.2) have been adjusted using parametrizations from the literature. A detailed overview of these parameters can be found in Section A.4 in the Annex.

Please note, for the following analysis, the concentration of the isotopologues is evaluated using the commonly used δ-notation that relates the ratio of isotopologues to $H_2^{16}O$ R_α^i to a standard value: R_{VSMOW}: $\delta_\alpha^i := \frac{R_\alpha^i - R_{VSMOW}}{R_{VSMOW}} \times 1000[‰]$ with $R_\alpha^i = \frac{N^i}{N^{H_2O}}$ (here: N^κ [-] describes the particle number) and R_{SMOW} the standard mean ocean water (Gonfiantini, 1978)) (here: $R_{VSMOW}^{{}^1H\,{}^2HO} = 0.00031152$ and $R_{VSMOW}^{H_2^{18}O} = 0.00200520$).

In transport simulations, isotopologue concentrations derived from isotopologue ratios are used, whereas mass spectrometers directly measure isotope ratios. For $H_2^{18}O$, the isotopologue ratio is identical to the corresponding isotope ratio. In contrast, when calculating the

δ value of HDO, the reference isotopologue ratio is approximately twice the isotope ratio, assuming the contribution of the two hydrogen atoms in HDO molecules is neglected. Nevertheless, the δ_{α}^{i} values calculated from isotope ratios are identical to those obtained from isotopologue ratios.

3.3.4 Study of the Dry Zone

Despite the different treatment of the dynamics of the boundary layer thickness and related to it, the aerodynamic resistance in the boundary condition, both models simulated similar cumulative evaporation curves (Figure A 6b). The impact of the definition of the boundary layer thickness gets more significant regarding the non-cumulative evaporation rates (Figure A 6a). The increase in the aerodynamic resistance (Figure A 7) directly after the start of the numerical simulation results in a rapid decrease in the simulated evaporation in SiSPAT-Isotope. When using a constant boundary layer thickness and thus a constant aerodynamic resistance, as it is used in DuMu^{x}, a nearly constant evaporation rate is modeled in the first 25 days of the simulation, which corresponds to the so-called stage-I evaporation or energy-limited evaporation. Later, due to transport limitations in soil, the evaporation rate simulated by DuMu^{x} drops as well and transits into the so-called stage-II evaporation or diffusion-limited evaporation. In SiSPAT-Isotope, this transport limitation is a result of the increasing aerodynamic resistance. Besides the different treatments of the aerodynamic resistance in the boundary conditions, the models use different approaches dealing with the drying of the soil (Figure 3-4).

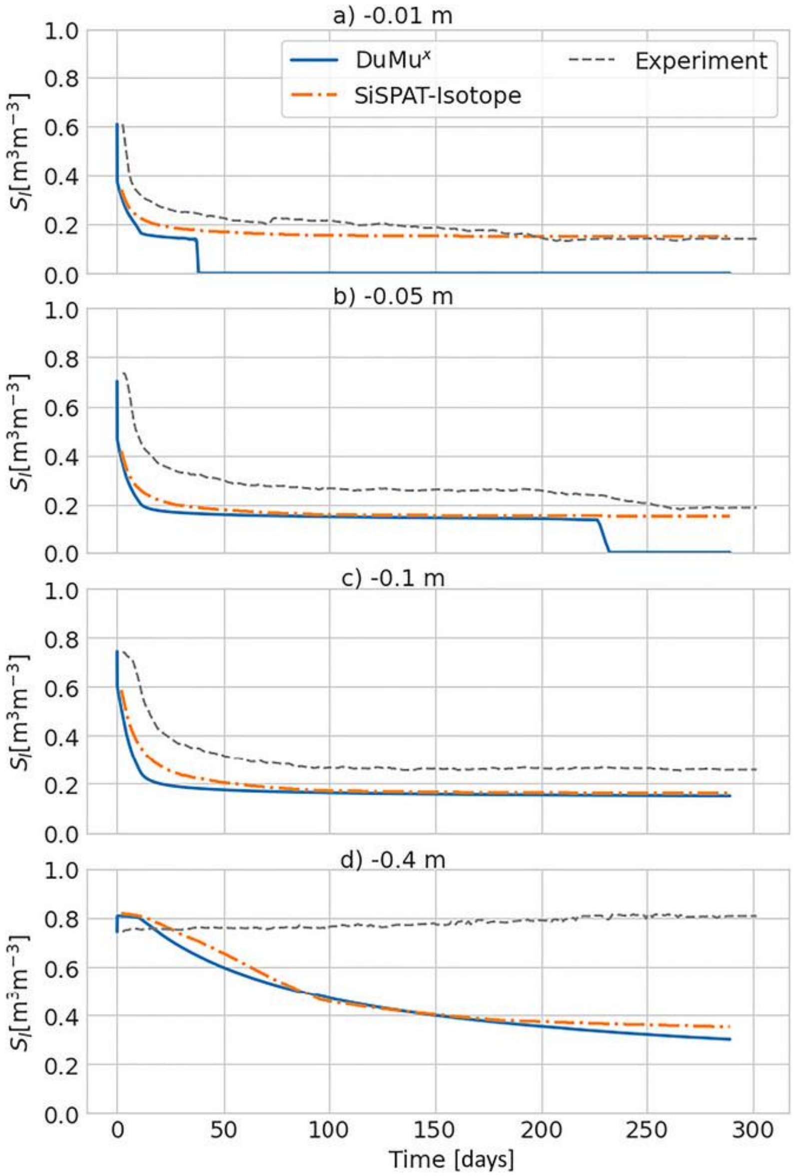

Figure 3-4: Water saturation S_l of over time at different soil column depths. The simulated values (DuMu^x [blue] and SiSPAT-Isotope [orange]) are plotted against experimental observations (gray).

The water saturation modeled by SiSPAT-Isotope reduces over time until it reaches a constant value that is equal to the residual water saturation. DuMu^x simulates a complete drying of the top-soil layers. Once the residual water saturation is reached, the saturation suddenly drops to zero saturation, for example, at -0.01 m depth after 40 days and at -0.05 m depth after 220 days. In DuMu^x, we assume that: (i) the hydraulic conductivity can drop to zero, which leads to a stoppage of the liquid flow, and (ii) that the water retention curve is linearly regularized in the regime below the residual water saturation. In the range where the saturation and capillary pressure are linearized, the capillary pressure is still quite low, which leads to a vapor concentration that is close to the saturated vapor concentration. Thus, the remaining residual liquid water can be removed via vapor diffusion. The regularization of the saturation-capillary pressure curve and assuming that no fluid flow could take place, that is, film flow was neglected, led to a rapid decrease in liquid saturation after reaching the residual saturation. Comparing the numerical results with the experimental data, the measured water saturation is higher than the simulated one. Only at -0.01 and -0.05 m depths, the water saturation gradually decreases toward the residual water saturation after 75 and 230 days of the experiment. The interpretation of the sensor measurements should be considered with caution. Since the simulations reproduce the cumulative evaporation well and the simulations close the soil water balance, the measurements seem to overestimate the water saturation. Figure 3-5 shows the relative abundance of $^{1}H\ ^{2}H^{16}O$ in pore water, expressed as $\delta_l^2 H$ and compared to measured $\delta_l^2 H$ values at different depths over time.

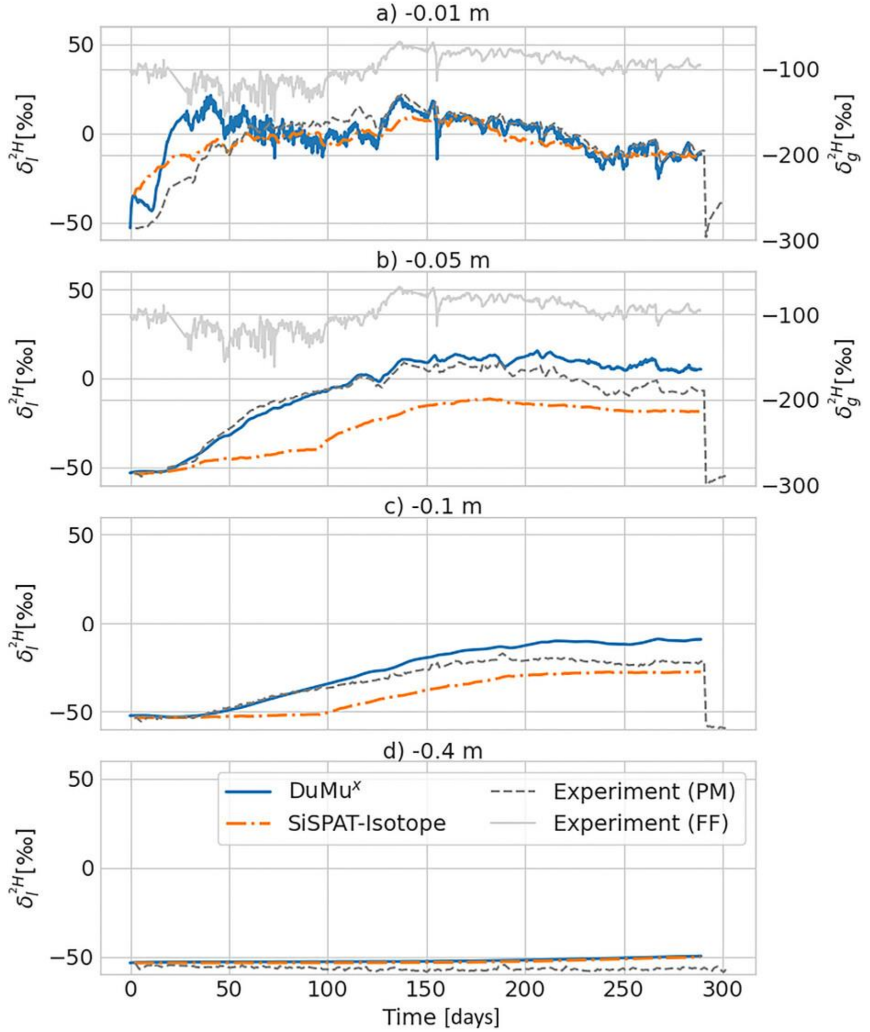

Figure 3-5: Relative abundance of ${}^1H\ {}^2H^{16}O$ in pore water, expressed as δ_l^2H, over time at different soil column depths. The simulated values (DuMu^x [blue] and SiSPAT-Isotope [orange]) are plotted against experimental observations (dark gray). In depths near the surface, the fluctuations of the atmospheric δ_g^2H values, are shown (note the different y-axis for the atmospheric δ_g^2H values (light grey line)). The abbreviation *FF* stands for the free flow (atmosphere) and *PM* for the porous medium (soil).

In Annex A.7, a similar plot for $H_2^{18}O$ is shown. We focus the discussion on the ${}^1H\ {}^2H^{16}O$ plots since the same conclusions can be drawn from the $H_2^{18}O$ plots. In the drying soil, an enrichment of ${}^1H\,{}^2H^{16}O$ and $H_2^{18}O$ toward the soil surface was observed. After reaching a maximum, δ_l^2H and $\delta_l^{18}O$ values decreased slowly, which reflects the intrusion of ${}^1H\,{}^2H^{16}O$ and $H_2^{18}O$ depleted atmospheric air into the soil's top layers. This behavior is modeled by both, SiSPAT-Isotope and DuMu^x.

Focusing on the ${}^1H\,{}^2H^{16}O$ ratios at -0.01 m, DuMu^x simulates a first local maximum directly after the start of the simulation, which was not observed in the experimental data and not modeled by SiSPAT-Isotope. This local maximum in heavy isotopologue enrichment occurred during stage-I evaporation and was also found in simulations described in Kiemle et al.(2023). We discussed the underlying mechanisms that caused this first peak in a sensitivity analysis later. For further discussions, we will refer to the first maximum as the stage-I peak and define the second peak as the stage-II peak.

To demonstrate the impact of ${}^1H\,{}^2H^{16}O$ and $H_2^{18}O$ concentrations in the atmosphere and their fluctuations on the concentrations in the soil, the measured δ_g^2H and $\delta_g^{18}O$ values in the atmosphere are included in the plots representing the near soil surface. High-frequency fluctuations in the atmospheric ${}^1H\,{}^2H^{16}O$ and $H_2^{18}O$ concentrations were observed. These fluctuations were transmitted to the concentrations in the soil and the coherence between the measured δ values in the soil and the atmosphere were strong after 120 days for both isotopologues (Figure A 7). DuMu^x reproduced these measured fluctuations in the soil after 120 days remarkably well, but they were smoothed in the SiSPAT-Isotope simulations. Since the top-soil layer in the SiSPAT-isotope simulations kept a residual water content, the buffer capacity of this layer to buffer ${}^1H\,{}^2H^{16}O$ and $H_2^{18}O$ concentration fluctuations in the atmosphere and the gas phase at the soil surface was larger than the buffer capacity of the completely dry surface layer in the DuMu^x simulations. The comparison study shows that both models are able to reproduce the general isotopic behavior from the experiments. However, the models use different assumptions with respect to water transport in the dry top-soil layer and the definition of the boundary layer at the porous medium-free flow interface.

The increase of the boundary layer thickness to describe the reduction of the evaporation rate in SISPAT-Isotope leads to a numerically stable solution. Its use should be avoided when simulating heavy isotopologue enrichment since it leads to an overestimation of the heavy isotopologue enrichment near the soil surface and does not reproduce δ_l^2H and $\delta_l^{18}O$ profiles correctly.

Under field conditions, the evaporative demand is much higher than in laboratory settings leading to comparable fast dry soil conditions after a wetting event. In combination, as laser-based measurement techniques are becoming state-of-the-art in isotopologue monitoring, we anticipate that describing the processes near the surface will be relevant to interpret the observation data. Our simulation showed a sensitivity of the isotopic composition once the soil was dried below residual saturation, which can be seen in the enrichment behavior of ${}^1H\ {}^2H^{16}O$ and $H_2^{18}O$ in response to the atmospheric fluctuations. To further study and highlight the impact of this difference in the handling of the dry zone, we next compare and analyze the sensitivity of the heavy isotopologue enrichment to the residual water saturation S_{wr}. In Figure 3-6, a comparison of DuMu^x and SiSPAT-Isotope can be seen for varying values of S_{wr}. To highlight the impact of that single parameter, the previous simulation setup was simplified by using constant boundary conditions. The values used for the constant setup are listed in Table A 5. With the change to stable atmospheric boundary conditions, the boundary layer thickness in SiSPAT-Isotope was kept constant. Thus, SiSPAT-Isotope and DuMu^x are using the same boundary conditions. To prevent numerical instabilities caused by the constant boundary layer thickness, the van Genuchten parameter was changed to n_{VG}=1.6.

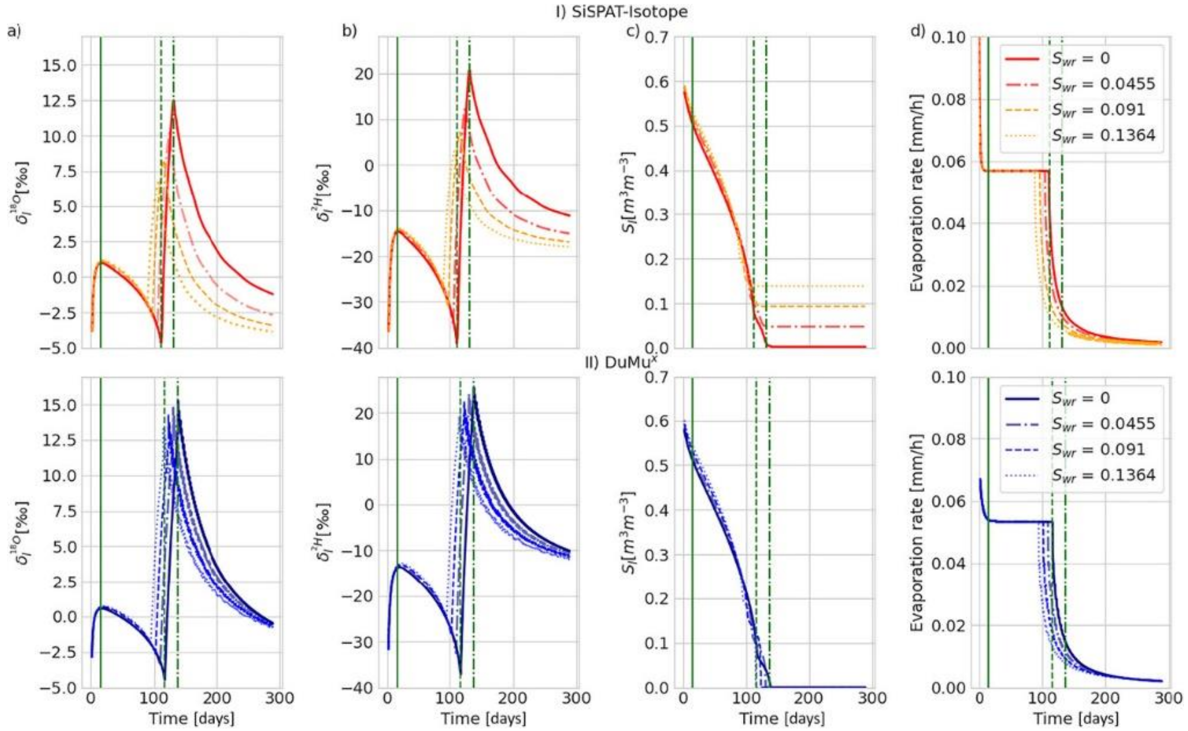

Figure 3-6: Impact of residual water saturation S_{wr} on the heavy isotopologue abundance of (a) $H_2^{18}O$ and (b) ${}^{1}H\,{}^{2}H\,{}^{16}O$, (c) the water saturation, and (d) the evaporation rate due to the different regularization methods of the drying on soils near the surface (-0.01 m depth) in SiSPAT-Isotope (orange) and DuMu^x (blue). The green lines indicate the time of occurrence of the different isotopic peaks (Case: $S_{wr} = 0$): stage-1 peak (straight; day 16), lowest isotopologue concentration (dashed; day 111 [SiSPAT-Isotope]; day 116 [DuMu^x]), and stage-II peak (dash-dotted; day 131 [SiSPAT-Isotope]; day 137 [DuMu^x]). Note, that this plot contains values only after 35 h of simulation time and no initial values. This illustration was chosen for better readability due to rapid and strong changes compared to the initial values.

With this setup, both models simulate stage-I evaporation before transferring to stage-II (Figure 3-6 d), which further results in the formation of a stage-I peak in both models (Figure 3-6 a,b). As the evaporation rate is transferring into stage-II evaporation, both models simulate a minimum in $\delta_l^2 H$ and $\delta_l^{18} O$ values followed by an enrichment of ${}^1H\,{}^2H^{16}O$ and $H_2^{18}O$ until the residual water saturation (SiSPAT-Isotope) or zero saturation (DuMu^x) is reached Figure 3-6 c). While DuMu^x allows further drying until reaching a saturation equal to zero, SiSPAT-Isotope limits its minimum saturation equal to the residual water saturation value resulting in a constant wet phase in soil. The choice of the residual water saturation and the choice of the method for describing the dry zone have an effect on the evaporation rate and on $\delta_l^2 H$ and $\delta_l^{18} O$ values.

Stage-I evaporation rate and the stage-I peak are barely affected by a higher residual water saturation (examined residual saturation range: 0-0.1364). With ongoing drying and the transition into stage-II, the impact of the residual water saturation value becomes relevant. The residual water saturation determines the availability of mobile water so that a higher residual saturation value corresponds with an earlier end of stage-I evaporation and with an earlier minimum in $\delta_l^2 H$ and $\delta_l^{18} O$ values. The stage-I peak and subsequent decline of $\delta_l^2 H$ and $\delta_l^{18} O$ values are a consequence of the very high evaporation rates at the beginning of the simulation that decline rapidly afterward until they reach a steady stage-I evaporation. This decline in evaporation rate is related to the equilibration of the soil-surface temperatures. Initially, the soil column and soil-surface temperatures are equal to the free-flow temperature. The consumption of heat for evaporation at the soil surface leads initially to a decrease in surface temperature, surface soil vapor concentration, and evaporation rate. The lower soil-surface temperatures generate a sensible heat flux from the free flow to the porous medium-free flow interface. Constant surface temperature and evaporation rates are reached when the sensible heat flux compensates for the latent heat flux. The initially high but rapidly decreasing evaporation rates correspond with an initially strong source of heavier isotopologues due to high kinetic fractionation. The decreasing source in combination with drying leads to an increasing air phase diffusion coefficient and more back diffusion of $^{1}H\,^{2}H^{16}O$ and $H_2^{18}O$ into the soil and to the advection of more depleted air into the column generating a decrease after a first strong rapid increase of δ_l^2H and $\delta_l^{18}O$ values near the soil surface during stage-I evaporation. At the onset of stage-II evaporation, the liquid flow with more water depleted in heavy isotopologues toward the evaporation surface decreases as water becomes immobile whereas the evaporation and the kinetic fractionation source continue. This leads to an increase in δ_l^2H and $\delta_l^{18}O$ values until a stage-II peak is formed. For SiSPAT-Isotope, this corresponds with reaching the residual water saturation level, and in DuMu^x, with a complete dried-out soil (S_{we}= 0). However, there is a marked difference in the dependence of the peak value on S_{wr} between the two models. In SiSPAT-Isotope simulations, the peak values decrease more with increasing S_{wr} than in DuMu^x simulations. There are two reasons that can explain this difference. When S_{wr} is larger than zero, there is always liquid water present in SiSPAT-Isotope. The liquid phase functions as a buffer to changes in δ_l^2H and $\delta_l^{18}O$ values that are generated by kinetic fractionation. The larger this buffer, the smaller the enrichment will be. Second, in DuMu^x, the residual water can evaporate. This is an additional source of evaporation at the observation depth, which leads to a stronger heavy isotopologue enrichment. The slightly higher peaks that are simulated by DuMu^x for a lower S_{wr} are due to the longer stage-I evaporation and the stronger drying with more enrichment of $^{1}H\,^{2}H^{16}O$ and $H_2^{18}O$. After the stage-II peak is reached at the observation depth, there is no evaporation happening at this depth anymore, the evaporation front moved deeper in the soil column, and the δ_l^2H and $\delta_l^{18}O$ values decreases due to intrusion of heavy isotopologue-depleted atmospheric water vapor.

3.3.5 Study of Evaporation Front

The localization of the evaporation front in drying soils is one aspect of analyzing stable water isotopologues (Walker et al., 1988). A small difference in the chemical potential between the isotopologues leads to an enrichment of the heavier isotopologues at the evaporation front. This can be seen in the δ_l^2H and $\delta_l^{18}O$ profiles in Figure 3-7. In Figure 3-7, the δ_l^2H and $\delta_l^{18}O$ profiles that are simulated by DuMu^x and SiSPAT-Isotope during a drying period are plotted together with experimental data points. The different stages of the drying period are represented through the liquid phase saturation. In Figure A 10, a detailed description of the δ_l^2H and $\delta_l^{18}O$ profiles simulated by DuMux and how they are affected by the different states of the evaporation rate is given.

a) Day 1

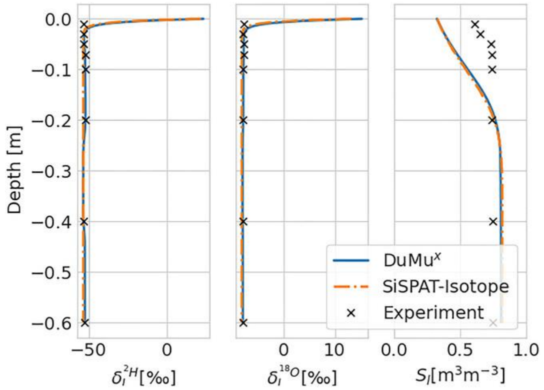

b) Day 140

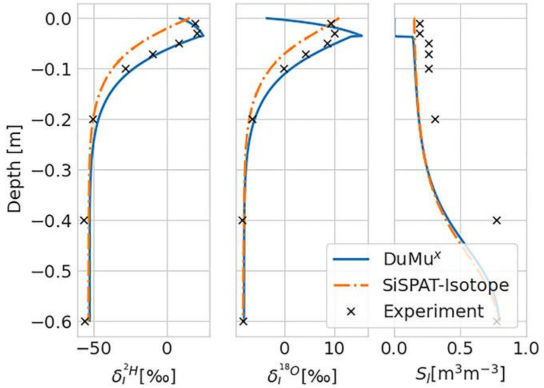

c) Day 289

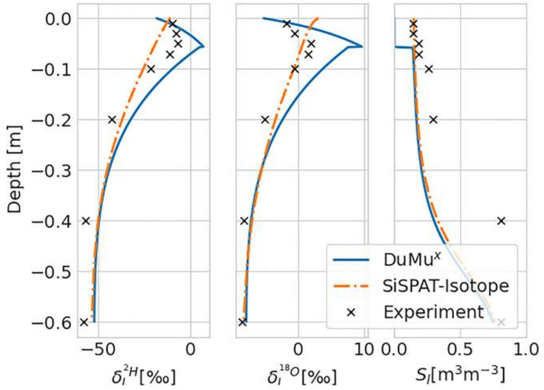

Figure 3-7: Comparison of simulated relative abundances of heavy isotopologs in the soil profile (left: $\delta_l^2 H$ middle: $\delta_l^{18} O$, right: S_l) against experimental measurements after (a) 1 day, (b) 140 days, and (c) 289 days of drying using DuMux (blue) and SiSPAT-Isotope (orange).

The results presented in Figure A 10 show three different stages of the drying soil: At day 1, the soil is still partly saturated in all soil layers. The atmospheric water demand can be fulfilled from the upper soil layers. Thus, the evaporation front and the maximum $^1H\,^2H^{16}O$ and $H_2^{18}O$ enrichment are located at the top of the domain. Both numerical models show this behavior.

Day 140 represents the middle of the drying scenario. The soil has dried out further, and the evaporation rate has switched to a stage-II evaporation behavior. In the experimental data and the numerical results derived by DuMu^x, the evaporation front indicated through a maximum in $^1H\,^2H^{16}O$ and $H_2^{18}O$ enrichment is well-defined. In SiSPAT-Isotope, the enrichment of $^1H\,^2H^{16}O$ and $H_2^{18}O$ in soils is modeled, but not the intrusion of $^1H\,^2H^{16}O$ and $H_2^{18}O$ depleted air in the dried-out zone. Here, the top boundary condition is defined by increasing the aerodynamic resistance. The higher atmospheric resistance ensures that the gas vapor concentration stays near the saturated concentration at the surface. The evaporation is simulated to occur mainly at the soil surface resulting in a maximal heavy isotopologue enrichment at the top. Switching to a constant aerodynamic resistance in the top boundary conditions, evaporation is simulated at the moving evaporation front, and SiSPAT-Isotope simulates a similar characteristic : δ_l^2H and $\delta_l^{18}O$ profile as simulated by DuMu^x (Figure A 8).

Day 289 states the end of the simulations and experiments. The findings from this state are similar to the ones on Day 140 (Figure A 10). However, the offset between the measurements and simulations is larger. The offset can have multiple reasons, for example, long runtime of experiments, correct description of drying soil.

Our results show the importance of defining the boundary conditions to simulate the correct isotopic behavior. If a decreasing evaporation rate is simulated by an increasing boundary layer thickness, the model can simulate the isotopic response in each layer, as demonstrated in Figure 3-5, but it fails to model the characteristic δ_l^2H and $\delta_l^{18}O$ profiles as depicted in Figure 3-7.

From an experimental perspective, a common measure to evaluate the evaporation front in soils is to equate the evaporation front with the height of the maximum δ_l^2H or $\delta_l^{18}O$ value (Rothfuss & Javaux, 2017). However, Rothfuss et al. (2015) stated that this measure can be used only at the isotopic steady state. For the transient state, they suggested equating the height of the maximum gradient of δ_l^2H or $\delta_l^{18}O$ values with the evaporation front. We used the highly resolved numerical models to analyze the suggestion made by Rothfuss et al. (2015). The fine resolution (600 cells (0.001 m cell^{-1}) in DuMu^x) of the numerical simulations allows us to analyze both methods on a detailed scale, but also on a coarser scale within an order of the sampling points of the experiments. Note, as we used the experimental setup on which this statement has been formulated, the numerical analysis is only performed with DuMu^x.

The procedure of both methods is quite similar. For a given time step, the sampling point where the maximal δ_l^2H or $\delta_l^{18}O$ value is observed, is used to determine the location of the evaporation front in the common approach. Sampling points were at: -0.01 m, -0.03 m, -0.05 m, -0.07 m, -0.10 m, - 0.20 m, -0.40 m, and -0.60 m. In the gradient approach, the average vertical gradient of δ_l^2H or $\delta_l^{18}O$ between each pair of neighboring observation points is calculated. The depth of the evaporation front is assigned to the layer above the interval where the maximal gradient is observed: -0.01 to -0.03 m: 0 m, -0.03 to -0.05 m: -0.02 m, -0.05 to - 0.07 m: -0.04 m, -0.07 to -0.1 m: -0.06 m. A more detailed explanation can be found in Rothfuss et al. (2015).

The comparison of both methods using the numerical simulation results using DuMu^x is displayed in Figure 3-8. To check on the performance of both methods, we compare the solutions against a refined solution where the resolution matches the resolution of the discretization grid. The analysis of the evaporation front with the fine resolution was carried out for both methods, the common and the alternative. If using a fine resolution, both methods show identical results. As the methods show identical results for the fine resolution, we compared the solutions of the coarse scale to the one of the fine scale. In

53.89 % of all data points, the alternative approach is closer to the refined solution than the common approach. The error analysis can be found in Kiemle et al. (2024). Based on these results, we cannot make a suggestion whose approach is more accurate, but we recommend further investigations on this topic to analyze under which conditions which approach is more suitable.

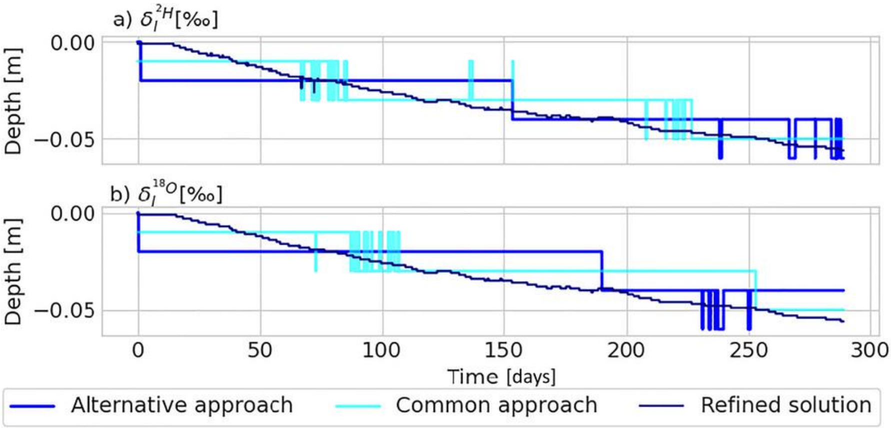

Figure 3-8: Evaporation front propagation in soil simulated by DuMu^x for (a) δ_l^2H, and (b) $\delta_l^{18}O$ values. Two approximation methods for the localization of the evaporation front, (i) alternative approach (blue line) and (ii) common approach (light-blue line), are compared against a refined solution (dark-blue line).

3.4 Conclusion and Discussion

In this study, we present a comparison study of two numerical simulators, SiSPAT-Isotope and DuMu^x. The description of water vapor movement and energy transport differs slightly between the models. Especially under very dry soil conditions, for example, occurring at the evaporation front, there are notable differences: While drying and before the soil water saturation reaches residual saturation, both models describe the relationship between capillary pressure and water saturation with the van Genuchten relationship. Once residual water saturation is reached, both models differ in their approach: In DuMu^x, the capillary pressure-saturation curve is regularized to avoid infinite capillary pressures, while in SiSPAT-Isotope, drying below residual water saturation is not possible.

Another difference between the two models is the treatment of the upper boundary conditions. In DuMu^x, a constant boundary layer thickness with a constant resistance was considered, whereas in SiSPAT-Isotope, the resistance in the boundary layer was increased to simulate a reduction in evaporation rate. We analyzed how these different methods affect isotopologue fractionation and compared the simulations with high-frequency experimental data. Furthermore, by resolving and coupling atmosphere and soil Dumu^x derive the kinetic fractionation process for the interface region without relying on a kinetic fractionation factor like SISPAT-Isotope does.

The high-frequency variations of δ_l^2H and $\delta_l^{18}O$ values that were measured in the dried-out soil layer in response to variations in the free air isotopic composition were reproduced very accurately by DuMu^x, which simulated a complete drying out of the surface layer. The reduction in water content below residual saturation was simulated to occur relatively fast and corresponded with an increase in drying rate that was observed at a certain depth. This is due to the rapid decrease in liquid water content with increasing capillary pressure whereas the vapor concentration remains close to saturation over the range of capillary pressures where the capillary pressure-saturation relation was regularized. Such high-frequency variations in δ_l^2H and $\delta_l^{18}O$ values were not simulated by SiSPAT-Isotope in which the soil did not dry out below the residual water content. Neither was an increase in drying rate at a certain depth simulated but the drying rate decreased over time.

We analyzed the influence of the value of the residual water saturation on the peak enrichment and showed that for lower residual water saturations the simulation results of both simulators match more closely. For higher residual water saturations, the simulated peaks in heavy isotopologue enrichement by SiSPAT-Isotope were considerably smaller than the peaks simulated by DuMu^x. This could be attributed to the presence of liquid water that functions as a buffer to changes in the δ_l^2H and $\delta_l^{18}O$ values, and to evaporation of residual water that is simulated in DuMu^x, which leads to a higher enrichment of ${}^1H\,{}^2H^{16}O$ and $H_2^{18}O$. However, the comparison with experimental data did not show that a larger simulated enrichment improved the prediction of the measurements considerably. A rapid and complete drying out of the soil surface layer was not observed by the soil moisture sensors in the experiment. However, an increase in drying rate was observed at -0.05 m at the time when the simulations predicted rapid drying. Such an increase in drying rate was also measured at -0.01 m depth but later and much smaller than in the DuMu^x simulation. To further analyze the impact of the water content (or its absence) in the dried-out soil layer on δ_l^2H and $\delta_l^{18}O$ values and their dynamics, alternative descriptions of the capillary pressure-water saturation relation in dry soil and the implementation of relationships that have been developed for this range (e.g.,Campbell & Schiozawa, 1992; Fayer & Simmons, 1995; Schneider & Goss, 2012 should be considered).

Based on the comparison between the experimental data and the simulation results, we can see that DuMu^x can simulate the vertical δ_l^2H and $\delta_l^{18}O$ profiles better than SiSPAT-Isotope. SiSPAT-Isotope did not simulate a downward movement of the peak in δ_l^2H and $\delta_l^{18}O$ values since the reduction in evaporation during soil drying was modeled by increasing the thickness of the laminar boundary layer. This kept the evaporation front near the soil surface. To simulate a downward movement of the evaporation front and of the peak in δ_l^2H and $\delta_l^{18}O$ values, the reduction in evaporation should be simulated due to an increased resistance to water transfer through a drying surface layer.

SiSPAT-Isotope can simulate such effects as well, but the numerical solution may become unstable, because soil water flow is solved using a partly implicit numerical scheme that approximates nonlinear soil properties. For soils with very sharp hydraulic retention curves, small changes in soil water potential cause very large changes in water content and conductivity. Because these rapid changes are only approximated, the numerical solution can become unstable.

This problem especially occurs in uniform sandy materials (large n value) that are often used in lab experiments. For field applications, this might be less of a problem since field soils typically have much more heterogeneous pore size distributions. Additionally, we showed that either using the maximum δ_l^2H or $\delta_l^{18}O$ value or using the maximum gradient between each pair of neighboring δ_l^2H or $\delta_l^{18}O$ observation points can determine the location of the evaporation front in soils.

The comparison shows both, the complexity of describing dry soil conditions in numerical models and the sensitivity of δ_l^2H and $\delta_l^{18}O$ values and isotope fractionation to transport processes in the dry soil layer and the free flow boundary layer. This sensitivity implies that high frequency in situ measurements of heavy isotopologue ratios can help to gain more insight into different transport processes in the free flow boundary layer and upper soil layer controlling the evaporation process but with different impacts on isotopologue fractionation. The dependency of isotopologue fractionation on diffusive transport, that is, kinetic fractionation, could therefore be used to evaluate the role of airflow fluctuations (turbulent pumping) and diffusive transport in the dry soil surface layer and the free flow boundary layer and how they are influenced by the pore network structure of the porous medium and the roughness of the porous medium-free flow interface. Advective processes are expected to play a more important role under field conditions than under the laboratory conditions of the experiment that were analyzed in this study. Both numerical models should be extended to include the impact of airflow fluctuations in the dry surface soil layer and across the porous medium-free flow interface to describe these processes and to infer their impact on evaporation from the isotopic behavior at the soil–atmosphere interface. In a further step, this can be expanded to include a comparison with data from larger scales and under outdoor conditions, for example, lysimeters.

For future studies of evaporation and isotopologue dynamics, we recommend using a regularized pressure-saturation relationship that avoids infinite capillary pressures as it allows drying below residual water saturation . This enables a physically consistent representation of the transition from liquid dominated to vapor dominated transport at the evaporation front. Combining the regularized pressure-saturation relationship with a water saturation threshold at which liquid connectivity is lost, the evaporation front can migrate downward and the associated heavy-isotopologue enrichment peak can shift with time, consistent with experimental observations. Furthermore, DuMu^x does not prescribe a kinetic fractionation factor; instead, kinetic fractionation emerges from the explicit representation of vapor-liquid phase exchange, gas phase diffusion, and isotope-specific binary diffusion coefficients in the surface boundary layer.

4 General Conclusions and Outlook

4.1 Conclusions

4.1.1 Modeling Evaporation

This thesis is based on two complementary and very unique datasets, a three-year record of bare soil evaporation from weighable lysimeters under natural outdoor conditions and high-resolution daily isotope profile measurements that display evaporation front dynamics in drying soil. Together, these datasets allowed an unprecedented evaluation of how well physical models reproduce soil evaporation across saturation states, temporal scales, and transport regimes.

We wanted to investigate if models based on the Richards equation can reproduce observed evaporation rates accurately on different temporal scales and at different saturation levels.

We hypothesized that the Richards equation would perform adequately as long as the soil is within a certain saturation range (stage-I evaporation), and soil temperature is relatively constant. We assumed a decreasing accuracy in predictions of evaporation rates as the soil is drying out, and vapor flow is dominating. Moreover, we expected inaccuracies on diurnal/hourly time scales due to limitations in accounting for temperature fluctuations and vapor flow. Instead, the Richards equation models would be more suitable for long-term predictions of evaporation (Chapter 1.12).

To test our hypothesis, we used a unique data set of measurements under natural outdoor conditions in natural undisturbed soils for three years (2016-2018) with different climatic conditions between harvest and sowing when evaporation was dominated by bare soil characteristics (Chapter 2.3.2). The data was compared with simulation results using the Richards equation.

With the right SHPs, the Richards equation simulated bare soil lysimeter evaporation losses accurately on a monthly scale (Chapter 2.4.4.1). But the use of the threshold boundary condition caused a monotonous decrease of the evaporation rate when the soil dries out. That is because the threshold boundary condition decouples the evaporation dynamics from the dynamics of evaporative forcing and heat fluxes during stage-II evaporation.

We confirmed by measurements that the Richards equation is not suitable to represent diurnal dynamics when vapor transport in the porous medium is more important than liquid flow and vapor concentration in the soil increases during the day due to increasing temperature (Chapter 2.4.4.2). Neither can an increase in daily evaporation during stage-II be reproduced by this model, due to higher radiative forcing leading to higher soil temperatures.

We observed that the disturbance of a surface layer by tillage affected hydraulic properties of the surface layer. A surface layer with aggregates formed by tillage and the presence of large pores can impact the evaporation process. Loose surface layers can suppress soil evaporation because of the capillary discontinuity between the loosened soil surface and the underlying soil and the disruption of the hydraulic connectivity, which would allow a water flow from deeper soil layers to the surface layer. Furthermore, a dry surface layer forms in the loosened surface due to fast drying, creating a barrier that only allows gas flow and diffusion in the gas phase. Once the surface layer dries, evaporation becomes limited by vapor diffusion through this dry surface layer. The implementation of a tilled surface layer shows the importance of including vertical heterogeneity into models which was not further tested in our study due to missing information about the tillage treatment and a homogenous soil profile.

For predicting SHPs, PTFs are an effective tool. In this context we wanted to investigate how adequate methods for estimating SHPs are and which impact PTFs from the ROSETTA model have on simulated evaporation rates compared to PTFs taken from field measurements.

We assumed that the use of PTFs leads to significant differences between modeled and observed evaporation rates, especially under non equilibrium conditions (Chapter 1.12).

To test our hypothesis, we compared three model approaches with different SHPs (Chapter 2):

- SHPs derived from soil texture using the ROSETTA PTFs

- SHPs derived from in situ measurements of water content and soil water pressure heads
- SHPs derived from L-band brightness temperatures

SHPs estimated from soil texture using the ROSETTA PTFs resulted in overestimation of the measured evaporation, suggesting that the hydraulic conductivities of the studied soils were overestimated by the PTFs. One reason for this overestimation could be the tillage treatment on the surface of the arable lysimeters (Chapter 2.4.4.1).

SHPs derived from in situ measurements of water content and soil water pressure heads improved evaporation rate estimations, although the saturated hydraulic conductivity was still estimated from soil texture. The in situ measured retention curves suggested a wider pore size distribution than the retention curves that were derived from PTFs. This resulted in lower estimates of unsaturated hydraulic conductivity using the vGM model (van Genuchten, 1980) and consequently lower simulated evaporation that more closely matched observations.

As mentioned above, the SHPs derived from L-band brightness temperature were applied to one soil to understand the effect of surface layer disturbance by tillage. Those SHPs were applied in Durner's bimodal model and reproduced the reduced evaporation rates caused by the disruption of the capillary continuity between the surface and deeper soil water due to tillage.

With our results we confirmed the statement of Lehmann et al. (2020) that SHP estimates should be limited by the characteristic length L_c. SHPs derived from soil texture using PTFs corresponded with very high characteristic lengths whereas SHPs obtained from to in situ measurements corresponded with smaller L_c and better predicted E_m. The tilled surface layer had a significant smaller L_c. The ranking of L_c reproduced the ranking of the simulated E in the different soils and different years. Therefore, L_c can be considered as a valuable characteristic for translating SHPs to evaporation properties of a soil.

Understanding these dynamics is important for designing systems to manage water loss through evaporation. Agricultural practices like tillage and mulching are effective for water conservation because they can create a natural barrier, limiting the upward movement of water and reducing evaporation losses. Not considering the effects of soil loosening or soil structure on unsaturated soil properties in environmental models could lead to an overestimation of evaporation from finer textured soils.

Further research is needed to evaluate and quantify the impact of soil surface management practices, which influence soil structure and surface roughness, and which aim to reduce soil evaporation losses (Chapter 2.5).

Despite the insights gained from this study, several limitations should be acknowledged when interpreting our results.

Our study focused on loamy soil types available at our lysimeter facility which does not represent the full range of agricultural soils. Other soil textures and structures with different hydraulic properties might show a different behavior under similar conditions.

Furthermore, although we selected bare soil periods between harvest and sowing to minimize vegetation influence, arable lysimeters cannot guarantee that bare soil conditions were maintained consistently throughout the study period. Minor vegetation growth and residual crop effects may have introduced variability in evaporation dynamics not accounted for in our models.

Another limitation of our study was the lack of a vertical spatial scale characterization, especially close to the surface. While lysimeters provide excellent temporal resolution of water fluxes, they represent point measurements that may not capture the spatial heterogeneity of field conditions. Changing hydraulic properties with depth, especially within the top few centimeters where evaporation processes have the greatest impact, is important for modeling.

4.1.2 Modeling Isotopologues

A further useful tool to analyze evaporation on a daily scale are isotopologue measurements, as described in Chapter 1.6. With isotopologue measurements we were able to measure changes in soil water isotopologue composition close to the surface, which we were not able to do in the lysimeter experiments. They can capture the isotopic fractionation that occurs during phase changes. The enrichment of heavier isotopes in remaining soil water provides a temporal signature that can be tracked as evaporation proceeds. Daily measurements allow correlating isotopic changes with environmental variables (temperature, humidity, wind) that influence evaporation mechanisms.

In our study, we used two different modeling approaches: SiSPAT-Isotope ("One-and-a-Half" phase, one component model) and DuMu^x (fully coupled heat and water flow model). Our research aimed to identify key differences between these two models in simulating isotopologue transport within drying unsaturated porous media (Chapter 3).

The focus of our comparison was understanding how different boundary conditions affect simulations of isotopologue transport. We put a focus on the impact of residual water content on isotopologue transport simulations, examining the critical differences between the vGM model implemented in SiSPAT-Isotope versus the approach of characterizing soil hydraulic properties for dry conditions used in DuMu^x.

We hypothesized that the results of the fully coupled DuMu^x model would differ from the "One-and-a-Half" phase approach in SiSPAT-Isotope because of its treatment of the gas phase and interface processes. Modeling gas phase dynamics would lead to differences in predicted vapor transport, especially during stage-II evaporation. The differences in how residual water content is handled between the models would lead to different predictions of isotope transport under very dry conditions.

DuMu^x accurately reproduced high frequency heavy isotopologue ratio variations in dried out soil by simulating complete drying of the surface. DuMu^x maintained vapor concentration close to saturation while liquid water content decreased sharply in the regularized capillary pressure range. SiSPAT-Isotope, which prevents drying below residual water content, simulated neither these high frequency heavy isotopologue ratio variations nor the downward movement of the evaporation front.

Analysis showed that lower residual water saturation values produced more similar results between both models. At higher residual water saturations, SiSPAT-Isotope simulated smaller peaks in heavy isotopologue enrichment than DuMu^x due to the residual liquid water buffering changes in heavy isotopologue enrichment.

Experimental data did not agree with any simulation approach, as sensors did not detect complete surface drying but did record increased drying rates that were delayed and less pronounced compared to DuMu^x predictions (Chapter 3.3.4).

As the vGM model and the concept of residual water content are not sufficient for describing dry soil conditions, future work should consider alternative capillary pressure-saturation relationships developed specifically for dry soil.

When comparing experimental data with simulations, DuMu^x better reproduced vertical δ_l^2H and $\delta_l^{18}O$ profiles than SiSPAT-Isotope. SiSPAT-Isotope failed to show downward movement of isotopologue enrichment peaks because the evaporation flux is implemented through an increasing boundary layer thickness with time, which keeps the evaporation front near the surface. For accurate simulation of downward movement, models should account for diffusive transport in the laminar boundary layer and in the dried-out surface soil layer.

This comparison highlights both the challenges in modeling dry soil conditions and the sensitivity of isotopologue behavior to boundary layers and to transport processes in dry soil. This sensitivity suggests high-frequency in situ isotopologue measurements could provide insights into different transport processes controlling evaporation.

Moreover, we investigated whether daily measurements of stable water isotopologues in soil profiles could effectively identify specific evaporation mechanisms, particularly the development of an evaporation front (Chapter 3.3.5).

Our hypothesis was that these daily isotopic measurements would provide sufficient temporal resolution to detect both the formation and movement of the evaporation front. We expected this front to be characterized by a distinct peak in heavy isotopic enrichment. We aimed to confirm Rothfuss et al. (2015) observation that the evaporation front occurs at the location of maximum isotopic gradient (of δ^2H and $\delta^{18}O$).

We compared two methodological approaches for determining the evaporation front location: (1) at the point with maximal heavy isotope enrichment, and (2) at the location of the maximum isotopic gradient (of δ^2H and $\delta^{18}O$) (Chapter 3.3.5). Experimental measurements and DuMu^x simulations were analyzed. To evaluate the performance of these approaches, we compared them against a refined solution with resolution matching the discretization grid of DuMu^x. While both methods yielded identical results at fine resolution, our comparison of coarse-scale to fine-scale solutions revealed that the approach of identifying the maximum isotopic gradient, was closer to the refined solution. Based on these findings, we cannot recommend one approach over the other, but suggest further investigations to determine the specific conditions under which each approach might be more suitable.

Several limitations of the study should be acknowledged.

Our study primarily relied on controlled laboratory conditions, which may not capture the complexity of field environments where advective processes play a significant role.

Looking at the water saturation measurements of Rothfuss et al. (2015), there is a visible drift with time in saturation, although the soil is drying, the saturation is slowly increasing below 40 cm depth over time. Since the simulations reproduce the cumulative evaporation well and the simulations close the soil water balance, the measurements seem to overestimate the water saturation.

The discrepancies observed between simulated results and experimental measurements of water saturation suggest potential challenges in sensor calibration or model assumptions that need further research. There should be some analysis of sensor accuracy over long time periods and under very dry conditions considering validation with alternative measurement methods.

To avoid numerical instability with SiSPAT-Isotope when modeling sand with a narrow pore size distribution, it was necessary to adjust the boundary layer thickness based on values derived from measured evaporation rates, which influenced the simulation results of isotopic fractionation. It did not simulate a downward movement of the heavy isotopologue enrichment peak since the reduction in evaporation during soil drying was modeled by increasing the thickness of the laminar boundary layer, keeping the evaporation front near the surface

The study focuses on a single soil type (uniform sand FH31) which restricts our results to sand. Simulations with a wide range of soil textures and characteristics found in natural settings are necessary.

Our examination was limited to one-dimensional vertical flow, neglecting potential lateral flow or three-dimensional effects that might influence fractionation in natural environments.

The regularization of the capillary pressure-saturation curve and assuming that no fluid flow could take place and film flow was neglected, led to a rapid decrease in liquid saturation after reaching the residual saturation. A more accurate understanding and representation of water behavior below residual saturation is needed.

4.1.3 Summary

This thesis evaluates the ability of Richards equation based evaporation models and isotope transport models to reproduce soil evaporation dynamics across moisture states and temporal scales by using two unique experimental datasets: (1) a three year bare soil weighable lysimeter dataset capturing natural climatic variability, and (2) high resolution isotope measurements under controlled drying conditions.

Our results show that the Richards equation can accurately simulate long term evaporation during stage-I when soil hydraulic properties are well constrained but cannot represent vapor dominated and temperature driven diurnal processes during stage-II. In contrast, isotopologue modeling highlights the importance of boundary layer dynamics, vapor diffusion, and the limitations of commonly used hydraulic models for evaporation. These combined findings emphasize the need for improved soil hydraulic parameterizations, explicit representation of vapor and heat transport, and integrated modeling approaches to describe evaporation across the full range of environmental conditions.

4.2 Outlook

4.2.1 Modeling Evaporation

We systematically evaluated how well the standard FAO PM method combined with Richards equation predict measured evaporation, and in showing that soil hydraulic parameter estimation critically affects predictions by comparing simulation with lysimeter data.

In summary, our research shows that the Richards equation provides good results for longer temporal scales for a certain range of water saturation. Accurate modeling of soil evaporation across various temporal scales and drying conditions require consideration of vapor flow dynamics, temperature fluctuations, soil treatment, and accurate determination of SHPs through direct measurements rather than generalized PTFs.

For future work with PTFs the following should be considered:

Natural soils typically exhibit bi- or multimodal pore size distributions, which are not represented by the vGM model (Dimitrov et al., 2014; Zhang et al., 2022). PTFs should be developed for models that capture these pore size distributions such as Durner’s bimodal model (Durner, 1994). Durner’s bimodal model extends the van Genuchten equation by using a weighted sum of two or more van Genuchten functions to represent different pore size distributions, which better represents inter- and intra-aggregate pore space.

The concept of residual water content has no physical justification as soil water can approach zero (Weber et al., 2024). Our isotope study confirms this (Chapter 3).

PTFs also do not consider the capillary hysteresis, which describes the different water retention curves for wetting and drying cycles. But the capillary hysteresis significantly influences water redistribution and is rarely incorporated in PTFs (Hannes et al., 2016; Weber et al., 2024). The capillary hysteresis plays an essential role in the complex dynamics of soil water and has to be included in future models to achieve appropriate representations of the water retention processes (Hannes et al., 2016).

Further research to evaluate and quantify this impact of soil surface management practices (like tillage) that influence pore size and surface roughness, which reduce soil evaporation losses is needed. It is also important to account for changes in soil properties over time due to soil management practices, climate or biological activity. As we show in our study, lysimeters as long-term field trials can help collect data of temporal changes in soil hydraulic properties.

To ensure physical plausibility in PTF derived parameters, secondary soil hydraulic properties like the characteristic length of evaporation L_c, introduced in Chapter 2.4.4.2 (Lehmann et al., 2020), ponding time or field capacity should be used (Twarakavi et al., 2009; Weber et al., 2024).

PTFs mostly fail to account for soil structure(Vereecken et al., 2022), hence future models need to better account for incorporating information from soil profile characterization and classification (Weber et al., 2024).

Another improvement for PTFs would be standardization of used data as different measurement methods create inconsistencies in datasets. Programs like SOPHIE (Soil Program on Hydro-Physics via International Engagement), already work on standardized protocols (Bakker et al., 2019).

For capturing diurnal evaporation dynamics, coupling the Richards equation with surface water and energy balance equations is important. Models should account for temperature-dependent vapor transport and implement resistance terms dependent on surface soil moisture to better reproduce evaporation.

Furthermore, to represent diurnal evaporation dynamics, other boundary conditions such as using resistance terms that depend on surface soil moisture could be implemented (van de Griend & Owe, 1994). For example, Saito and Šimůnek et al. (2009) coupled the Richards equation with equations for the surface water and energy balance to achieve better reproduction of evaporation during diurnal cycles. Therefore, they solved the energy balance equation at each time step to determine evaporation rates and heat fluxes at the boundary. The model iteratively solved the water flow and heat transport equations with these updated boundary conditions. They demonstrated that proper coupling of Richards equation with energy balance models significantly improved predictions at finer temporal scales compared to uncoupled approaches, particularly for capturing diurnal temperature fluctuations.

By addressing the above mentioned points, we can improve our representations of soil evaporation processes, increasing accuracy for different temporal scales and soil conditions.

4.2.2 Isotope Measurements and Simulation

We combined stable isotope data with fully coupled mass and energy flow models to improve understanding of how evaporation affects water and isotope distributions especially focusing on model behavior under different residual saturation conditions.

Our results helped to understand evaporation driven isotopic fractionation in unsaturated porous media. Both numerical models demonstrated their ability to reproduce the general isotopic behavior observed in experiments.

These numerical models should be extended to incorporate the impact of airflow fluctuations in the dry surface soil layer and across the porous medium-free flow interface, which would enable more accurate representation of field conditions where turbulent pumping and diffusive transport processes significantly influence evaporation and isotopic signatures.

The comparison between modeled and measured isotopic profiles suggested that correctly representing diffusive transport processes in both the laminar boundary layer and the dried out surface soil layer is crucial for accurately reproducing the downward movement of the evaporation front.

Kiemle et al. (2023) developed a model that couples the free-flow domain with the porous medium domain to investigate how atmospheric flow conditions affect isotopic fractionation. They solve compositional flow equations with suitable coupling conditions at the soil-atmosphere interface. This allows for a better understanding of how airflow affects isotope transport. They test both laminar and turbulent flow conditions with varying wind velocities (0.1 to 3.0 m/s), showing that these different atmospheric conditions significantly impact the evaporation rate and subsequently the isotopic composition in soil. Moreover, the model confirms that equilibrium fractionation is temperature sensitive, with higher evaporative cooling leading to greater isotope partitioning.

The model of Kiemle et al. (2023) can be used as a supporting tool to refine parameterizations of fractionation processes, especially for kinetic fractionation at the soil atmosphere interface. In their approach, kinetic fractionation emerges naturally from the resolved transport processes in DuMu^X and does not rely on any imposed kinetic fractionation parameterizations. Because kinetic fractionation depends on the balance between diffusive and turbulent transfer above the soil surface and these contributions themselves depend on surface roughness, using isotopologue measurements to infer kinetic effects may help improve parameterizations of exchange processes across rough surfaces. The model of Kiemle et al. (2023) is therefore suitable for exploring or quantifying kinetic fractionation, since the kinetic effects arise physically rather than from empirical factors.

Kiemle et al. (2023) also performed isolated process tests to verify how individual kinetic and equilibrium components influence fractionation, following the qualitative approach of Mathieu and Bariac (1996). A direct numerical comparison with classical analytical models (e.g., Barnes & Allison (1984), Craig & Gordon (1965)) is not possible because those analytical formulations do not resolve a free flow domain, assume constant evaporation rates, and require parameterized kinetic fractionation factors. The model of Kiemle et al. (2023) does not prescribe a boundary layer thickness; instead, the atmospheric boundary layer develops dynamically from the solution of the free flow equations (laminar or turbulent) in the atmospheric domain.

Field scale applications of isotopologue measurements represent an essential next step, as evaporative demands under natural conditions typically exceed those in laboratory settings.

Quade et al. (2019) applied the same gas-permeable membrane technology of Rothfuss et al. (2013) in the field to investigate partitioning of water isotopologues in a sugar beet field. The evaporation was measured in situ and identified large differences between the isotope δ values derived from destructive and non-destructive measurements. Their analysis using a transfer resistance model revealed discrepancies in T/ET (transpiration fraction) ratio estimations, which are critical for understanding how water moves through the soil-plant-atmosphere continuum.

Oerter et al. (2017) employed a vapor-permeable membrane technique to measure soil water isotopes in situ at four locations across North America. They validated the water vapor probe method through comparison with the bag equilibration method and vacuum extraction, followed by liquid water analysis. Their assessment demonstrated that while the accuracy of all three methods was comparable, the water vapor probe method provided significant advantages in ease of use and higher sample throughput.

Comparing the systems described by Rothfuss et al. (2015) and Oerter's (2017) both methods use similar underlying principles of gas-permeable membranes for isotope measurements. Oerter's (2017) system represents a significant evolution in design that prioritized field applicability, validation across multiple environments, and practical usability considerations. The main advancement in Oerter's (2017) method was translating the gas-permeable membrane technology from a primarily research-focused implementation to a more field-ready system with practical improvements in deployment flexibility, calibration, and efficiency.

With the increasing adoption of laser-based measurement techniques for isotopologue monitoring, describing the processes near the soil surface will become increasingly important for interpreting observational data.

Expanding this research to include a variety of soil types beyond the uniform sand used in this study would enhance the applicability of the findings. The interplay between soil texture and pore network is especially important for heterogeneous field soils with more complex pore size distributions. Soils with more complex pore networks are challenging for modeling vapor transport and isotopic exchange processes.

Understanding how these factors affect the position and movement of the evaporation front which gives us information on how water is lost from the soil through evaporation can be applied in agricultural water management to support precision irrigation strategies aimed at minimizing water loss in water scarce regions.

Future research should focus on dry soil capillary pressure-saturation relationships, broader soil texture analyses, and integrated water balance-isotopologue models to improve evaporation predictions and agricultural water management.

5 Appendix

A.1 Soil Textures of the Different Lysimeters

Table A 1: Soil textures of the different lysimeters located in Selhausen (Herbrich et al., 2017). For the Selhausen soil (SE) only profile information of the field side is available (Weihermüller et al., 2006).

Lysimeter and code in TERENO database	**Layer**	**Depth [cm]**	**Layer thickness [cm]**	**Sand [%]**	**Silt [%]**	**Clay [%]**
BL4 **SE_Y_031**	Ap	28	28	4.90	72.91	22.18
	Axh1-2	48	20	4.27	82.66	13.07
	Axh3	72	24	4.05	81.66	14.30
	C1	128	56	5.60	67.47	26.93
	C2	141	13	5.15	71.98	22.87
	C3	>141	n.a.	65.04	15.96	19.00
BL5 **SE_Y_035**	Ap	29	29	4.90	72.91	22.18
	Axh1-2	40	11	4.27	82.66	13.07
	Axh3	68	28	4.05	81.66	14.30
	C1	123	55	5.60	67.47	26.93
	C2	141	18	5.15	71.98	22.87
	C3	>141	n.a.	65.04	15.96	19.00
BL6 **SE_Y_036**	Ap	28	28	4.90	72.91	22.18
	Axh1-2	46	18	4.27	82.66	13.07
	Axh3	73	27	4.05	81.66	14.30
	C1	145	72	5.60	67.47	26.93
	C2			5.15	71.98	22.87
	C3	>145	n.a.	65.04	15.96	19.00
SB10 **SE_Y_042**	Ap	26	26	13.40	61.49	25.11
	M1	83	57	15.69	69.69	14.63
	M2	112	29	11.28	74.08	14.64
	M3	>112	n.a.	5.99	75.50	18.51
SB11 **SE_Y_043**	Ap	23	23	13.40	61.49	25.11
	M1	92	69	15.69	69.69	14.63
	M2	112	20	11.28	74.08	14.64
	M3	>112	n.a.	5.99	75.50	18.51
SB12 **SE_Y_044**	Ap	30	30	13.40	61.49	25.11
	M1	76	46	15.69	69.69	14.63
	M2	102	26	11.28	74.08	14.64
	M3	131	29	5.99	75.50	18.51

Lysimeter and code in TERENO database	**Layer**	**Depth [cm]**	**Layer thickness [cm]**	**Sand [%]**	**Silt [%]**	**Clay [%]**
	C	>131	n.a.	12.59	68.98	18.43
DD9 **SE_Y_041**	Ap	30	30	45.5	39.7	14.8
	Bt	55	25	50	23.6	26.4
	elCcv	100	45	65.5	24	10.5
	elCv	150	50	61.1	27.4	11.5
DD7 **SE_Y_045**	Ap	37	37	60.6	26.7	12.7
	Bt	75	38	50	23.6	26.4
	elCcv	150	75	65.5	24	10.5
DD8 **SE_Y_046**	Ap	29	29	51.2	33.5	15.3
	Bt	75	46	50	23.6	26.4
	Bvt	84	9	50	23.6	26.4
	elCcv	105	21	65.5	24	10.5
	elCv	150	45	61.1	27.4	11.5
SE **SE_Y_032** **SE_Y_033** **SE_Y_034**	Ap	7.5	7.5	15.4	67.5	17.1
	Ap	22.5	15	15.6	67.7	16.6
	Al-Bv	37.5	15	14.2	66.2	19.6
	Al-Bv	52.5	15	18.1	60	22
	II-Btv	72.5	20	12.4	63.3	24.3
	II-Btv	92.5	20	9.8	65.1	25
	II-Btv	125.5	33	21.9	58.9	20.2

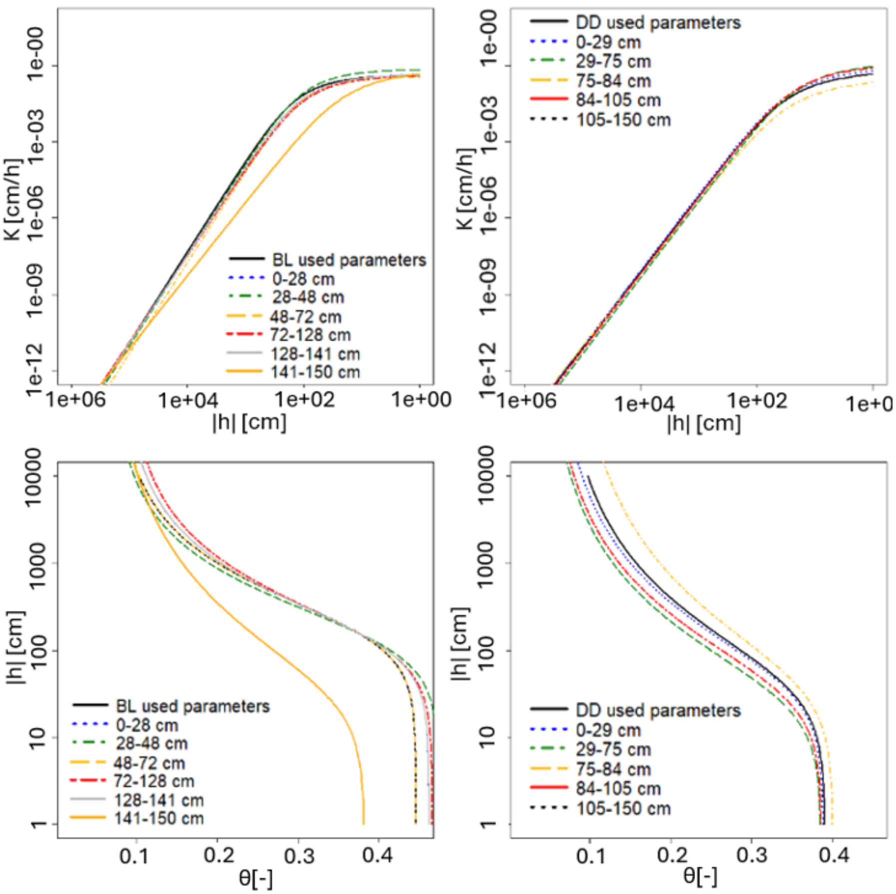

Figure A 1: Hydraulic conductivity plotted against the pressure head (left) and the water retention curve for the Bad Lauchstädt (BL) and Dedelow (DD) soil type in different depths

A.2 Net Radiation Measurements

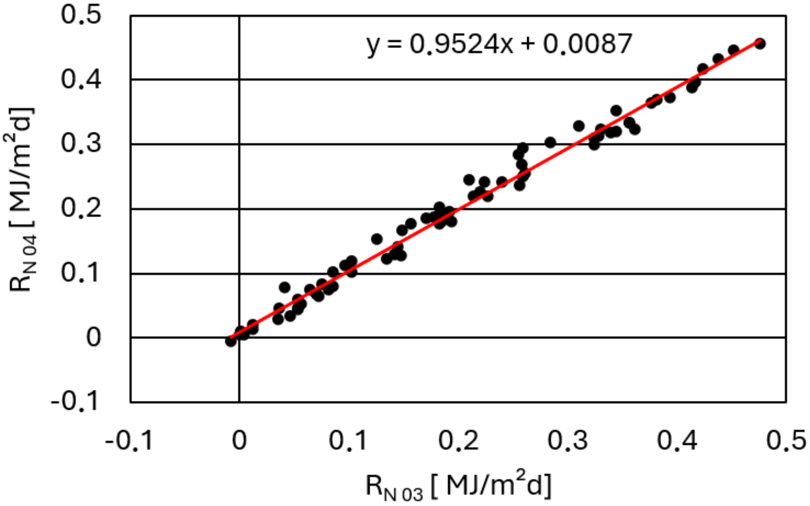

Figure A 2: Values for R_N measured above two different lysimeters in Selhausen containing different soil types. $R_{N\,03}$ was measured above SE $R_{N\,04}$ was measured above SB soil.

In a first attempt, potential evaporation was calculated from R_N that was estimated from the short-wave radiation and the atmospheric water vapor concentration according to the approach proposed by Allen et al. (1998). In a second attempt, measured R_N was taken for calculations. Aim was to avoid errors in potential evaporation given by the measurement of R_N, being influenced by the soil surface and its cover. The approach proposed by Allen et al. (1998) does not use measurements of long wave radiation but uses an empirical relation that may have to be recalibrated for a specific location. The measured net long wave radiation depends on the surface temperature of the soil, which is higher than the surface temperature of a reference well-watered surface that is evaporating at a potential rate when the soil is dry and is evaporating less. The differences between both calculations can be neglected. In general, the calculated R_N varies more and shows greater negative values by night while the R_N during daylight periods are corresponding (Figure A 3).

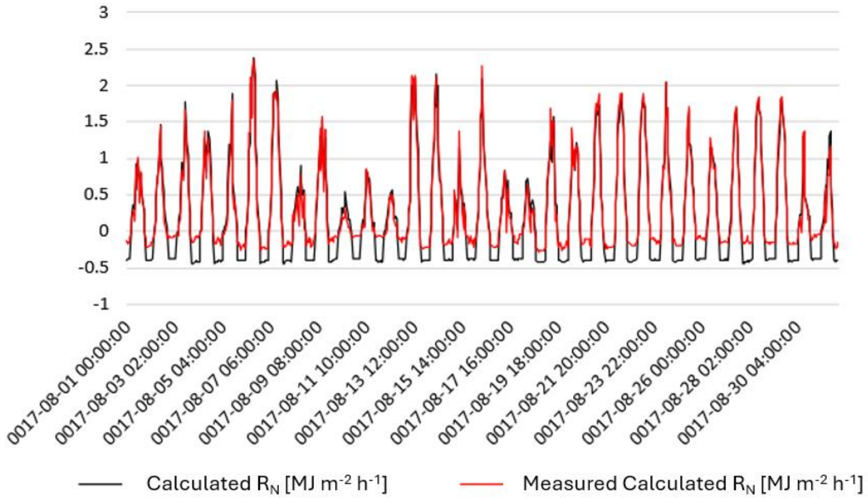

Figure A 3: Comparison of calculated and measured diurnal net radiation [MJ m^{-2}h^{-1}] for August 2017.

A.3 Additional Information ANOVA Analysis

Evaporation from lysimeter l installed in soil s on day d was analyzed using an additive analysis of variance (ANOVA) model. The observed evaporation was expressed as the sum of an overall mean evaporation and four additive components: (i) the effect of time (day), (ii) the effect of soil type, (iii) the interaction between soil type and time, and (iv) the effect of the individual lysimeter. The temporal effect represents the influence of time varying meteorological conditions, such as rainfall and potential evaporation, on evaporation rates. The influence of soil type on evaporation is captured by both a main soil effect, representing differences in mean evaporation between soils, and a soil x time interaction term, which reflects differences among soils in their temporal response to changing meteorological conditions.

The model assumes that there is no interaction between lysimeter and time; that is, the lysimeter effect is considered constant over the entire observation period. Consequently, potential interactions between lysimeter and time are not explicitly modelled but are included in the residual error term. Although this assumption simplifies the model, it implies that temporal changes in lysimeter specific behaviour are treated as random variation.

Lysimeters were treated as a nested factor within soil type, such that each lysimeter is uniquely associated with a single soil. Under this nested ANOVA framework, the lysimeter effect represents a constant deviation of an individual lysimeter from the mean evaporation of its corresponding soil across all observation days. This approach allows testing whether observed differences in evaporation between soils both in terms of mean evaporation over time and soil specific temporal patterns can be attributed to systematic soil effects or are instead due to random variation arising from the selection of lysimeters.

A key assumption of the ANOVA model is that residual errors are uncorrelated in time. This assumption was evaluated by calculating the autocovariance of the residual error terms derived from the fitted model. The analysis revealed significant temporal autocorrelation of residuals for lag times of up to five days (Figure A 4). Such autocorrelation leads to an underestimation of residual variance and consequently to an overestimation of the statistical significance of model effects.

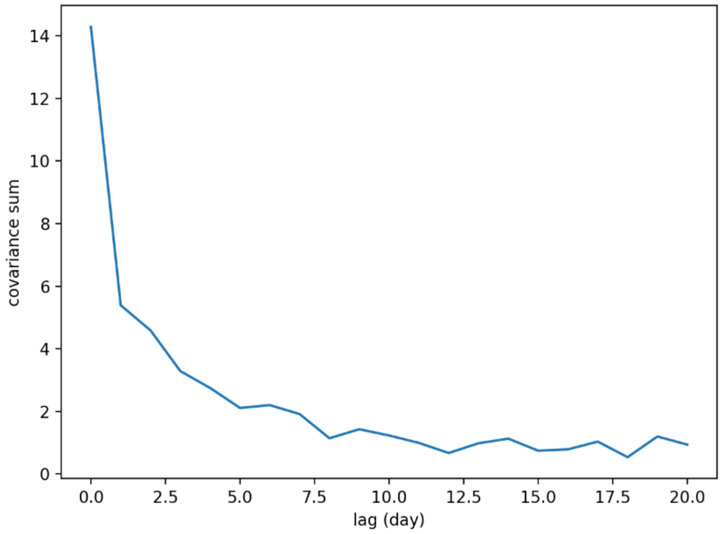

Figure A 4: Autocovariance of residuals of original model

To assess the impact of this violation of the independence assumption, the ANOVA was repeated using a reduced dataset consisting only of evaporation observations separated by at least five days. While this approach reduced the effective temporal autocorrelation (Figure A 5), it did not alter the overall conclusions regarding the significance of the main effects and interactions. However, the corresponding significance levels were lower, indicating a more conservative and robust statistical inference (Table A 2).

Table A 2: ANOVA analysis showing the significance of differences caused by time, soil, lysimeters and the unexplained error.

Source	**Sum of squares**	**df**	**Mean square**	***F***	**Prob > *F***
Time	210.884	43	4.90427	417	0
Soil	0.353	3	0.1177	2.85	0.1049
Lysimeter(soil)	0.33	8	0.04128	3.51	0.0006
Time × soil	4.191	129	0.03249	2.76	0
Error	4.046	344	0.01176		
Total	219.804	527			

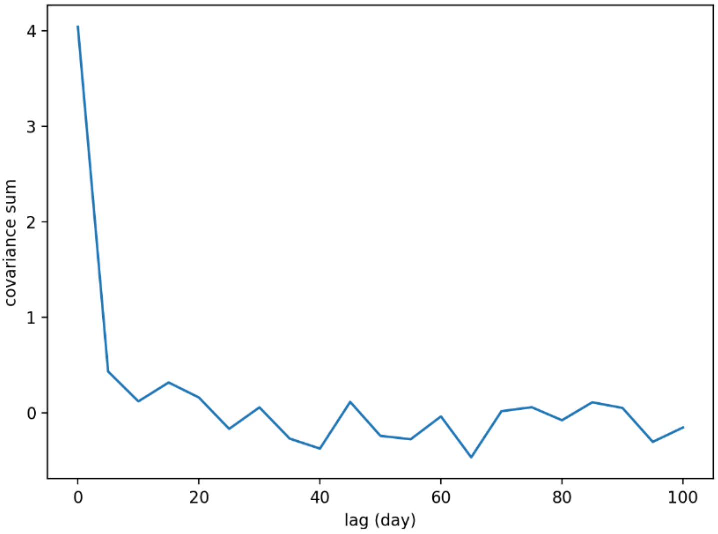

Figure A 5: Autocovariance of residuals of original model using data with 5 days intervals.

A.4 Component Specific Factors

As mentioned before, the component description and, thereof, the fractionation of the isotopologues are dependent on parametrizations. In Table A 3, the values for the equilibrium fractionation factor are listed. The kinetic fractionation is driven by diffusion in the liquid and the gas phase. The respective diffusion coefficients and the parametrization values are listed in Table A 4:

Table A 3: Parametrization values for the equilibrium fractionation factor for isotopologues $^{1}H\ ^{2}H^{16}O$ and $H_2^{18}O$.

Coefficient	a	b	c
$^{1}H\ ^{2}H^{16}O$	24844	-76.248	0.052612
$H_2^{18}O$	1137	-0.4156	-0.00206677

Table A 4: Binary diffusion coefficients for $^{1}H\ ^{2}H^{16}O$ and $^{1}H_2{}^{18}O$.

Definition	**Parameterization value**
Liquid diffusion coefficients Self-diffusion coefficient of H_2O in the liquid phase $D_l^{H_2O,self} = 10^{-9} \exp\left(-\frac{535400}{T^2} + \frac{1393.3}{T} + 2.1876 \right)$	
Binary diffusion coefficient of $H_2O - i$ in the liquid phase $D_l^{H_2O,i} = a^i D_l^{H_2O,self}, i \in \left\{ ^{1}H\,^{2}H\,^{16}O, ^{1}H_2^{18}O \right\}$	(Mathieu & Bariac, 1996) $a^{H_2^{18}O} = 0.9669$ $a^{\,^{1}H\ ^{2}H^{16}O}$ $= 0.9833$
Gas diffusion coefficients Binary diffusion coefficient of $H_2O -\ air$ in the gas phase $D_g^{air,H_2O} = 2.17 \cdot 10^{-7} \left(\frac{T}{273.15} \right)^{1.88}$	
Binary diffusion coefficient coefficient $i -\ air$ in the gas phase $D_g^{air,i} = \frac{1}{b_i} D_g^{air,H_2O}, i \in \left\{ ^{1}H\,^{2}H\,^{16}O, ^{1}H_2^{18}O \right\}$	(Merlivat, 1978) $b^{H_2^{18}O} = 1.0285$ $b^{\,^{1}H\ ^{2}H^{16}O}$ $= 1.0251$

Table A 5: Initial and boundary conditions for analyzing the impact of residual water saturation on the dry zone.

Parameter	**Values**
Soil conditions (initial)	
Water saturation, S_l	0.74 [m^3 m^{-3}]
Temperature, T	289 [K]
δ_l^{2H} value	-52 [‰]
δ_l^{18O} $value$	-8 [‰]
Gas pressure, p_s	10^5 [Pa]
Atmospheric conditions (initial and boundary)	
Relative humidity, RH	0.4 [-]
Temperature, T	289 [K]
Isotopologue concentration, δ_l^{2H}	-100 [‰]
Isotopologue concentration, δ_l^{18O}	-15 [‰]
Gas pressure, p_s	10^5 [Pa]
Boundary layer thickness, δ_z	0.005 [m]
Hydraulic parameters	
Van Genuchten parameter, n_{VG}	1.6 [-]

A.5 Derivation of Boundary Layer Thickness for the Upper Boundary Flux

The boundary layer thickness is an unknown degree of freedom in the upper boundary conditions. As the total evaporation rate is measured in the experiments, the boundary layer thickness can be derived from the measured total evaporation rate and used to define the component evaporation fluxes. The derivation of the boundary layer thickness was different for DuMu^x and SiSPAT-Isotope. The calculated total evaporation rate with the derived boundary layer thickness is compared with the measured evaporation rate in Figure A 6.

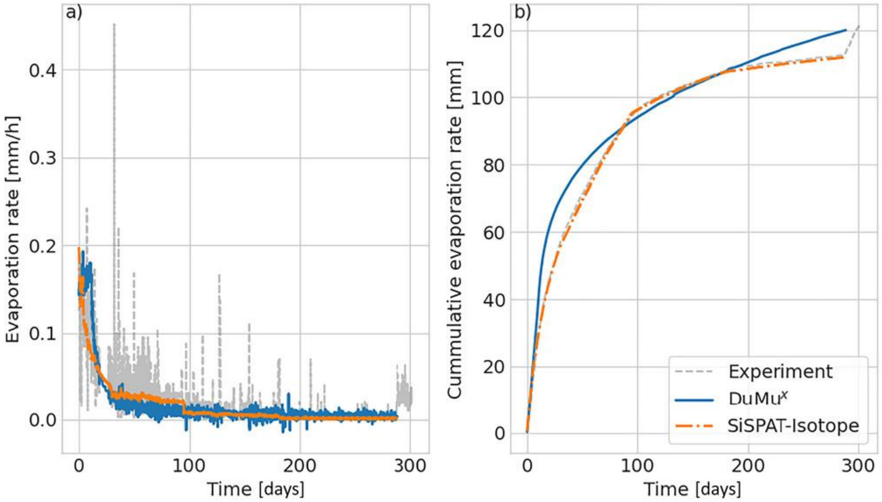

Figure A 6: Resulting total evaporation fluxes for DuMux (blue) and SiSPAT-Isotope (orange) compared to to experimental data (gray).

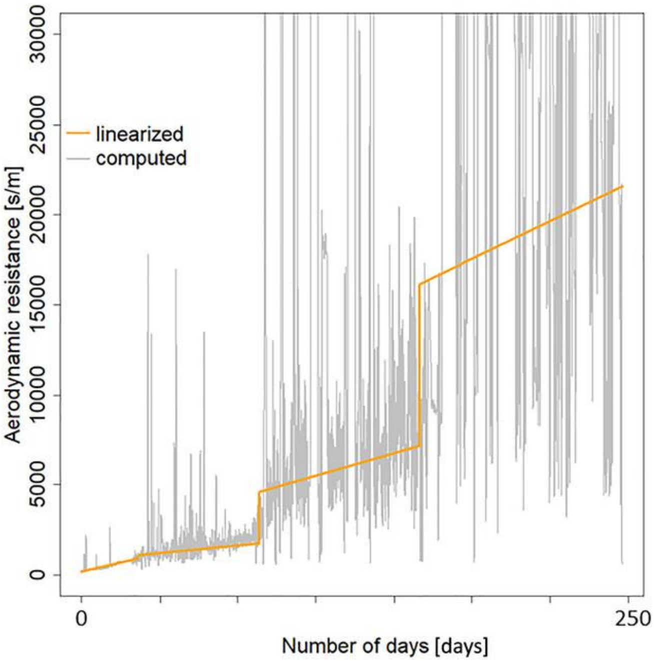

Figure A 7: Derivation of the aerodynamic resistance in SiSPAT-Isotope over time. The aerodynamic resistance is either imposed by using the measured evaporation flux (gray lines) or further modified by stepwise linearizing the computed aerodynamic resistance (orange line).

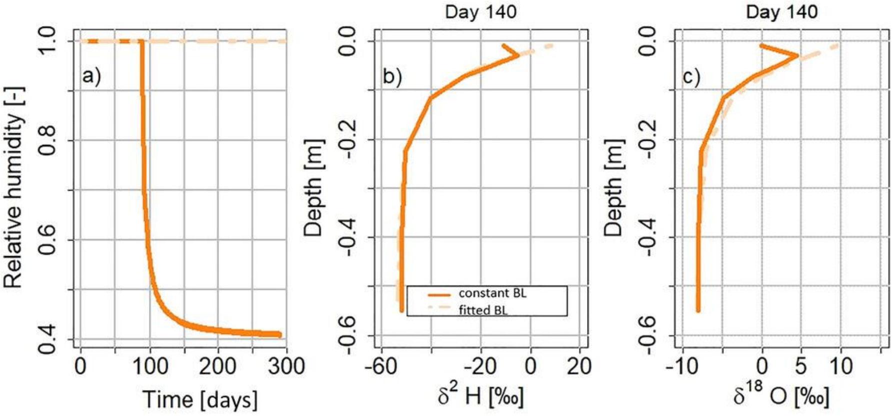

Figure A 8: Effect of different boundary layer conditions in SiSPAT-Isotope on: (a) relative humidity at soil surface level, (b) the $\delta\,^2H$, and (c) $\delta^{18}O$ profiles on day 140. Constant (straight line) and fitted (dashed line) boundary layer thickness has been chosen as variants for the boundary layer conditions.

In DuMu^x, a constant boundary layer thickness is set for the entire simulation period. The boundary layer thickness is derived through an interactive process until the deviation of the calculated evaporation rate to the measured evaporation rate is minor.

In SiSPAT-Isotope, it is assumed that the boundary layer thickness changed over time. The boundary layer thickness is derived by introducing the aerodynamic resistance, r_a [s m^{-1}], which is defined as $r_a := \frac{\delta_z}{D_g^{H_2O,air}}$. The aerodynamic resistance is then derived in two steps. In the first step, the daily measured evaporation flux is imposed on SiSPAT-Isotope, so the aerodynamic resistance is inversely calculated (Figure A 7). In the second step, the aerodynamic resistance over time is described using a stepwise linear function. A detailed description of the optimization of the aerodynamic resistance can be found in Braud et al. (2009) and Hernández-López et al. (2016). Figure A 8 shows how different descriptions of the boundary layer thickness (here: constant and fitted) affect the relative humidity and the isotopologue concentrations in SiSPAT-Isotope (Section 3.3.4).

A.6 Supplementary Material About the Description of the Isotopologue Concentration Profiles

Figure A 9 supplements the findings in Figure 3-5. Figure A 10 describes in detail the impact of the phase status of the evaporation rate on the isotopologue concentration profile in soil. Here, we highlighted the enrichment of isotopologues during stage-I evaporation and the transition into stage-II.

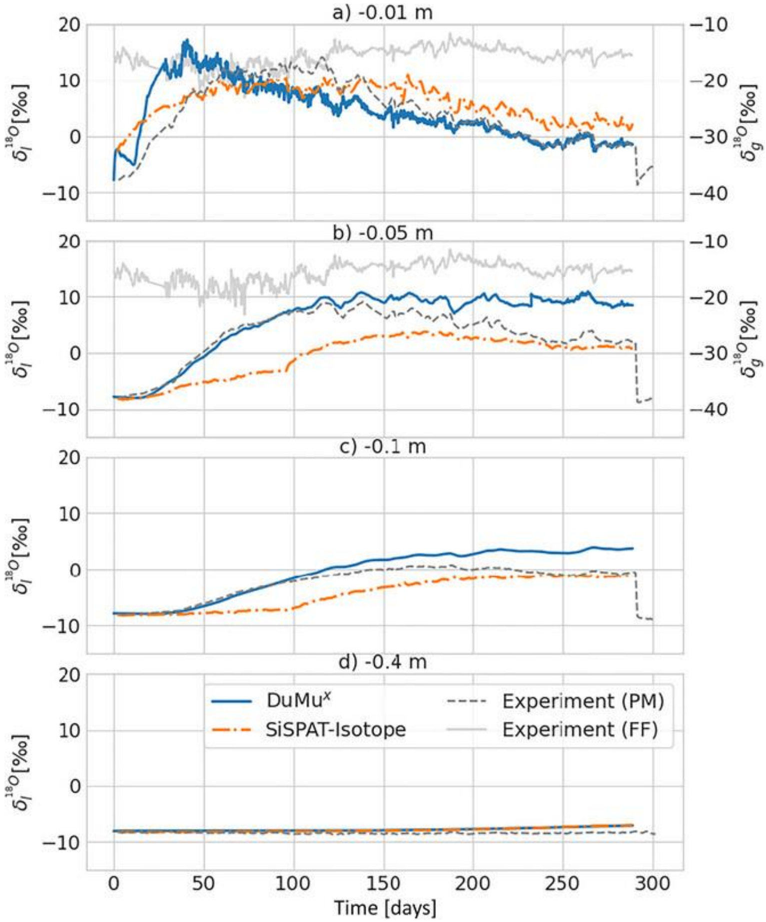

Figure A 9: Abundance of $H_2^{18}O$ isotopologs expressed in $\delta_l^{18}O$ over time at different depths. The simulated values (DuMu^x [blue] and SiSPAT-Isotope [orange]) are plotted against experimental observations (gray).

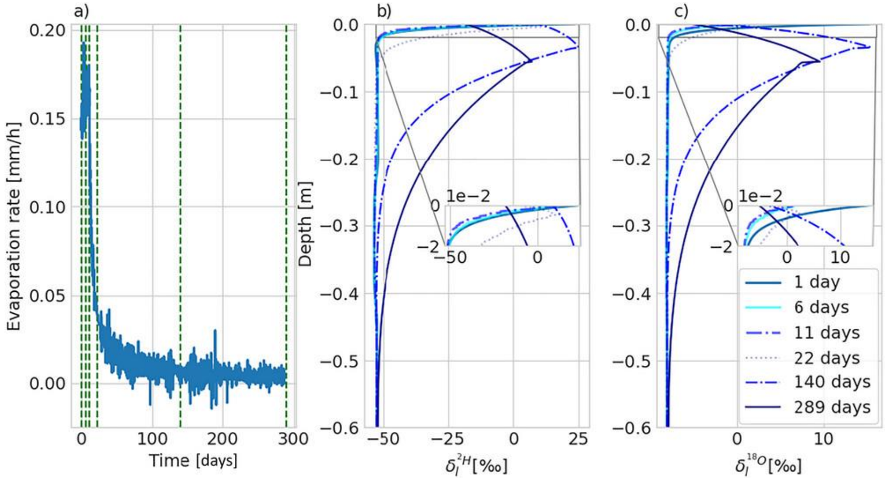

Figure A 10: Simulated abundance of $^{1}H\ ^{2}H^{16}O$ and $H_2^{18}O$ expressed in (b) δ_l^2H and (c) δ_l^{18O} by DuMu^x at different phases of (a) the evaporation rate.

A.7 Input and boundary condition values for setup change used for analyzing the dry zone

In Table A 3, we summarize the conditions used for analyzing the variations of the residual water saturation S_{wr}. Concerning the transport, hydraulic, and thermal property parameters, the values remained as listed in Table 3-1 beside the van Genuchten parameter n_{VG}.

Use of Generative AI

I did use generative AI assistance tools during the writing process of my thesis.

I did use the generative AI assistance tool claude.ai (Haiku 3.5, Sonnet 3.7 and Sonnet 4) and ChatGPT 5.2 from 23.02.2025 to 11.01.2025 in Chapters 1 and 4.

Generative AI assistance was used for language assistance, including translation, grammar and spelling correction, and optimizing consistency throughout the introduction, conclusion and outlook.

Generative AI was used for carrying out a literature review. This includes assistance with finding relevant literature related to specific topics, generating overviews for my own understanding and recall.

The text and images in this thesis are my own (unless otherwise specified) and generative AI has only been used in accordance with the KU Leuven guidelines and appropriate references have been added. I have reviewed and edited the content as needed and I take full responsibility for the content of the thesis.

6 List of Scientific Publications

Schneider, J., Kiemle, S., Heck, K., Rothfuss, Y., Braud, I., Helmig, R., & Vanderborght, J. (2024). Analysis of experimental and simulation data of evaporation-driven isotopic fractionation in unsaturated porous media. *Vadose Zone Journal*, 23(5), e20363. doi: 10.1002/vzj2.20363

Schneider, J., Groh, J., Pütz, T., Helmig, R., Rothfuss, Y., Vereecken, H., & Vanderborght, J. (2021). Prediction of soil evaporation measured with weighable lysimeters using the FAO Penman–Monteith method in combination with Richards' equation. *Vadose Zone Journal*, 20(1), e20102. doi: 10.1002/vzj2.20102

Heck, K., Coltman, E., Schneider, J., & Helmig, R. (2020). Influence of radiation on evaporation rates: A numerical analysis. *Water Resources Research*, 56(10), e2020WR027332., doi: 10.1029/2020WR027332

Al Yacoubi, L., Bouchaou, B., Jaillard, E., Masrour, M., Ait Brahim, Y., El Mouden, A., Schneider, J. & Reichert, B. (2017). Impact of rock-water interactions and recharge on water resources quality of the Agadir-Essaouira basin, southwestern Morocco. *Arabian Journal of Geosciences*, 10(7), 169., doi: 10.1007/s12517-017-2968-2

7 List of References

Aboukhaled, A., Alfaro, A., & Smith, M. (1982). Lysimeter. In *FAO (Ed.): Irrigation and Drainage Paper 39*. Food and Agriculture Organization of the United Nation.

Allen, R. G., Pereira, L. S., Raes, D., & Smith, M. (1998). Crop evapotranspiration: Guidelines for computing crop water requirements. *FAO Irrigation and Drainage Paper 56*.

Allen, R. G., Pruitt, W. O., Raes, D., Smith, M., & Pereira, L. S. (2005). Estimating Evaporation from Bare Soil and the Crop Coefficient for the Initial Period Using Common Soils Information. *Journal of Irrigation and Drainage Engineering*, *131*(1), 14–23. https://doi.org/10.1061/(asce)0733-9437(2005)131:1(14)

Allison, G. B., Colin-Kaczala, C., Filly, A., & Fontes, J. C. (1987). Measurement of isotopic equilibrium between water, water vapour and soil CO2 in arid zone soils. *Journal of Hydrology*, *95*(1–2), 131–141. https://doi.org/10.1016/0022-1694(87)90120-X

An, N., Tang, C. S., Xu, S. K., Gong, X. P., Shi, B., & Inyang, H. I. (2018). Effects of soil characteristics on moisture evaporation. *Engineering Geology*, *239*, 126–135. https://doi.org/10.1016/j.enggeo.2018.03.028

Anderson, R. G., Zhang, X., & Skaggs, T. H. (2017). Measurement and Partitioning of Evapotranspiration for Application to Vadose Zone Studies. *Vadose Zone Journal*, *16*(13), 1–9. https://doi.org/10.2136/vzj2017.08.0155

Arora, B., Dwivedi, D., Faybishenko, B., Jana, R. B., & Wainwright, H. M. (2019). Understanding and Predicting Vadose Zone Processes. *Reviews in Mineralogy and Geochemistry*, *85*(1), 303–328. https://doi.org/10.2138/rmg.2019.85.10

Arthur, E., Tuller, M., Moldrup, P., & Wollesen de Jonge, L. (2014). Evaluation of a Fully Automated Analyzer for Rapid Measurement of Water Vapor Sorption Isotherms for Applications in Soil Science. *Soil Science Society of America Journal*, *78*(3), 754–760. https://doi.org/10.2136/sssaj2013.11.0481n

Assouline, S., & Narkis, K. (2019). Evaporation From Multilayered Heterogeneous Bare Soil Profiles. *Water Resources Research*, *55*(7), 5770–5783. https://doi.org/10.1029/2018WR024560

Assouline, S., Narkis, K., Gherabli, R., Lefort, P., & Prat, M. (2014). Analysis of the impact of surface layer properties on evaporation from porous systems using column experiments and modified definition of characteristic length. *Water Resources Research*, *50*(5), 3933–3955. https://doi.org/10.1002/2013WR014489

Assouline, S., Russo, D., Silber, A., & Or, D. (2015). Balancing water scarcity and quality for sustainable irrigated agriculture. *Water Resources Research*, *51*(5), 3419–3436. https://doi.org/10.1002/2015WR017071

Assouline, S., Tyler, S. W., Selker, J. S., Lunati, I., Higgins, C. W., & Parlange, M. B. (2013). Evaporation from a shallow water table: Diurnal dynamics of water and heat at the surface of drying sand. *Water Resources Research*, *49*(7), 4022–4034. https://doi.org/10.1002/wrcr.20293

Aydin, M. (1998). A new model for predicting evaporation from bare field soil. *Proceedings of International Symposium and Second Chinese National Conference on Rainwater Utilization*, 283–287.

Bakker, G., van der Ploeg, M., Visser, S., Degre, A., & Nemes, A. (2019). *Harmonization, innovation, and standardization of soil hydrophysics properties through international engagement (SOPHIE)* (Vol. 21, p. 1). EGU General Assembly 2019. https://meetingorganizer.copernicus.org/EGU2019/EGU2019-15055.pdf

Barnes, C. J., & Allison, G. B. (1984). The distribution of deuterium and 18O in dry soils: 3. Theory for non-isothermal water movement. *Journal of Hydrology*, *74*, 119–135.

Bear, Jacob. (2014). *Dynamics of fluids in porous media*. Dover Publications Incorporated.

Beier, F. D., Bodirsky, B. L., Heinke, J., Karstens, K., Dietrich, J. P., Müller, C., Stenzel, F., von Jeetze, P. J., Popp, A., & Lotze-

Campen, H. (2023). Technical and Economic Irrigation Potentials Within Land and Water Boundaries. *Water Resources Research*, *59*(4). https://doi.org/10.1029/2021WR031924

Benettin, P., Queloz, P., Bensimon, M., McDonnell, J. J., & Rinaldo, A. (2019). Velocities, Residence Times, Tracer Breakthroughs in a Vegetated Lysimeter: A Multitracer Experiment. *Water Resources Research*, *55*(1), 21–33. https://doi.org/10.1029/2018WR023894

Boesten, J. J. T. I., & Stroosnijder, L. (1986). Simple model for daily evaporation from fallow tilled soil under spring conditions in a temperate climate. *Netherlands Journal of Agricultural Science*, *34*(1), 75–90. https://doi.org/10.18174/njas.v34i1.16818

Bogena, H. R., Montzka, C., Huisman, J. A., Graf, A., Schmidt, M., Stockinger, M., von Hebel, C., Hendricks-Franssen, H. J., van der Kruk, J., Tappe, W., Lücke, A., Baatz, R., Bol, R., Groh, J., Pütz, T., Jakobi, J., Kunkel, R., Sorg, J., & Vereecken, H. (2018). The TERENO-Rur Hydrological Observatory: A Multiscale Multi-Compartment Research Platform for the Advancement of Hydrological Science. *Vadose Zone Journal*, *17*(1), 1–22. https://doi.org/10.2136/vzj2018.03.0055

Boretti, A., & Rosa, L. (2019). Reassessing the projections of the World Water Development Report. *Npj Clean Water*, *2*(1). https://doi.org/10.1038/s41545-019-0039-9

Boutraa, T., Akhkha, A., Al-Shoaibi, A. A., & Alhejeli, A. M. (2010). Effect of water stress on growth and water use efficiency (WUE) of some wheat cultivars (*Triticum durum*) grown in Saudi Arabia. *Journal of Taibah University for Science*, *3*(1), 39–48. https://doi.org/10.1016/S1658-3655(12)60019-3

Brandes, D., & Wilcox, B. P. (2000). Evapotranspiration and soil moisture dynamics on a semiarid ponderosa pine hillslope. *JAWRA Journal of the American Water Resources Association*, *36*(5), 965–974. https://doi.org/10.1111/j.1752-1688.2000.tb05702.x

Braud, I., Bariac, T., Biron, P., & Vauclin, M. (2009). Isotopic composition of bare soil evaporated water vapor. Part II: Modeling of RUBIC IV experimental results. *Journal of Hydrology*, *369*(1–2), 17–29. https://doi.org/10.1016/j.jhydrol.2009.01.038

Braud, I., Bariac, T., Gaudet, J. P., & Vauclin, M. (2005). SiSPAT-Isotope, a coupled heat, water and stable isotope (HDO and $H_2$18O) transport model for bare soil. Part I: Model description and first verifications. *Journal of Hydrology*, *309*(1–4), 277–300. https://doi.org/10.1016/j.jhydrol.2004.12.013

Brooks, R. , H., & Corey, A. , T. (1964). Hydraulic properties of porous media. *Hydrology Papers*, *3*, 37.

Brunke, M., Groh, J., Vanderborght, J., Vereecken, H., & Pütz, T. (2019). Tau: Ein bedeutsamer Bestandteil des Wasserhaushaltes eines Grünlandstandortes – eine lysimeterbasierte Studie [Tau: An important component of the water balance of a grassland site – a lysimeter-based study] (In German, with English abstract). *Gumpensteiner Lysimetertagung*, 49–58.

Brutsaert, W. (2014). Daily evaporation from drying soil: Universal parameterization with similarity. *Water Resources Research*, *50*(4), 3206–3215. https://doi.org/10.1002/2013WR014872

Burt, C. M., Mutziger, A. J., Allen, R. G., & Howell, T. A. (2005). Evaporation Research: Review and Interpretation. *Journal of Irrigation and Drainage Engineering*, *131*(1), 37–58. https://doi.org/10.1061/(asce)0733-9437(2005)131:1(37)

Campbell, G. S. (1974). A simple method for determining unsaturated conductivity from moisture retention data. *Soil Science*, *117*(6), 311–314. https://doi.org/10.1097/00010694-197406000-00001

Campbell, G., & Schiozawa, S. (1992). Prediction of hydraulic properties of soils using particle-size distribution and bulk density data. *Proceedings of International Workshop on Indirect Methods for Estimating the Hydraulic Properties of Unsaturated Soils*, 317–328.

Carminati, A., Kaestner, A., Flühler, H., Lehmann, P., Or, D., Lehmann, E., & Stampanoni, M. (2007). Hydraulic contacts controlling water flow across porous grains. *Physical Review E - Statistical, Nonlinear, and Soft Matter Physics*, *76*(2). https://doi.org/10.1103/PhysRevE.76.026311

Carminati, A., Kaestner, A., Ippisch, O., Koliji, A., Lehmann, P., Hassanein, R., Vontobel, P., Lehmann, E., Laloui, L., Vulliet, L., & Flühler, H. (2007). Water flow between soil aggregates. *Transport in Porous Media*, *68*(2), 219–236. https://doi.org/10.1007/s11242-006-9041-z

Chartzoulakis, K., & Bertaki, M. (2015). Sustainable Water Management in Agriculture under Climate Change. *Agriculture and Agricultural Science Procedia*, *4*, 88–98. https://doi.org/10.1016/j.aaspro.2015.03.011

Chukalla, A. D., Mekonnen, M. M., Gunathilake, D., Wolkeba, F. T., Gunasekara, B., & Vanham, D. (2025). Global spatially explicit crop water consumption shows an overall increase of 9% for 46 agricultural crops from 2010 to 2020. *Nature Food*, *6*(10), 983–994. https://doi.org/10.1038/s43016-025-01231-x

Class, H. (2007). *Models for non-isothermal compositional gas-liquid flow and transport in porous media*. Universität Stuttgart.

Coltmann, N. E. (2024). *Coupled Free-Flow and Porous-Medium Flow Systems: An Analysis of Soil Water Evaporation on Multiple Scales*. Institut für Wasser- und Umweltsystemmodellierung der Universität Stuttgart.

Cooper, P. J. M., Gregory, P. J., Keatinge, J. D. H., & Brown, S. C. (1987). Effects of Fertilizer, Variety and Location on Barley Production under Rainfed Conditions in Northern Syria 2. Soil Water Dynamics and Crop Water Use. *Field Crops Research*, *16*, 67–84. https://doi.org/https://doi.org/10.1016/0378-4290(87)90054-2

Craig, H., & Gordon, L. , I. (1965). Deuterium and oxygen 18 variationsin the ocean and the marine atmosphere, Stable Isotopes in Oceanographic Studies and Paleotemperatures E. In E. Tongiori (Ed.), *Proceedings of the Third Spoleto Conference* (pp. 9–130).

Craig, H., Gordon, L. I., & Horibe, Y. (1963). Isotopic exchange effects in the evaporation of water: 1. Low-temperature experimental results. *Journal of Geophysical Research*, *68*(17), 5079–5087. https://doi.org/10.1029/JZ068i017p05079

Dai, A. (2011). Characteristics and trends in various forms of the Palmer Drought Severity Index during 1900-2008. *Journal of Geophysical Research Atmospheres*, *116*(12). https://doi.org/10.1029/2010JD015541

Dar, S. S., Ghosh, P., Swaraj, A., & Kumar, A. (2020). Craig–Gordon model validation using stable isotope ratios in water vapor over the Southern Ocean. *Atmospheric Chemistry and Physics*, *20*(19), 11435–11449. https://doi.org/10.5194/acp-20-11435-2020

Davarzani, H., Smits, K., Tolene, R. M., & Illangasekare, T. (2014). Study of the effect of wind speed on evaporation from soil through integrated modeling of the atmospheric boundary layer and shallow subsurface. *Water Resources Research*, *50*(1), 661–680. https://doi.org/10.1002/2013WR013952

Dijkema, J., Koonce, J. E., Shillito, R. M., Ghezzehei, T. A., Berli, M., van der Ploeg, M. J., & van Genuchten, M. Th. (2018). Water Distribution in an Arid Zone Soil: Numerical Analysis of Data from a Large Weighing Lysimeter. *Vadose Zone Journal*, *17*(1), 1–17. https://doi.org/10.2136/vzj2017.01.0035

Dimitrov, M., Vanderborght, J., Kostov, K. G., Debecker, B., Schulze Lammers, P., Damerow, L., & Vereecken, H. (2015). Soil Hydraulic Parameters of Bare Soil Plots with Different Soil Structure Inversely Derived from L-Band Brightness Temperatures. *Vadose Zone Journal*, *14*(8), 1–23. https://doi.org/10.2136/vzj2014.09.0133

Dimitrov, M., Vanderborght, J., Kostov, K. G., Jadoon, K. Z., Weihermüller, L., Jackson, T. J., Bindlish, R., Pachepsky, Y., Schwank, M., & Vereecken, H. (2014). Soil Hydraulic Parameters and Surface Soil Moisture of a Tilled Bare Soil Plot Inversely Derived from L-Band Brightness Temperatures. *Vadose Zone Journal*, *13*(1), 1–18. https://doi.org/10.2136/vzj2013.04.0075

Doležal, F., Hernandez-Gomis, R., Matula, S., Gulamov, M., Miháliková, M., & Khodjaev, S. (2018). Actual Evapotranspiration of Unirrigated Grass in a Smart Field Lysimeter. *Vadose Zone Journal*, *17*(1), 1–13. https://doi.org/10.2136/vzj2017.09.0173

Dourado Neto, D., de Jong van Lier, Q., van Genuchten, M. Th., Reichardt, K., Metselaar, K., & Nielsen, D. R. (2011). Alternative Analytical Expressions for the General van Genuchten–Mualem and van Genuchten–Burdine Hydraulic Conductivity Models. *Vadose Zone Journal*, *10*(2), 618–623. https://doi.org/10.2136/vzj2009.0191

Dubbert, M., & Werner, C. (2019). Water fluxes mediated by vegetation: emerging isotopic insights at the soil and atmosphere interfaces. *New Phytologist*, *221*(4), 1754–1763. https://doi.org/10.1111/nph.15547

Durner, W. (1994). Hydraulic conductivity estimation for soils with heterogeneous pore structure. *Water Resources Research*, *30*(2), 211–223. https://doi.org/10.1029/93WR02676

Evett, S. R., Lascano, R. J., Howell, T. A., Tolk, J. A., O’Shaughnessy, S. A., & Colaizzi, P. D. (2012). Single- and Dual-Surface Iterative Energy Balance Solutions for Reference ET. *Transactions of the ASABE*, *55*(2), 533–541. https://doi.org/10.13031/2013.41388

Farrell, D. A., Greacen, E. L., & Gurr, C. G. (1966). Vapor transfer in soil due to air turbulence. *Soil Science*, *102*(5), 305–313. https://doi.org/10.1097/00010694-196611000-00005

Fatichi, S., Or, D., Walko, R., Vereecken, H., Young, M. H., Ghezzehei, T. A., Hengl, T., Kollet, S., Agam, N., & Avissar, R. (2020). Soil structure is an important omission in Earth System Models. *Nature Communications*, *11*(1). https://doi.org/10.1038/s41467-020-14411-z

Fayer, M. J., & Simmons, C. S. (1995). Modified Soil Water Retention Functions for All Matric Suctions. *Water Resources Research*, *31*(5), 1233–1238. https://doi.org/10.1029/95WR00173

Feng, J., Zhang, K., Zhan, H., & Chao, L. (2023). Improved soil evaporation remote sensing retrieval algorithms and associated uncertainty analysis on the Tibetan Plateau. *Hydrology and Earth System Sciences*, *27*(2), 363–383. https://doi.org/10.5194/hess-27-363-2023

Fetzer, T. (2018). *Coupled free and porous-medium flow processes affected by turbulence and roughness: models, concepts and analysis*. Stuttgart.

Fetzer, T., Vanderborght, J., Mosthaf, K., Smits, K. M., & Helmig, R. (2017). Heat and water transport in soils and across the soil-atmosphere interface: 2. Numerical analysis. *Water Resources Research*, *53*(2), 1080–1100. https://doi.org/10.1002/2016WR019983

Gebler, S., Hendricks Franssen, H.-J., Pütz, T., Post, H., Schmidt, M., & Vereecken, H. (2015). Actual evapotranspiration and precipitation measured by lysimeters: a comparison with eddy covariance and tipping bucket. *Hydrology and Earth System Sciences*, *19*(5), 2145–2161. https://doi.org/10.5194/hess-19-2145-2015

Ghanbarian, B., Sahimi, M., & Daigle, H. (2016). Modeling relative permeability of water in soil: Application of effective-medium approximation and percolation theory. *Water Resources Research*, *52*(7), 5025–5040. https://doi.org/10.1002/2015WR017903

Gonfiatini, R. (1978). Standards for stable isotope measurements in natural compounds. *Nature*, *271*(5645), 534–536. https://doi.org/10.1038/271534a0

Gong, C., Berli, M., Zhang, Z., Wang, W., & Wang, Y. (2025). A novel method for estimating film-flow-controlled bare soil evaporation. *Journal of Hydrology: Regional Studies*, *62*, 102784. https://doi.org/10.1016/j.ejrh.2025.102784

Good, S. P., Noone, D., & Bowen, G. (2015). Hydrologic connectivity constrains partitioning of global terrestrial water fluxes. *Science*, *349*(6244), 175–177. https://doi.org/10.1126/science.aaa5931

Goss, M. J., & Ehlers, W. (2009). The role of lysimeters in the development of our understanding of soil water and nutrient dynamics in ecosystems. *Soil Use and Management*, *25*(3), 213–223. https://doi.org/10.1111/j.1475-2743.2009.00230.x

Graf, A., Herbst, M., Weihermüller, L., Huisman, J. A., Prolingheuer, N., Bornemann, L., & Vereecken, H. (2012). Analyzing spatiotemporal variability of heterotrophic soil respiration at the field scale using orthogonal functions. *Geoderma*, *181–182*, 91–101. https://doi.org/10.1016/j.geoderma.2012.02.016

Groh, J., Pütz, T., Gerke, H. H., Vanderborght, J., & Vereecken, H. (2019). Quantification and Prediction of Nighttime Evapotranspiration for Two Distinct Grassland Ecosystems. *Water Resources Research*, *55*(4), 2961–2975. https://doi.org/10.1029/2018WR024072

Groh, J., Slawitsch, V., Herndl, M., Graf, A., Vereecken, H., & Pütz, T. (2018). Determining dew and hoar frost formation for a low mountain range and alpine grassland site by weighable lysimeter. *Journal of Hydrology*, *563*, 372–381. https://doi.org/10.1016/j.jhydrol.2018.06.009

Groh, J., Vanderborght, J., Pütz, T., Gründling, R., Rupp, H., Rahmati, M., Sommer, M., Sommer, M., Vereecken, H., & Gerke, H. H. (2020). Responses of soil water storage and crop water use efficiency to changing climatic conditions: A lysimeter-based space-for-time approach. *Hydrology and Earth System Sciences*, *24*(3), 1211–1225. https://doi.org/10.5194/hess-24-1211-2020

Groh, J., Vanderborght, J., Pütz, T., & Vereecken, H. (2016). How to Control the Lysimeter Bottom Boundary to Investigate the Effect of Climate Change on Soil Processes? *Vadose Zone Journal*, *15*(7), 1–15. https://doi.org/10.2136/vzj2015.08.0113

Haghighi, E., & Or, D. (2015). Evaporation from Wavy Porous Surfaces into Turbulent Airflows. *Transport in Porous Media*, *110*(2), 225–250. https://doi.org/10.1007/s11242-015-0512-y

Hannes, M., Wollschläger, U., Schrader, F., Durner, W., Gebler, S., Pütz, T., Fank, J., Von Unold, G., & Vogel, H. J. (2015). A comprehensive filtering scheme for high-resolution estimation of the water balance components from high-precision lysimeters. *Hydrology and Earth System Sciences*, *19*(8), 3405–3418. https://doi.org/10.5194/hess-19-3405-2015

Hannes, M., Wollschläger, U., Wöhling, T., & Vogel, H. -J. (2016). Revisiting hydraulic hysteresis based on long-term monitoring of hydraulic states in lysimeters. *Water Resources Research*, *52*(5), 3847–3865. https://doi.org/10.1002/2015WR018319

Haverd, V., & Cuntz, M. (2010). Soil–Litter–Iso: A one-dimensional model for coupled transport of heat, water and stable isotopes in soil with a litter layer and root extraction. *Journal of Hydrology*, *388*(3–4), 438–455. https://doi.org/10.1016/j.jhydrol.2010.05.029

Haverd, V., Cuntz, M., Griffith, D., Keitel, C., Tadros, C., & Twining, J. (2011). Measured deuterium in water vapour concentration does not improve the constraint on the partitioning of evapotranspiration in a tall forest canopy, as estimated using a soil vegetation atmosphere transfer model. *Agricultural and Forest Meteorology*, *151*(6), 645–654. https://doi.org/10.1016/j.agrformet.2011.02.005

Heinlein, F., Biernath, C., Klein, C., Thieme, C., & Priesack, E. (2017). Evaluation of Simulated Transpiration from Maize Plants on Lysimeters. *Vadose Zone Journal*, *16*(1), 1–16. https://doi.org/10.2136/vzj2016.05.0042

Herbrich, M., Gerke, H. H., Bens, O., & Sommer, M. (2017). Water balance and leaching of dissolved organic and inorganic carbon of eroded Luvisols using high precision weighing lysimeters. *Soil and Tillage Research*, *165*, 144–160. https://doi.org/10.1016/j.still.2016.08.003

Herczeg, A. L., & Leaney, F. W. (2011). Review: Environmental tracers in arid-zone hydrology. *Hydrogeology Journal*, *19*(1), 17–29. https://doi.org/10.1007/s10040-010-0652-7

Hernández-López, M. F., Braud, I., Gironás, J., Suárez, F., & Muñoz, J. F. (2016). Modelling evaporation processes in soils from the Huasco salt flat basin, Chile. *Hydrological Processes*, *30*(25), 4704–4719. https://doi.org/10.1002/hyp.10987

Hillel, Daniel. (2004). *Introduction to environmental soil physics*. Elsevier Academic Press.

Hoffmann, M., Schwartengräber, R., Wessolek, G., & Peters, A. (2016). Comparison of simple rain gauge measurements with precision lysimeter data. *Atmospheric Research*, *174–175*, 120–123. https://doi.org/10.1016/j.atmosres.2016.01.016

Hu, Z., Wang, G., Sun, X., Zhu, M., Song, C., Huang, K., & Chen, X. (2018). Spatial-Temporal Patterns of Evapotranspiration Along an Elevation Gradient on Mount Gongga, Southwest China. *Water Resources Research*, *54*(6), 4180–4192. https://doi.org/10.1029/2018WR022645

Huxman, T. E., Wilcox, B. P., Breshears, D. D., Scott, R. L., Snyder, K. A., Small, E. E., Hultine, K., Pockman, W. T., & Jackson, R. B. (2005). ECOHYDROLOGICAL IMPLICATIONS OF WOODY PLANT ENCROACHMENT. *Ecology*, *86*(2), 308–319. https://doi.org/10.1890/03-0583

Iden, S. C., Peters, A., & Durner, W. (2015). Improving prediction of hydraulic conductivity by constraining capillary bundle models to a maximum pore size. *Advances in Water Resources*, *85*, 86–92. https://doi.org/10.1016/j.advwatres.2015.09.005

Idso, S. B., Reginato, R. J., Jackson, R. D., Kimball, B. A., & Nakayama, F. S. (1974). The Three Stages of Drying of a Field Soil. *Soil Science Society of America Journal*, *38*(5), 831–837. https://doi.org/10.2136/sssaj1974.03615995003800050037x

Imukova, K., Ingwersen, J., Hevart, M., & Streck, T. (2016). Energy balance closure on a winter wheat stand: Comparing the eddy covariance technique with the soil water balance method. *Biogeosciences*, *13*(1), 63–75. https://doi.org/10.5194/bg-13-63-2016

Ineson, P., Taylor, K., Harrison, A. F., Poskitt, J., Benham, D. G., Tipping, E., & Woof, C. (1998). Effects of climate change on nitrogen dynamics in upland soils. 1. A transplant approach. *Global Change Biology*, *4*(2), 143–152. https://doi.org/10.1046/j.1365-2486.1998.00118.x

Ishihara, Y., Shimojima, E., & Harada, H. (1992). Water vapor transfer beneath bare soil where evaporation is influenced by a turbulent surface wind. *Journal of Hydrology*, *131*(1–4), 63–104. https://doi.org/10.1016/0022-1694(92)90213-F

Jensen, M. E. ., & Allen, R. G. . (2016). *Evaporation, Evapotranspiration, and Irrigation Water Requirements*. American Society of Civil Engineers.

Jung, M., Reichstein, M., Ciais, P., Seneviratne, S. I., Sheffield, J., Goulden, M. L., Bonan, G., Cescatti, A., Chen, J., de Jeu, R., Dolman, A. J., Eugster, W., Gerten, D., Gianelle, D., Gobron, N., Heinke, J., Kimball, J., Law, B. E., Montagnani, L., ... Zhang, K. (2010). Recent decline in the global land evapotranspiration trend due to limited moisture supply. *Nature*, *467*(7318), 951–954. https://doi.org/10.1038/nature09396

Karimov, A. K., Šimůnek, J., Hanjra, M. A., Avliyakulov, M., & Forkutsa, I. (2014). Effects of the shallow water table on water use of winter wheat and ecosystem health: Implications for unlocking the potential of groundwater in the Fergana Valley (Central Asia). *Agricultural Water Management*, *131*, 57–69. https://doi.org/10.1016/j.agwat.2013.09.010

Keating, B. A., Carberry, P. S., Hammer, G. L., Probert, M. E., Robertson, M. J., Holzworth, D., Huth, N. I., Hargreaves, J. N. G., Meinke, H., Hochman, Z., McLean, G., Verburg, K., Snow, V., Dimes, J. P., Silburn, M., Wang, E., Brown, S., Bristow, K. L., Asseng, S., ... Smith, C. J. (2003). An overview of APSIM, a model designed for farming systems simulation. *European Journal of Agronomy*, *18*(3–4), 267–288. https://doi.org/10.1016/S1161-0301(02)00108-9

Kiemle, S. (2019). *Modelling of Isotope Transport and Evaporation Rates at the Porous Medium Free-Flow Interface*. Universität Stuttgart.

Kiemle, S., Heck, K., Coltman, E., & Helmig, R. (2023). Stable Water Isotopologue Fractionation During Soil-Water Evaporation: Analysis Using a Coupled Soil-Atmosphere Model. *Water Resources Research*, *59*(2). https://doi.org/10.1029/2022WR032385

Kiemle, S., Schneider, J., & Heck, K. (2024). Replication data for analyzing stable water isotopologue transport within soils using fractionation parameterizations [Data set]. *DARUS*.

Kimball, B. A., & Lemon, E. R. (1971). Air Turbulence Effects upon Soil Gas Exchange. *Soil Science Society of America Journal*, *35*(1), 16–21. https://doi.org/10.2136/sssaj1971.03615995003500010013x

Knaps, A. (2019). *Table of annual value since 1961*. Longterm Climate Observation from the Climate Station at the Research Center.

Koch, T., Gläser, D., Weishaupt, K., Ackermann, S., Beck, M., Becker, B., Burbulla, S., Class, H., Coltman, E., Emmert, S., Fetzer, T., Grüninger, C., Heck, K., Hommel, J., Kurz, T., Lipp, M., Mohammadi, F., Scherrer, S., Schneider, M., … Flemisch, B. (2021). DuMux 3 – an open-source simulator for solving flow and transport problems in porous media with a focus on model coupling. *Computers & Mathematics with Applications*, *81*, 423–443. https://doi.org/10.1016/j.camwa.2020.02.012

Kohfahl, C., Molano-Leno, L., Martínez, G., Vanderlinden, K., Guardiola-Albert, C., & Moreno, L. (2019). Determining groundwater recharge and vapor flow in dune sediments using a weighable precision meteo lysimeter. *Science of the Total Environment*, *656*, 550–557. https://doi.org/10.1016/j.scitotenv.2018.11.415

Kool, D., Ben-Gal, A., Agam, N., Šimůnek, J., Heitman, J. L., Sauer, T. J., & Lazarovitch, N. (2014). Spatial and diurnal below canopy evaporation in a desert vineyard: Measurements and modeling. *Water Resources Research*, *50*(8), 7035–7049. https://doi.org/10.1002/2014WR015409

Kroes, J. G., van Dam, J. C., Bartholomeus, R. P., Groenendijk, P., Heinen, M., Hendriks, R. F. A., Mulder, H. M., Supit, I., & van Walsum, P. E. V. (2017). *SWAP version 4*. https://doi.org/10.18174/416321

Lehmann, P., Assouline, S., & Or, D. (2008). Characteristic lengths affecting evaporative drying of porous media. *Physical Review E - Statistical, Nonlinear, and Soft Matter Physics*, *77*(5). https://doi.org/10.1103/PhysRevE.77.056309

Lehmann, P., Berli, M., Koonce, J. E., & Or, D. (2019). Surface Evaporation in Arid Regions: Insights From Lysimeter Decadal Record and Global Application of a Surface Evaporation Capacitor (SEC) Model. *Geophysical Research Letters*, *46*(16), 9648–9657. https://doi.org/10.1029/2019GL083932

Lehmann, P., Bickel, S., Wei, Z., & Or, D. (2020). Physical Constraints for Improved Soil Hydraulic Parameter Estimation by Pedotransfer Functions. *Water Resources Research*, *56*(4). https://doi.org/10.1029/2019WR025963

Levine, S., & Cuthiell, D. L. (1986). Relative permeabilities in two-phase flow through porous media: An application of effective medium theory. *Journal of Canadian Petroleum Technology*, *25*(05). https://doi.org/10.2118/86-05-10

Li, Z., Vanderborght, J., & Smits, K. M. (2019). Evaluation of Model Concepts to Describe Water Transport in Shallow Subsurface Soil and Across the Soil–Air Interface. *Transport in Porous Media*, *128*(3), 945–976. https://doi.org/10.1007/s11242-018-1144-9

Li, Z., Vanderborght, J., & Smits, K. M. (2020). The effect of the top soil layer on moisture and evaporation dynamics. *Vadose Zone Journal*, *19*(1). https://doi.org/10.1002/vzj2.20049

Lipman, C. B., & Waynick, D. D. (1916). A detailed study of effects of climate on important properties of soils. *Soil Science*, *1*, 5–48.

Luo, Y., & Sophocleous, M. (2010). Seasonal groundwater contribution to crop-water use assessed with lysimeter observations and model simulations. *Journal of Hydrology*, *389*(3–4), 325–335. https://doi.org/10.1016/j.jhydrol.2010.06.011

Maier, M., Schack-Kirchner, H., Aubinet, M., Goffin, S., Longdoz, B., & Parent, F. (2012). Turbulence Effect on Gas Transport in Three Contrasting Forest Soils. *Soil Science Society of America Journal*, *76*(5), 1518–1528. https://doi.org/10.2136/sssaj2011.0376

Majoube, M. (1971). Fractionnement en oxygène 18 et en deutérium entre l'eau et sa vapeur. *Journal de Chimie Physique*, *68*, 1423–1436. https://doi.org/10.1051/jcp/1971681423

Marek, G., Gowda, P., Marek, T., Auvermann, B., Evett, S., Colaizzi, P., & Brauer, D. (2016). Estimating preseason irrigation losses by characterizing evaporation of effective precipitation under bare soil conditions using large weighing lysimeters. *Agricultural Water Management*, *169*, 115–128. https://doi.org/10.1016/j.agwat.2016.02.024

Mathieu, R., & Bariac, T. (1996). An Isotopic Study (2 H and 18 O) of Water Movements in Clayey Soils Under a Semiarid Climate. *Water Resources Research*, *32*(4), 779–789. https://doi.org/10.1029/96WR00074

Mathworks. (2019). *MATLAB version 9.7 (R2019b). Natick, MA:*

Meissner, R., Seeger, J., Rupp, H., Seyfarth, M., & Borg, H. (2007). Measurement of dew, fog, and rime with a high-precision gravitation lysimeter. *Journal of Plant Nutrition and Soil Science*, *170*(3), 335–344. https://doi.org/10.1002/jpln.200625002

Melayah, A., Bruckler, L., & Bariac, T. (1996). Modeling the Transport of Water Stable Isotopes in Unsaturated Soils Under Natural Conditions: 1. Theory. *Water Resources Research*, *32*(7), 2047–2054. https://doi.org/10.1029/96WR00674

Mellouli, H. J., van Wesemael, B., Poesen, J., & Hartmann, R. (2000). Evaporation losses from bare soils as influenced by cultivation techniques in semi-arid regions. *Agricultural Water Management, 42*(3), 355–369. https://doi.org/10.1016/S0378-3774(99)00040-2

Merlin, O., Stefan, V. G., Amazirh, A., Chanzy, A., Ceschia, E., Er-Raki, S., Gentine, P., Tallec, T., Ezzahar, J., Bircher, S., Beringer, J., & Khabba, S. (2016). Modeling soil evaporation efficiency in a range of soil and atmospheric conditions using a meta-analysis approach. *Water Resources Research*, *52*(5), 3663–3684. https://doi.org/10.1002/2015WR018233

Merlivat, L., & Jouzel, J. (1979). Global climatic interpretation of the deuterium-oxygen 18 relationship for precipitation. *Journal of Geophysical Research: Oceans*, *84*(C8), 5029–5033. https://doi.org/10.1029/JC084iC08p05029

Milly, P. C. D. (1982). Moisture and heat transport in hysteretic, inhomogeneous porous media: A matric head-based formulation and a numerical model. *Water Resources Research*, *18*(3), 489–498. https://doi.org/10.1029/WR018i003p00489

Milly, P. C. D. (1984). A Simulation Analysis of Thermal Effects on Evaporation From Soil. *Water Resources Research*, *20*(8), 1087–1098. https://doi.org/10.1029/WR020i008p01087

Milly, P. C. D., Dunne, K. A., & Vecchia, A. V. (2005). Global pattern of trends in streamflow and water availability in a changing climate. *Nature*, *438*(7066), 347–350. https://doi.org/10.1038/nature04312

Montzka, C., Moradkhani, H., Weihermüller, L., Franssen, H.-J. H., Canty, M., & Vereecken, H. (2011). Hydraulic parameter estimation by remotely-sensed top soil moisture observations with the particle filter. *Journal of Hydrology*, *399*(3–4), 410–421. https://doi.org/10.1016/j.jhydrol.2011.01.020

Mosthaf, K. (2014). *Modeling and analysis of coupled porous-medium and free flow with application to evaporation processes*. Universität Stuttgart.

Mosthaf, K., Helmig, R., & Or, D. (2014). Modeling and analysis of evaporation processes from porous media on the REV scale. *Water Resources Research*, *50*(2), 1059–1079. https://doi.org/10.1002/2013WR014442

Mualem, Y. (1976). Hysteretical models for prediction of the hydraulic conductivity of unsaturated porous media. *Water Resources Research*, *12*(6), 1248–1254. https://doi.org/10.1029/WR012i006p01248

Muller, P. (1994). Glossary of terms used in physical organic chemistry (IUPAC Recommendations 1994). *Pure and Applied Chemistry,* *66*(5), 1077–1184. https://doi.org/10.1351/pac199466051077

Mutziger, A. J., Burt, C. M., Howes, D. J., & Allen, R. G. (2005). Comparison of Measured and FAO-56 Modeled Evaporation from Bare Soil. *Journal of Irrigation and Drainage Engineering*, *131*(1), 59–72. https://doi.org/10.1061/(ASCE)0733-9437(2005)131:1(59)

Nehls, T., Nam, R., & Wessolek, G. (2011). Technical note on measuring run-off dynamics from pavements using a new device: The weighable tipping bucket. *Hydrology and Earth System Sciences*, *15*(5), 1379–1386. https://doi.org/10.5194/hess-15-1379-2011

Nolz, R., Kammerer, G., & Cepuder, P. (2013). Interpretation of lysimeter weighing data affected by wind. *Journal of Plant Nutrition and Soil Science*, *176*(2), 200–208. https://doi.org/10.1002/jpln.201200342

Oerter, E. J., & Bowen, G. (2017). In situ monitoring of H and O stable isotopes in soil water reveals ecohydrologic dynamics in managed soil systems. *Ecohydrology*, *10*(4). https://doi.org/10.1002/eco.1841

Oerter, E. J., & Bowen, G. J. (2019). Spatio-temporal heterogeneity in soil water stable isotopic composition and its ecohydrologic implications in semiarid ecosystems. *Hydrological Processes*, *33*(12), 1724–1738. https://doi.org/10.1002/hyp.13434

Oerter, E., Singleton, M., & Davisson, L. (2017). Hydrogen and oxygen stable isotope signatures of goethite hydration waters by thermogravimetry-enabled laser spectroscopy. *Chemical Geology*, *475*, 14–23. https://doi.org/10.1016/j.chemgeo.2017.10.025

Oki, T., & Kanae, S. (2006). Global Hydrological Cycles and World Water Resources. *Science*, *313*(5790), 1068–1072. https://doi.org/10.1126/science.1128845

Or, D., & Lehmann, P. (2019). Surface Evaporative Capacitance: How Soil Type and Rainfall Characteristics Affect Global-Scale Surface Evaporation. *Water Resources Research*, *55*(1), 519–539. https://doi.org/10.1029/2018WR024050

Or, D., Lehmann, P., Shahraeeni, E., & Shokri, N. (2013). Advances in Soil Evaporation Physics—A Review. *Vadose Zone Journal*, *12*(4), 1–16. https://doi.org/10.2136/vzj2012.0163

Padrón, R. S., Gudmundsson, L., Michel, D., & Seneviratne, S. I. (2020). Terrestrial water loss at night: global relevance from observations and climate models. *Hydrology and Earth System Sciences*, *24*(2), 793–807. https://doi.org/10.5194/hess-24-793-2020

Parlange, J.-Y., Vauclin, M., Haverkamp, R., & Lisle, I. (1985). Note: The relation between desorptivity and soil-water diffusivity. *Soil Science*, *139*(5), 458–461. https://doi.org/10.1097/00010694-198505000-00012

Peters, A., Durner, W., & Iden, S. (2024). The PDI model system for parameterizing soil hydraulic properties. *Vadose Zone Journal*, *23*(4). https://doi.org/10.1002/vzj2.20338

Peters, A., Groh, J., Schrader, F., Durner, W., Vereecken, H., & Pütz, T. (2017). Towards an unbiased filter routine to determine precipitation and evapotranspiration from high precision lysimeter measurements. *Journal of Hydrology*, *549*, 731–740. https://doi.org/10.1016/j.jhydrol.2017.04.015

Peters, A., Hohenbrink, T. L., Iden, S. C., & Durner, W. (2021). A Simple Model to Predict Hydraulic Conductivity in Medium to Dry Soil

From the Water Retention Curve. *Water Resources Research*, *57*(5). https://doi.org/10.1029/2020WR029211

Peters, A., Nehls, T., Schonsky, H., & Wessolek, G. (2014). Separating precipitation and evapotranspiration from noise - A new filter routine for high-resolution lysimeter data. *Hydrology and Earth System Sciences*, *18*(3), 1189–1198. https://doi.org/10.5194/hess-18-1189-2014

Peters, A., Nehls, T., & Wessolek, G. (2016). Technical note: Improving the AWAT filter with interpolation schemes for advanced processing of high resolution data. *Hydrology and Earth System Sciences*, *20*(6), 2309–2315. https://doi.org/10.5194/hess-20-2309-2016

Philip, J. R., & de Vries, D. A. (1957). Moisture movement in porous materials under temperature gradients. *Eos, Transactions American Geophysical Union*, *38*(2), 222–232. https://doi.org/10.1029/TR038i002p00222

Priesack, E., & Durner, W. (2006). Closed-Form Expression for the Multi-Modal Unsaturated Conductivity Function. *Vadose Zone Journal*, *5*(1), 121–124. https://doi.org/10.2136/vzj2005.0066

Priestley, C. H. B., & Taylor, R. J. (1972). On the Assessment of Surface Heat Flux and Evaporation Using Large-Scale Parameters. *Monthly Weather Review*, *100*(2), 81–92. https://doi.org/10.1175/1520-0493(1972)100<0081:OTAOSH>2.3.CO;2

Pütz, T., Fank, J., & Flury, M. (2018). Lysimeters in Vadose Zone Research. *Vadose Zone Journal*, *17*(1), 1–4. https://doi.org/10.2136/vzj2018.02.0035

Pütz, T., Kiese, R., Wollschläger, U., Groh, J., Rupp, H., Zacharias, S., Priesack, E., Gerke, H. H., Gasche, R., Bens, O., Borg, E., Baessler, C., Kaiser, K., Herbrich, M., Munch, J. C., Sommer, M., Vogel, H. J., Vanderborght, J., & Vereecken, H. (2016). TERENO-SOILCan: a lysimeter-network in Germany observing soil processes and plant diversity influenced by climate change. *Environmental*

Earth Sciences, *75*(18). https://doi.org/10.1007/s12665-016-6031-5

Quade, M., Klosterhalfen, A., Graf, A., Brüggemann, N., Hermes, N., Vereecken, H., & Rothfuss, Y. (2019). In-situ monitoring of soil water isotopic composition for partitioning of evapotranspiration during one growing season of sugar beet (Beta vulgaris). *Agricultural and Forest Meteorology*, *266–267*, 53–64. https://doi.org/10.1016/j.agrformet.2018.12.002

Quinn, R., Parker, A., & Rushton, K. (2018). Evaporation from bare soil: Lysimeter experiments in sand dams interpreted using conceptual and numerical models. *Journal of Hydrology*, *564*, 909–915. https://doi.org/10.1016/j.jhydrol.2018.07.011

Rianna, G., Reder, A., & Pagano, L. (2018). Estimating actual and potential bare soil evaporation from silty pyroclastic soils: Towards improved landslide prediction. *Journal of Hydrology*, *562*, 193–209. https://doi.org/10.1016/j.jhydrol.2018.05.005

Riou, C. (1977). *Évaporation du sol nu et répartition des pluies: relations établies en Tunisie à partir des résultats des cases lysimétriques*. INRAT.

Ritchie, J. T. (1972). Model for predicting evaporation from a row crop with incomplete cover. *Water Resources Research*, *8*(5), 1204–1213. https://doi.org/10.1029/WR008i005p01204

Ross, P. J. (2006). Fast solution of Richards' equation for flexible soil hydraulic property descriptions (Land and Water Technical Report). *CSIRO*, *39*(6).

Rost, S., Gerten, D., Bondeau, A., Lucht, W., Rohwer, J., & Schaphoff, S. (2008). Agricultural green and blue water consumption and its influence on the global water system. *Water Resources Research*, *44*(9). https://doi.org/10.1029/2007WR006331

Rothfuss, Y., Biron, P., Braud, I., Canale, L., Durand, J. L., Gaudet, J. P., Richard, P., Vauclin, M., & Bariac, T. (2010). Partitioning evapotranspiration fluxes into soil evaporation and plant transpiration using water stable isotopes under controlled conditions. *Hydrological Processes*, *24*(22), 3177–3194. https://doi.org/10.1002/hyp.7743

Rothfuss, Y., & Javaux, M. (2017). Reviews and syntheses: Isotopic approaches to quantify root water uptake: a review and comparison of methods. *Biogeosciences*, *14*(8), 2199–2224. https://doi.org/10.5194/bg-14-2199-2017

Rothfuss, Y., Merz, S., Vanderborght, J., Hermes, N., Weuthen, A., Pohlmeier, A., Vereecken, H., & Brüggemann, N. (2015). Long-term and high-frequency non-destructive monitoring of water stable isotope profiles in an evaporating soil column. *Hydrology and Earth System Sciences*, *19*(10), 4067–4080. https://doi.org/10.5194/hess-19-4067-2015

Rothfuss, Y., Quade, M., Brüggemann, N., Graf, A., Vereecken, H., & Dubbert, M. (2021). Reviews and syntheses: Gaining insights into evapotranspiration partitioning with novel isotopic monitoring methods. *Biogeosciences*, *18*(12), 3701–3732. https://doi.org/10.5194/bg-18-3701-2021

Rothfuss, Y., Vereecken, H., & Brüggemann, N. (2013). Monitoring water stable isotopic composition in soils using gas-permeable tubing and infrared laser absorption spectroscopy. *Water Resources Research*, *49*(6), 3747–3755. https://doi.org/10.1002/wrcr.20311

Rudiyanto, Sakai, M., van Genuchten, M. Th., Alazba, A. A., Setiawan, B. I., & Minasny, B. (2015). A complete soil hydraulic model accounting for capillary and adsorptive water retention, capillary and film conductivity, and hysteresis. *Water Resources Research*, *51*(11), 8757–8772. https://doi.org/10.1002/2015WR017703

Saito, H., & Šimůnek, J. (2009). Effects of meteorological models on the solution of the surface energy balance and soil temperature variations in bare soils. *Journal of Hydrology*, *373*(3–4), 545–561. https://doi.org/10.1016/j.jhydrol.2009.05.019

Salvucci, G. D. (1997). Soil and moisture independent estimation of stage-two evaporation from potential evaporation and albedo or surface temperature. *Water Resources Research*, *33*(1), 111–122. https://doi.org/10.1029/96WR02858

Schaap, M. G., Leij, F. J., & van Genuchten, M. Th. (2001). rosetta : a computer program for estimating soil hydraulic parameters with hierarchical pedotransfer functions. *Journal of Hydrology*, *251*(3–4), 163–176. https://doi.org/10.1016/S0022-1694(01)00466-8

Schlesinger, W. H., & Jasechko, S. (2014). Transpiration in the global water cycle. *Agricultural and Forest Meteorology*, *189–190*, 115–117. https://doi.org/10.1016/j.agrformet.2014.01.011

Schlüter, S., Vogel, H.-J., Ippisch, O., Bastian, P., Roth, K., Schelle, H., Durner, W., Kasteel, R., & Vanderborght, J. (2012). Virtual Soils: Assessment of the Effects of Soil Structure on the Hydraulic Behavior of Cultivated Soils. *Vadose Zone Journal*, *11*(4). https://doi.org/10.2136/vzj2011.0174

Schneider, M., & Goss, K.-U. (2012). Prediction of the water sorption isotherm in air dry soils. *Geoderma*, *170*, 64–69. https://doi.org/10.1016/j.geoderma.2011.10.008

Schoen, R., Gaudet, J. P., & Bariac, T. (1999). Preferential flow and solute transport in a large lysimeter, under controlled boundary conditions. *Journal of Hydrology*, *215*(1–4), 70–81. https://doi.org/10.1016/S0022-1694(98)00262-5

Schrader, F., Durner, W., Fank, J., Gebler, S., Pütz, T., Hannes, M., & Wollschläger, U. (2013). Estimating Precipitation and Actual Evapotranspiration from Precision Lysimeter Measurements. *Procedia Environmental Sciences*, *19*, 543–552. https://doi.org/10.1016/j.proenv.2013.06.061

Schwartz, R. C., Baumhardt, R. L., & Evett, S. R. (2010). Tillage effects on soil water redistribution and bare soil evaporation throughout a season. *Soil and Tillage Research*, *110*(2), 221–229. https://doi.org/10.1016/j.still.2010.07.015

Scotter, D. R., & Raats, P. A. C. (1969). Dispersion of water vapor in soil due to air turbulence. *Soil Science*, *108*(3), 170–176. https://doi.org/10.1097/00010694-196909000-00004

Seager, R., Ting, M., Held, I., Kushnir, Y., Lu, J., Vecchi, G., Huang, H. P., Harnik, N., Leetmaa, A., Lau, N. C., Li, C., Velez, J., & Naik, N. (2007). Model projections of an imminent transition to a more arid climate in southwestern North America. *Science*, *316*(5828), 1181–1184. https://doi.org/10.1126/science.1139601

Shahraeeni, E., & Or, D. (2010). Pore-Scale Analysis of Evaporation and Condensation Dynamics in Porous Media. *Langmuir*, *26*(17), 13924–13936. https://doi.org/10.1021/la101596y

Shahraeeni, E., & Or, D. (2012a). Pore scale mechanisms for enhanced vapor transport through partially saturated porous media. *Water Resources Research*, *48*(5). https://doi.org/10.1029/2011WR011036

Shahraeeni, E., & Or, D. (2012b). Pore-scale evaporation-condensation dynamics resolved by synchrotron x-ray tomography. *Physical Review E*, *85*(1), 016317. https://doi.org/10.1103/PhysRevE.85.016317

Sharp, Z. (2017). *Principles of Stable Isotope Geochemistry* (2nd ed.).

Shokri, N., Lehmann, P., & Or, D. (2010). Evaporation from layered porous media. *Journal of Geophysical Research: Solid Earth*, *115*(6). https://doi.org/10.1029/2009JB006743

Shurbaji, A.-R. M., & Phillips, F. M. (1995). A numerical model for the movement of H_2O, H_218O, and $2H_2O$ in the unsaturated zone. *Journal of Hydrology*, *171*(1–2), 125–142. https://doi.org/10.1016/0022-1694(94)02604-A

Šimůnek, J., Šejna, M., Saito, H., Sakai, M., & van Genuchten, M. T. (2018). *The HYDRUS-1D software package for simulating the movement of water, heat, and multiple solutes in variably saturated media Version 4.17*.

Šimůnek, J., Sejna, M., van Genuchten, M. , T., Šimůnek, J., Šejna, M., Jacques, D., & Sakai, M. (1998). *HYDRUS-1D. Simulating the one-*

dimensional movement of water, heat, and multiple solutes in variably-saturated media. https://www.pc-progress.com/en/porous-media-software/hydrus-1d

Šimůnek, J., Šejna, M., & van Genuchten, M. Th. (2013). *HYDRUS-1D Manual version 4.16. Software package for simulating one dimensional movement of water, heat and multiple solutes in variably saturated media.* University of California.

Šimůnek, J., van Genuchten, M. Th., & Šejna, M. (2016). Recent Developments and Applications of the HYDRUS Computer Software Packages. *Vadose Zone Journal*, *15*(7), 1–25. https://doi.org/10.2136/vzj2016.04.0033

Smits, K. M., Cihan, A., Sakaki, T., & Illangasekare, T. H. (2011). Evaporation from soils under thermal boundary conditions: Experimental and modeling investigation to compare equilibrium and non equilibrium-based approaches. *Water Resources Research*, *47*(5). https://doi.org/10.1029/2010WR009533

Sobaga, A., Decharme, B., Habets, F., Delire, C., Enjelvin, N., Redon, P. O., Faure-Catteloin, P., & Le Moigne, P. (2023). Assessment of the interactions between soil-biosphere-atmosphere (ISBA) land surface model soil hydrology, using four closed-form soil water relationships and several lysimeters. *Hydrology and Earth System Sciences*, *27*(13), 2437–2461. https://doi.org/10.5194/hess-27-2437-2023

Steenpass, C., Vanderborght, J., Herbst, M., Šimůnek, J., & Vereecken, H. (2010). Estimating Soil Hydraulic Properties from Infrared Measurements of Soil Surface Temperatures and TDR Data. *Vadose Zone Journal*, *9*(4), 910–924. https://doi.org/10.2136/vzj2009.0176

Stephens, D. B., Kron, A. J., & Kron, A. (2018). *Vadose Zone Hydrology*. CRC Press. https://doi.org/10.1201/9780203734490

Stewart, M. K. (1975). Stable isotope fractionation due to evaporation and isotopic exchange of falling waterdrops: Applications to atmospheric processes and evaporation of lakes. *Journal of Geophysical Research*, *80*(9), 1133–1146. https://doi.org/10.1029/JC080i009p01133

Stingaciu, L. R., Weihermüller, L., Haber-Pohlmeier, S., Stapf, S., Vereecken, H., & Pohlmeier, A. (2010). Determination of pore size distribution and hydraulic properties using nuclear magnetic resonance relaxometry: A comparative study of laboratory methods. *Water Resources Research*, *46*(11). https://doi.org/10.1029/2009WR008686

Su, Q., & Singh, V. P. (2023). Calibration-Free Priestley-Taylor Method for Reference Evapotranspiration Estimation. *Water Resources Research*, *59*(3). https://doi.org/10.1029/2022WR033198

Tehrani, K., Zhang, Y., Scheuermann, A., & Williams, D. J. (2019). Comparison of air entry values from soil water retention and volumetric shrinkage characteristic curves. *Japanese Geotechnical Society Special Publication*, *7*(2), 340–343. https://doi.org/10.3208/jgssp.v07.055

Teuling, A. J. (2018). A Forest Evapotranspiration Paradox Investigated Using Lysimeter Data. *Vadose Zone Journal*, *17*(1), 1–7. https://doi.org/10.2136/vzj2017.01.0031

Tolk, J. A., Evett, S. R., & Schwartz, R. C. (2015). Field-Measured, Hourly Soil Water Evaporation Stages in Relation to Reference Evapotranspiration Rate and Soil to Air Temperature Ratio. *Vadose Zone Journal*, *14*(7), 1–14. https://doi.org/10.2136/vzj2014.07.0079

Tran, D. K., Ralaizafisoloarivony, N., Charlier, R., Mercatoris, B., Léonard, A., Toye, D., & Degré, A. (2019). Studying the effect of desiccation cracking on the evaporation process of a Luvisol – From a small-scale experimental and numerical approach. *Soil and Tillage Research*, *193*, 142–152. https://doi.org/10.1016/j.still.2019.05.018

Trigo, I. F., de Bruin, H., Beyrich, F., Bosveld, F. C., Gavilán, P., Groh, J., & López-Urrea, R. (2018). Validation of reference evapotranspiration from Meteosat Second Generation (MSG) observations. *Agricultural and Forest Meteorology*, *259*, 271–285. https://doi.org/10.1016/j.agrformet.2018.05.008

Tuller, M., & Or, D. (2005). Water films and scaling of soil characteristic curves at low water contents. *Water Resources Research*, *41*(9). https://doi.org/10.1029/2005WR004142

Twarakavi, N. K. C., Sakai, M., & Šimůnek, J. (2009). An objective analysis of the dynamic nature of field capacity. *Water Resources Research*, *45*(10). https://doi.org/10.1029/2009WR007944

van de Griend, A. A., & Owe, M. (1994). Bare soil surface resistance to evaporation by vapor diffusion under semiarid conditions. *Water Resources Research*, *30*(2), 181–188. https://doi.org/10.1029/93WR02747

Van Der Ent, R. J., Savenije, H. H. G., Schaefli, B., & Steele-Dunne, S. C. (2010). Origin and fate of atmospheric moisture over continents. *Water Resources Research*, *46*(9). https://doi.org/10.1029/2010WR009127

van Genuchten, M. Th. (1980). A Closed-form Equation for Predicting the Hydraulic Conductivity of Unsaturated Soils. *Soil Science Society of America Journal*, *44*(5), 892–898. https://doi.org/10.2136/sssaj1980.03615995004400050002x

Van Looy, K., Bouma, J., Herbst, M., Koestel, J., Minasny, B., Mishra, U., Montzka, C., Nemes, A., Pachepsky, Y. A., Padarian, J., Schaap, M. G., Tóth, B., Verhoef, A., Vanderborght, J., van der Ploeg, M. J., Weihermüller, L., Zacharias, S., Zhang, Y., & Vereecken, H. (2017). Pedotransfer Functions in Earth System Science: Challenges and Perspectives. *Reviews of Geophysics*, *55*(4), 1199–1256. https://doi.org/10.1002/2017RG000581

Vanderborght, J., Fetzer, T., Mosthaf, K., Smits, K. M., & Helmig, R. (2017). Heat and water transport in soils and across the soil-atmosphere interface: 1. Theory and different model concepts. *Water Resources Research*, *53*(2), 1057–1079. https://doi.org/10.1002/2016WR019982

Vereecken, H., Amelung, W., Bauke, S. L., Bogena, H., Brüggemann, N., Montzka, C., Vanderborght, J., Bechtold, M., Blöschl, G., Carminati, A., Javaux, M., Konings, A. G., Kusche, J., Neuweiler, I., Or, D., Steele-Dunne, S., Verhoef, A., Young, M., & Zhang, Y. (2022). Soil hydrology in the Earth system. *Nature Reviews Earth & Environment*, *3*(9), 573–587. https://doi.org/10.1038/s43017-022-00324-6

Vereecken, H., Weynants, M., Javaux, M., Pachepsky, Y., Schaap, M. G., & van Genuchten, M. Th. (2010). Using Pedotransfer Functions to Estimate the van Genuchten–Mualem Soil Hydraulic Properties: A Review. *Vadose Zone Journal*, *9*(4), 795–820. https://doi.org/10.2136/vzj2010.0045

Volk, J. M., Huntington, J. L., Melton, F. S., Allen, R., Anderson, M., Fisher, J. B., Kilic, A., Ruhoff, A., Senay, G. B., Minor, B., Morton, C., Ott, T., Johnson, L., Comini de Andrade, B., Carrara, W., Doherty, C. T., Dunkerly, C., Friedrichs, M., Guzman, A., ... Yang, Y. (2024). Assessing the accuracy of OpenET satellite-based evapotranspiration data to support water resource and land management applications. *Nature Water*, *2*(2), 193–205. https://doi.org/10.1038/s44221-023-00181-7

Von Unold, G., & Fank, J. (2008). Modular design of field lysimeters for specific application needs. *Water, Air, and Soil Pollution: Focus*, *8*(2), 233–242. https://doi.org/10.1007/s11267-007-9172-4

Walker, G. R., Hughes, M. W., Allison, G. B., & Barnes, C. J. (1988). The movement of isotopes of water during evaporation from a bare soil surface. *Journal of Hydrology*, *97*(3–4), 181–197. https://doi.org/10.1016/0022-1694(88)90114-X

Weber, T. K. D., Durner, W., Streck, T., & Diamantopoulos, E. (2019). A Modular Framework for Modeling Unsaturated Soil Hydraulic Properties Over the Full Moisture Range. *Water Resources Research*, *55*(6), 4994–5011. https://doi.org/10.1029/2018WR024584

Weber, T. K. D., Weihermüller, L., Nemes, A., Bechtold, M., Degré, A., Diamantopoulos, E., Fatichi, S., Filipović, V., Gupta, S., Hohenbrink, T. L., Hirmas, D. R., Jackisch, C., de Jong van Lier, Q., Koestel, J., Lehmann, P., Marthews, T. R., Minasny, B., Pagel, H., van der Ploeg, M., … Bonetti, S. (2024). Hydro-pedotransfer functions: a roadmap for future development. *Hydrology and Earth System Sciences*, *28*(14), 3391–3433. https://doi.org/10.5194/hess-28-3391-2024

Weihermüller, L., Huisman, J. A., Herbst, M., & Graf, A. (2006). *Physical and chemical characterization of the FLOWatch trench*.

Weihermüller, L., Lehmann, P., Herbst, M., Rahmati, M., Verhoef, A., Or, D., Jacques, D., & Vereecken, H. (2021). Choice of Pedotransfer Functions Matters when Simulating Soil Water Balance Fluxes. *Journal of Advances in Modeling Earth Systems*, *13*(3). https://doi.org/10.1029/2020MS002404

Wilcox, B. P., Breshears, D. D., Seyfried, M. S., & Trimble, S. (2003). Water balance on rangelands. In *Encyclopedia of water science* (pp. 791–794). CRC Press.

Willmott, C. J., Ackleson, S. G., Davis, R. E., Feddema, J. J., Klink, K. M., Legates, D. R., O'Donnell, J., & Rowe, C. M. (1985). Statistics for the evaluation and comparison of models. *Journal of Geophysical Research: Oceans*, *90*(C5), 8995–9005. https://doi.org/10.1029/JC090iC05p08995

Wilmott, C. J. (1982). Some Comments on the Evaluation of Model Performance. *Bulletin of the American Meteorological Society*, *63*, 1309–1313.

Xu, C., Widén, E., & Halldin, S. (2005). Modelling hydrological consequences of climate change—Progress and challenges. *Advances in Atmospheric Sciences*, *22*(6), 789–797. https://doi.org/10.1007/BF02918679

Yakir, D., & Sternberg, L. da S. L. (2000). The use of stable isotopes to study ecosystem gas exchange. *Oecologia*, *123*(3), 297–311. https://doi.org/10.1007/s004420051016

Yang, J., Li, B., & Shiping, L. (2000). A large weighing lysimeter for evapotranspiration and soil-water-groundwater exchange studies. *Hydrological Processes*, *14*(10), 1887–1897. https://doi.org/10.1002/1099-1085(200007)14:10<1887::AID-HYP69>3.0.CO;2-B

Yaron, B., Calvet, R., & Prost, R. (1996). *Soil Pollution*. Springer Berlin Heidelberg. https://doi.org/10.1007/978-3-642-61147-6

Young, M. H., Wierenga, P. J., & Mancino, C. F. (1996). Large weighing lysimeters for water use and deep percolation studies. In *Soil Science Issue* (Vol. 161, Issue 8). https://doi.org/10.1097/00010694-199608000-00004

Zacharias, S., Bogena, H., Samaniego, L., Mauder, M., Fuß, R., Pütz, T., Frenzel, M., Schwank, M., Baessler, C., Butterbach-Bahl, K., Bens, O., Borg, E., Brauer, A., Dietrich, P., Hajnsek, I., Helle, G., Kiese, R., Kunstmann, H., Klotz, S., … Vereecken, H. (2011). A Network of Terrestrial Environmental Observatories in Germany. *Vadose Zone Journal*, *10*(3), 955–973. https://doi.org/10.2136/vzj2010.0139

Zha, Y., Yang, J., Zeng, J., Tso, C. M., Zeng, W., & Shi, L. (2019). Review of numerical solution of Richardson–Richards equation for variably saturated flow in soils. *WIREs Water*, *6*(5). https://doi.org/10.1002/wat2.1364

Zhang, Y., Weihermüller, L., Toth, B., Noman, M., & Vereecken, H. (2022). Analyzing dual porosity in soil hydraulic properties using soil databases for pedotransfer function development. *Vadose Zone Journal*, *21*(5). https://doi.org/10.1002/vzj2.20227

Zhou, T., Šimůnek, J., & Braud, I. (2021). Adapting HYDRUS-1D to simulate the transport of soil water isotopes with evaporation fractionation. *Environmental Modelling & Software*, *143*, 105118. https://doi.org/10.1016/j.envsoft.2021.105118

Zimmermann, U., Ehhalt, D., & Münnich, K. O. (1967). Soil-water movement and evapotranspiration: Changes in the isotopic composition of the water. *Proceedings of a Symposium*, 567–585.

Zotarelli, L., Dukes, M. D., Romero, C. C., Migliaccio, K. W., & Morgan, K. T. (2010). Step by step calculation of the Penman-Monteith Evapotranspiration (FAO-56 Method). In *Institute of Food and Agricultural Sciences. University of Florida*. https://edis.ifas.ufl.edu/publication/AE459

Zundel, G., Miekeley, W., Grisi, B. M., & Förstel, H. (1978). The H2 18O enrichment in the leaf water of tropic trees: Comparison of species from the tropical rain forest and the semi-arid region in Brazil. *Radiation and Environmental Biophysics*, *15*(2), 203–212. https://doi.org/10.1007/BF01323265